REPORT DOCUMENTATION PAGE

Form Approved
OMB No. 0704-0188

1. REPORT DATE *(DD-MM-YYYY)*	2. REPORT DATE	3. DATES COVERED *(From - To)*
30/05/2003	Final	01-03-2000 to 31-03-2003

4. TITLE AND SUBTITLE
ELASTIC POLYPEPTIDES AS ACOUSTIC ABSORBERS FOR NAVY APPLICATIONS

5a. CONTRACT NUMBER
N00014-00-C-0178

5b. GRANT NUMBER

5c. PROGRAM ELEMENT NUMBER

6. AUTHOR(S)
Urry, Dan W.; Xu, Jie; Wang, Weijun; Hayes, Larry C.; Prochazka, Frederic; Parker, Timothy M.

5d. PROJECT NUMBER

5e. TASK NUMBER

5f. WORK UNIT NUMBER

7. PERFORMING ORGANIZATION NAME(S) AND ADDRESS(ES)
Bioelastics Research, Ltd.
2800 Milan Court, Suite 386
Birmingham, AL 35211

8. PERFORMING ORGANIZATION REPORT NUMBER
BRL-0012

9. SPONSORING/MONITORING AGENCY NAME(S) AND ADDRESS(ES)
Same as 7

10. SPONSOR/MONITOR'S ACRONYM(S)

11. SPONSORING/MONITORING AGENCY REPORT NUMBER

12. DISTRIBUTION AVAILABILITY STATEMENT
Approved for Public Release; Distribution Unlimited

13. SUPPLEMENTARY NOTES

14. ABSTRACT

Elastic protein-based polymers comprised of repeating pentapeptide sequences, $(GXGXP)_n$, exhibit mechanical resonances that have been observed to date with frequency maxima near 5 MHz and 3 kHz. Because the 3 kHz resonance is in the middle of the acoustic frequency range, the purpose here is to substantiate the relevance of the 3 kHz resonance to acoustic absorption and to demonstrate means of improving mechanical properties for the sound absorption application. Previously reported loss factor data in the 100 Hz to 10 kHz range is substantiated by relevant but distinctly different measurements of loss shear modulus and loss permittivity. Furthermore cross-linking approaches are reported that result in increase elastic moduli by an order of magnitude to 4×10^6 Pa at 20% strain and that increase break stress by two orders of magnitude to 1.3×10^7 Pa while exhibiting break stain values of several hundred per cent.

15. SUBJECT TERMS
Medhanical Resonances, loss shear modulus, loss permittivity

16. SECURITY CLASSIFICATION OF:			17. LIMITATION OF ABSTRACT	18. NUMBER OF PAGES	19a. NAME OF RESPONSIBLE PERSON
a. REPORT	b. ABSTRACT	c. THIS PAGE			Dan W. Urry
UU	UU	UU	UU		19b. TELEPONE NUMBER *(Include area code)* 205-943-6590

Standard Form 298 (Rev. 8-98)
Prescribed by ANSI-Std Z39-18

Distribution List:

Final Report of Contract N00014-00-C-0178

Keith Ward Program Officer Office of Naval Research Ballston Tower One 800 North Quincy Street Arlington, VA 22217-5660	1 copy
Patricia Curry Administrative Contracting Officer DCMA P.O. Box 5130 Fort McClellan, AL 36205-0130	Transmittal letter only
Director, Naval Research Laboratory ATTN: Code 5227 Washington, D.C. 20375	1 copy
Defense Technical Information Center 8725 John J. Kingman Road STE 0944 Ft. Belvoir, VA 22060-6218	2 copies

FINAL PROGRESS REPORT

ELASTOMERIC POLYPEPTIDES AS ACOUSTIC ABSORBERS FOR NAVY APPLICATIONS

Dan W. Urry, Jie Xu, Weijun Wang, Larry Hayes, Frederic Prochazka, and Timothy M. Parker.

Bioelastics Research Ltd.,
2800 Milan Court, Suite 386,
Birmingham, AL, 35211

Prepared for
Office of Naval Research
Under Contract No. N00014-00-C-0178

May 2003

UNCLASSIFIED

ABSTRACT

Elastic protein-based polymers comprised of repeating pentapeptide sequences, $GXGXP)_n$, exhibit mechanical resonances that have been observed to date with frequency maxima near 5 MHz and 3 kHz. Because the 3 kHz resonance is in the middle of the acoustic frequency range, the purpose here is to substantiate the relevance of the 3 kHz resonance to acoustic absorption and to demonstrate means of improving mechanical properties for the sound absorption application. Previously reported loss factor data in the 100 Hz to 10 kHz range is substantiated by relevant but distinctly different measurements of loss shear modulus and loss permittivity. Furthermore cross-linking approaches are reported that result in increase elastic moduli by an order of magnitude to 4×10^6 Pa at 20% strain and that increase break stress by two orders of magnitude to 1.3×10^7 Pa while exhibiting break stain values of several hundred per cent.

Table of Contents

LIST OF FIGURES AND TABLE

FINAL PROGRESS REPORT
01 March 2000 to 31 March 2003

Elastomeric Polypeptides as Acoustic Absorbers for Navy Applications

Principal Investigator: Dan W. Urry, Ph.D.

PI Institution: Bioelastics Research, Ltd.
2800 Milan Court, Suite 386
Birmingham, AL 35211-6918
Phone: 205-943-6592; Fax: 205-943-6591
(e-mail:brl@oadi.uab.edu)

Contract Number; N00014-00-C-0178

Award Date: 27 April 2000

Authors: Dan W. Urry, Jie Xu, Weijun Wang, Larry Hayes, Frederic Prochazka, and Timothy M. Parker

SUMMARY

The problem addressed in this effort is the development of elastomeric polypeptides for acoustic absorption applications. The basic problem facing this objective is the continued fixation by authorities in the area on the idea that elastic materials must be (must have the properties of) random chain networks. The staid authorities simply will not entertain the possibility that elastic polymers can have mechanical resonances and that such resonances can exhibit intense absorptions (loss factors) in the acoustic frequency ranges. A quotation due to Maurice Maeterlinck, seems particularly appropriate, "At every crossway on the road that leads to the future, tradition, has placed against each of us, 10,000 men to guard the past." This report, buttressed by three papers in the APPENDIX, is believed to demonstrate the unique opportunity that elastic protein-based polymers present to satisfy sound absorption needs of the Navy.

Specifically, elastic protein-based polymers comprised of repeating pentapeptide sequences, $(GXGXP)_n$, exhibit mechanical resonances that have been observed to date with frequency maxima near 5 MHz and 3 kHz. As the 3 kHz resonance is in the middle of the acoustic frequency range, the principal result of this report substantiates the relevance of the 3 kHz resonance to acoustic absorption. Additional results demonstrate means of improving mechanical properties for the sound absorption application.

In particular, previously reported loss factor data in the 100 Hz to 10 kHz range was declared to be artifact by one particularly influential man of the 10,000 men that "guard the past." The principal result of this report is that loss shear modulus and loss permittivity data substantiate the intense absorption capacity of γ-irradiation cross-linked $(GVGIP)_{320}$ centered near 3 kHz with moduli in the range of 5×10^6 Pa and with the potential to reach 10^7 Pa. Furthermore, cross-linking approaches are reported that result in materials exhibiting, in the most favorable examples so far, elastic moduli and break stresses as high as 2×10^7 Pa while exhibiting break strain values of several hundred per cent.

We recommend that the NAVY give serious consideration to further development of these unique sound absorbing protein-based materials, and that those who believe that they have the instrumentation with which to measure artifact free acoustic absorption of elastomeric materials find it in their wisdom to reconsider doing so.

INTRODUCTION

When seeking materials suitable for low frequency sound absorption, compliant or elastomeric materials become a natural consideration. Classical elastomers, or rubbers, are reasonable and commonly used materials, but they have a fundamental limitation. They are composed of random chain networks that necessarily exhibit low intensity, very broad and essentially featureless frequency dependences of relaxation (or absorption). Because of this, the possibilities of tuning or designing classical elastomers to maximize sound absorption over a desired frequency range are limited.

On the other hand certain elastic protein-based polymers can exhibit good elastic moduli and yet contain dynamic structural regularities that exhibit mechanical modes. In fact elastic protein-based polymers can be designed to exhibit mechanical resonances with high loss factors over interesting frequency ranges.

Preliminary acoustic absorption studies on elastic protein-based polymeric materials:

The elastic protein-based polymer, (glycyl-valyl-glycyl-isoleucyl-prolyl)$_n$ abbreviated as (GVGIP)$_n$, emerged as a particularly interesting composition; it exhibited a large hysteresis in macroscopic stress-strain studies and in atomic force microscopy(AFM)-based single-chain force-extension studies.[1] Therefore, (GVGIP)

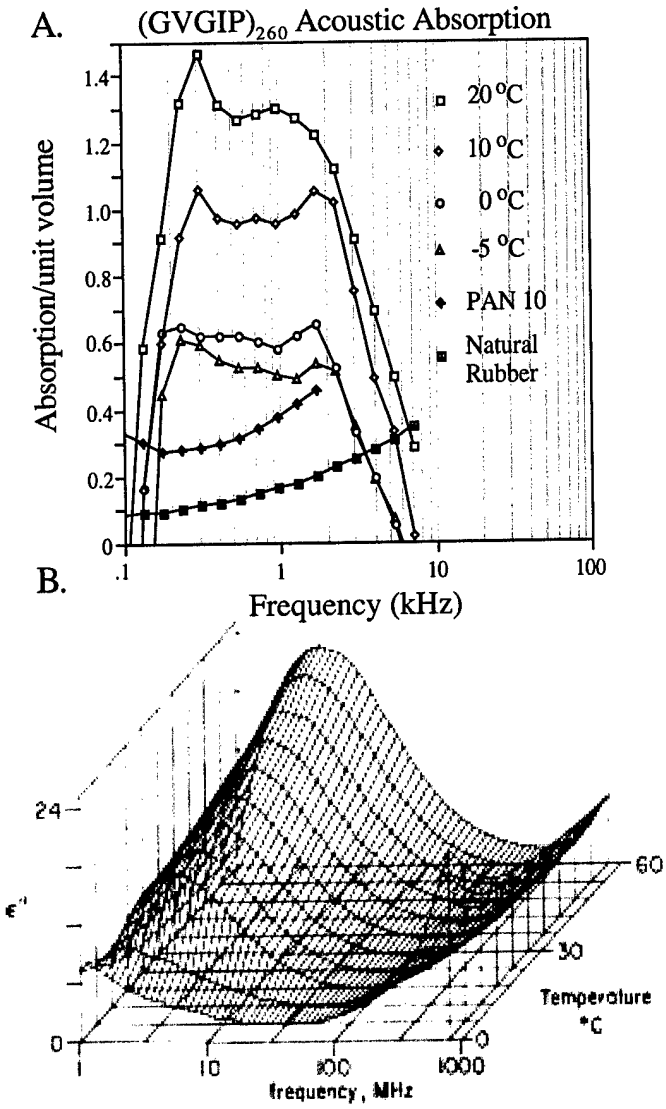

Figure 1: A. Acoustic absorption of 20 Mrad γ-irradiation cross-linked (GVGIP)$_{260}$
B. 5MHz dielectric relaxation of poly(GVGIP) (imaginary part, ε'')

might be expected to exhibit substantial loss factors as required for good acoustic absorption.

Accordingly, two γ-irradiation (20 Mrad) cross-linked cylinders of X^{20}-$(GVGIP)_{260}$ were prepared with diameters of 2.5 cm and lengths of 0.5 cm and 1.0 cm. Lev Sheiba and Jack Dea examined the absorption properties of these cylinders at the SPAWAR (Spatial Warfare) Systems Center in San Diego. The results are given in **Figure 1A** where the elastic protein-based polymer is compared to natural rubber and an absorption enhanced polyurethane.[1] As to be expected for the random chain networks of natural rubber and polyurethane, both exhibited broad featureless dependences on frequency and relatively low intensity loss factors (sound absorption/unit volume). On the other hand, the elastic protein-based polymer exhibited a localized relaxation that grew in intensity as the temperature increased, just as had been observed in the dielectric relaxation spectra, specifically in the imaginary part of the dielectric permittivity, of $(GVGIP)_n$ at 5 MHz (See **Figure 1B**).[2]

Molecular structure of (GXGXP)-type elastic protein-based polymers:

(GXGXP)-type protein-based elastomers form β-spiral structures described as a series of β-turns arranged in helical array with dynamic suspended segments between the β-turns. For discussion of the single secondary structural feature of the β-turn, the repeating conformational feature is considered in terms of the sequence permutation, $X^1P^2G^3X^4G^5$. With this residue numbering, the β-turn is a ten-atom hydrogen-bonded ring involving the C-O of the X^1 residue preceding the proline residue and the NH of the X^4 residue. The β-spiral structure in band representation of the backbone is shown on the left side of **Figure 2**, and cross-eye stereo views of the detailed molecular structure are seen in side and spiral axis views in the center structures of

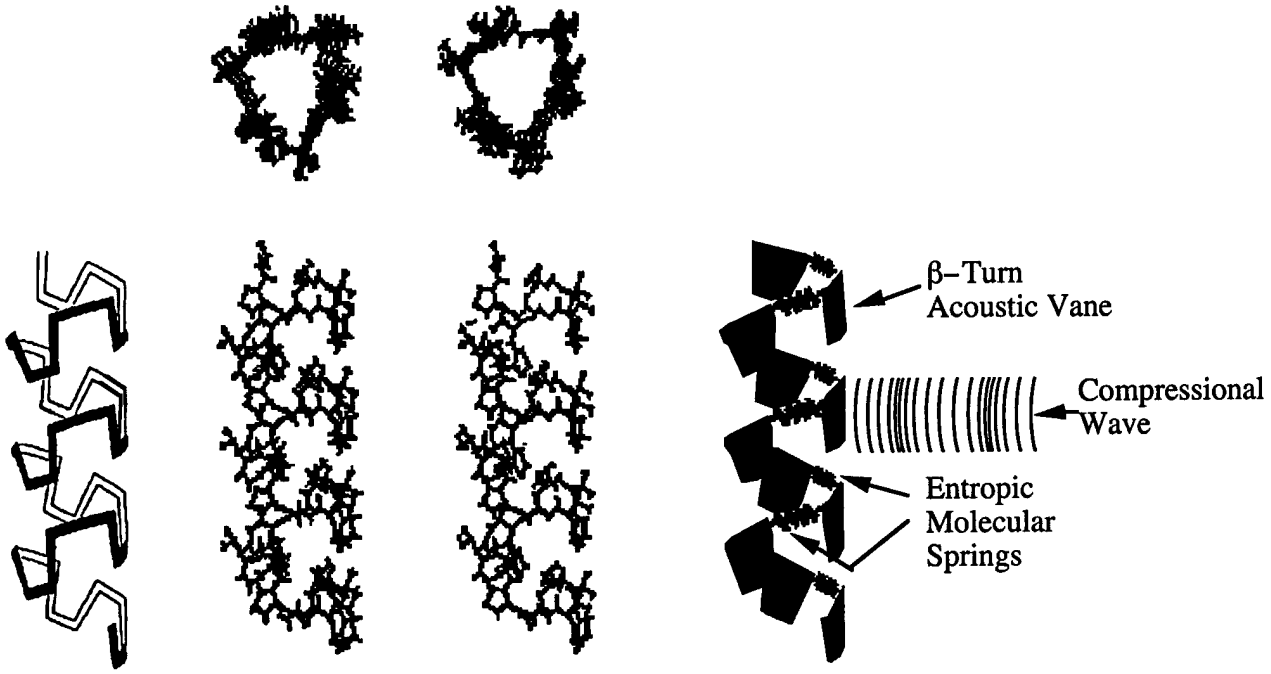

Figure 2: Molecular structure and acoustic absorption cartoon for elastic protein-based polymers of the GXGXP-type repeating pentapeptide sequence.

Figure 2. At the molecular level, there occur suspended segments connecting the β-turns that contain peptide moieties capable of large amplitude rocking motions. The suspended segments exhibit large amplitude torsional oscillations that become damped on extension. Thus, the suspended segments that link the β-turns function as entropic molecular springs.

The β-turns themselves provide dynamically active surface elements, effectively forming a series of plates on the surface of the wide dynamic helix that is the β-spiral. A macroscopic-classical analog would be equivalent to springs connecting the β-turn plates. The β-turn surface elements may be thought of as molecular acoustic veins attached to springs that are tunable to resonate at desired frequencies. A cartoon demonstrating these structural features is shown as the right-most illustration of **Figure 2.** The four spiral structures are separated, such that when the two central detailed structures are viewed in stereo, the backbone band representation and the cartoon also overlap with detailed molecular structures.

Mechanism of elasticity and mechanical resonances in repeating peptide sequences:

By means of AFM (atomic force microscopy), single-chain force-extension curves have been obtained on Cys-$(GVGIP)_{nx260}$-Cys and Cys-$(GVGVP)_{nx251}$-Cys, where Cys is the cysteinyl residue with a sulfhydryl for attachment to surfaces.[1] In the experiment, one end of the single chain is attached to the cantilever tip and the other end to a surface. Force is measured as a function of chain length, and elastic moduli of several pN/chain have been obtained. In this experiment, a single chain held fixed at both ends gives rise to entropic elastic force. Since total molecule rotations and translations are not possible, the decrease in entropy, that gives rise to an entropic elastic force on extension to a particular fixed length, must come from the damping of internal chain dynamics.[3] Therefore, it is established that entropic elasticity can occur without random chain networks and without a random, or Gaussian, distribution of end-to-end chain lengths.

Importantly, the intensity of the 5 MHz dielectric relaxation of $(GVGVP)_n$ can be calculated from the molecular dynamics of the structure of the repeating unit in **Figure 2** using Onsagers's equation for polar liquids.[4,5] Quoting from the *McGraw-Hill Concise Encyclopedia of Science and Technology*, 2nd Edition, 1989, page 1599, "When a mechanical or acoustical system is acted upon by an external periodic driving force whose frequency equals a natural free oscillation frequency of the system, the amplitude of the oscillation becomes large and the system is said to be in a state of resonance." The repeating structural units of **Figure 2** effectively resonate, and the absorption (loss factor) peaks in the relaxation spectra may be called mechanical resonances. Furthermore, the occurrence of mechanical resonances in elastic-protein-based polymers makes the classical theory of rubber elasticity only marginally relevant to these polymers and the use of related considerations in treatments of acoustic absorption by such polymers would also be suspected of similar limitations. Finally, the occurrence of mechanical resonances in these elastic protein-based polymers presents unique opportunities for designing materials with acoustic absorption properties that can be improved over current elastomeric materials.

Acoustic absorption data claimed to be artifact:

In spite of the occurrence of the same temperature dependent phenomena near 5 MHz (**Figure 1B**) and near 3 kHz (**Figure 1A**) using the same elastic protein-based polymer

composition, the acoustic absorption data of **Figure 1A** on the elastic protein-based polymer has been declared to be an artifact by academic professionals concerned with acoustic absorption applications for the Navy. This is in spite of the fact that the similarly determined data for natural rubber and polyurethane did not appear to be in question. At the same time that the data from SPAWAR has been declared to be artifact, the party making the claim refuses to measure, in their "uniquely artifact-free" instrumentation, the base polymer composition as well as additional analogues designed to extend further the acoustic absorption properties of this family of elastic protein-based polymers. Because of this, independent approaches have been sought and they have been found to evaluate the significance of the data in **Figure 1A**.

Content of this report:

This report presents a family of ten elastic protein-based polymers that have been designed to achieve even more potent acoustic absorption materials. They have been prepared using recombinant DNA technology and transformation of *E. coli* and have been expressed in large quantities through *E. coli* fermentation. Improved mechanical properties – such as essential work of fracture, elastic modulus, break stress and break strain – have been achieved by obtaining higher molecular weight, monodisperse polymers and by improved cross-linking approaches. The design for improved chemical cross-linking utilized the concept of apolar-polar repulsive free energies of hydration. Importantly for developing improved acoustic absorption materials, using the base composition of the family, X^{20}–$(GVGIP)_{320}$, a combination of loss shear modulus, G", measurements and loss permittivity, ε", data have been obtained that substantiate the existence of an intense temperature dependent acoustic absorption, that is a mechanical resonance, centered near 3kHz.

METHODS, ASSUMPTIONS, AND PROCEDURES

Production of polymers by recombinant DNA technology:

The list of elastic protein-based polymers of **Table 1** were prepared by recombinant DNA technology. This involves the construction of a monomer gene from two chemically synthesized, overlapping DNA sequences that were made into the complete double-stranded DNA by the polymerase chain reaction (PCR). Trace amounts of the monomer genes so prepared were inserted into an appropriate plasmid and a strain of *E. coli* was transformed that produced a large number of copies of the monomer gene. The isolated, relatively large quantity of monomer gene was polymerized (in terms molecular biology, concatemerized or concatenated) and ultimately used to transform a strain of *E. coli* that was suitable for expression of the elastic protein-based polymer.[6] **Table 1** gives the size of the gene for the resulting elastic protein-based polymer in terms of the number of repeating peptide units and the amount of polymer prepared for subsequent characterization.

Preparation of Polymers I' through VI' was for chemical cross-linking efforts, whereas Polymers VII' through XI' and XV' and XVII' were prepared for systematic change in hydrophobicity and for inclusion of a sulfate to introduce the effect on acoustic absorption of $MgSO_4$ association/dissociation in polymers of different hydrophobicities. Finally, Polymer

XVII' was specifically prepared for its higher molecular weight and for a more monodisperse molecular weight than had been prepared previously.

Table 1:		prepared grams	pentamers per polymer
Polymer I'	$[(GVGIP\ GEGIP\ GVGIP)_3]_n$	17	240
		34	108
Polymer II'	$[(GVGIP\ GVGIP\ GEGIP\ GVGIP\ GVGIP\ GVGIP)]_n$	58	276
Polymer III'	$[(GEGIP\ GVGIP\ GEGIP\ GVGIP\ GVGIP\ GVGIP)]_n$	31	180
Polymer IV'	$[(GVGIP\ GKGIP\ GVGIP)_3]_n$	0	
Polymer V'	$[(GVGIP\ GVGIP\ GKGIP\ GVGIP\ GVGIP\ GVGIP)]_n$	20	252
		20	144
Polymer VI'	$[(GKGIP\ GVGIP\ GKGIP\ GVGIP\ GVGIP\ GVGIP)]_n$	0	
Polymer VII'	$[(GVGIP)_{21}(GYGIP)]_n$,	60	242
Polymer IX'	$[(GVGIP)_{11}(GYGIP)]_n$,	40	216
Polymer XI'	$[(GVGIP)_8(GYGIP)]_n$,	47	288
Polymer XIII'	$[(GVGIP)_5(GYGIP)]_n$,	30	240
Polymer XV'	$\{[(GVGIP)_2(GYGIP)]_3\}_n$,	trace	135
Polymer XVII'	$[(GVGIP)_{10}]_n$	247	320
Polymer VIII'	$[(GVGIP)_{21}(GY\{SO_4^{=}\}GIP)]_n$	19	242
Polymer X'	$[(GVGIP)_{11}(GY\{SO_4^{=}\}GIP)]_n$	19	216

Cross-linking of polymers:

Preparation of γ-irradiation cross-linked matrices: In preparation for γ-irradiation cross-linking, the polymer is dissolved in water at low temperature. On raising the temperature above that of the inverse temperature transition for hydrophobic association, phase separation occurs. The phase-separated state is then exposed to 20 Mrad of γ-irradiation from a cobalt-60 source.

Preparation of chemically cross-linked fibers: Chemical cross-linking was achieved by extrusion of solutions of E- and K- pairs of polymers at equal concentrations of functional groups into a saturated solution at 50°C of water soluble carbodiimide (EDC, 1-(3-dimethylaminopropyl)-3-ethylcarbodiimide) to form amide bonds between the carboxyl of glutamic acid (E) residues and the ε-amino groups of lysine (K) residues.[7] When in an adequately hydrophobic elastic protein-based polymer, the charged carboxylate and amino functions experience a driving force for ion-pairing. The force arises due to an apolar-polar repulsive free energy of hydration, ΔG_{ap}, that is measurable from the hydrophobic-induced pKa shifts.[8] Cross-linking occurred on extrusion to form fibers and also in a manner to result in disks. When using microbially prepared elastic protein-based polymers with functional groups occurring every thirty residues and with the favorable ΔG_{ap}, materials of exceptional mechanical properties are

obtained, for example fibers exhibited elastic moduli and break stresses that are one to two orders of magnitude greater than obtained with γ-irradiation cross-linking.

Determination of shear moduli:
The instrument for determination of shear moduli was a Rheometric Scientific dynamic mechanical thermal analyzer, model DMTA V. Round shear sandwich geometry was used. The instrument was inverted so that the sandwich fixtures and sample were in water. A water-jacketed 1000 mL Pyrex cylinder supplied by Rheometric Scientific allowed control of temperature with a circulating temperature bath. A sinusoidal linear shear was applied by moving a flat plate between two identical disk-shaped samples over a specified range of frequencies. The two identical disk-shaped samples were sandwiched between the moving plate and two 12 mm diameter plates (called studs) fastened to a frame. The dynamic frequency sweeps to obtain the loss shear modulus, G", from 0.16 Hz to 318 Hz were reported in log scale.[9] For our purposes Initial static force was 0.05 N. Sample size was 12 mm diameter and 0.7 mm thickness. The sample was equilibrated at 40°C for 12 hours prior to starting the series of measurements. Shear moduli were measured from high to low temperature with an equilibration time of 2 hours at each temperature. The sequence of measurements was 40°C, 30°C, 25°C, and 15°C.

Determination of low frequency dielectric relaxation:
Low frequency dielectric relaxation data was obtained with a Rheometric Scientific dielectric thermal analyzer (DETA) system, model MK-II. The unit consists of a temperature programmer, dielectric thermal analyzer, and water-jacketed inverted can-shaped enclosure, called a furnace. Within the inverted can-shaped enclosure is a pair of disk-shaped parallel plates between which the sample is placed. The sample was sealed between 0.01mm Teflon sheets (Goodfellow, Cambridge, England) and the sealed packet was placed between the two 15mm-diameter parallel plates. An alternating electric field is applied to the sample by means of a sinusoidal voltage and an out of phase current is measured to obtain the loss permittivity, ε". An external temperature bath was used for temperature control. Sample size for X^{20}-$(GVGIP)_{320}$ was 15mm diameter and 0.6 mm thickness. The system was equilibrated overnight at 40°C. Temperature was decreased in 5-degree increments with 2 hours of equilibration between temperature changes and 3 sets of measurements were made from 20 Hz to 100 kHz at each temperature.

Basis for correlation between loss shear modulus and loss permittivity:
When a polymer exhibits a maximum in the imaginary part of the dielectric permittivity (the loss permittivity, ε") at frequencies less than 200 Hz, it becomes possible to make comparisons with the frequency dependence of shear moduli and most specifically with the loss shear modulus, G". This has been done for polypropylene diol, also called poly(oxypropylene), where there is reported a near perfect superposition of the frequency dependence of the normalized loss shear modulus with that of the normalized loss permittivity as reproduced in **Figure 3**.[10,11] The acoustic absorption frequency range of interest here is 100 Hz to 10 kHz, yet present

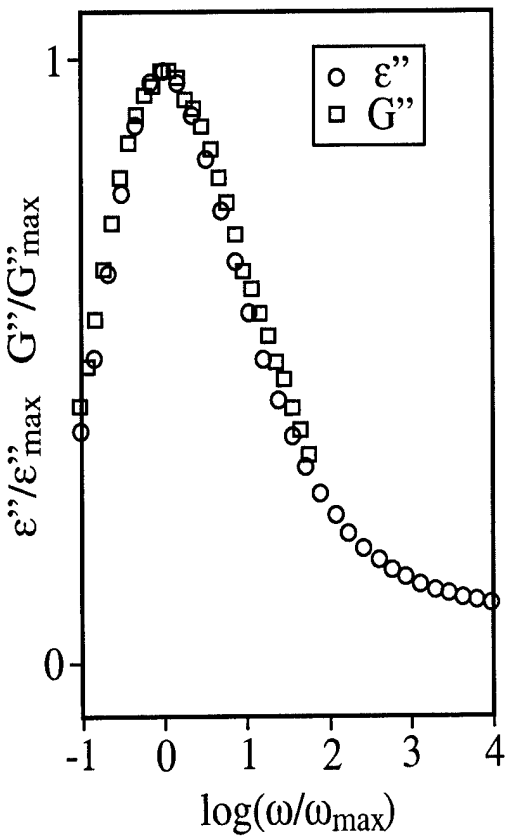

Figure 3: Superposition of loss permittivity and loss shear modulus for polypropylene diol. Adapted with permission from references 10 and 11.

macroscopic loss shear modulus data can be determined at most up to a few hundred Hz. Nonetheless, for X^{20}-$(GVGIP)_{320}$ there is a maximum in loss permittivity, ε", near 3 kHz that develops on raising the temperature through the temperature range of the inverse temperature transition. With the width of the loss permittivity curve a distinct set of curves as a function of temperature become defined as low as the 100 to 200 Hz frequency range. Accordingly, if these loss permittivity curves are sufficiently distinctive and compare favorably with the exactly corresponding set of loss shear modulus curves, the melding of the two sets of data in the overlap region provide for calibration of the loss permittivity curves in terms of loss shear modulus of recognized relevance to acoustic absorption data.

Determination of essential work of fracture:

Samples of X^{20}-$(GVGIP)_{320}$ were run on an in house custom-built vertical stress-strain apparatus. A water-jacketed chamber allowed grips and sample to be submerged at all times with temperature control. Sample size was 4x5x0.5 mm. Samples were double notched with a fresh razor blade and stretched at a speed of 2.2 mm/min until fractured.[12] Several different ligament lengths (distance between notches) were used and work of fracture was plotted against ligament length.

RESULTS AND DISCUSSION

Unique temperature and frequency dependence of loss shear modulus data:

It is generally recognized that the loss shear modulus, G", data in the 1 Hz to 200 Hz frequency range is relevant to acoustic absorption in the 100 Hz to 10 kHz frequency range. Commonly, data obtainable at lower frequencies, generally 100 Hz or less, has been extrapolated into the acoustic frequency range in order to evaluate candidates for good acoustic absorption properties. Such an extrapolation requires an assumption about the frequency dependence. While this becomes a reasonable practice for classical elastomers that occur as random chain networks with the broad, featureless frequency dependence of natural rubber and polyurethane seen in **Figure 1A**, it is not a reasonable assumption for elastic protein-based polymers that exhibit mechanical resonances as seen in **Figure 1B** for the loss permittivity of $(GVGIP)_n$.

The variable temperature dependence of the steepness of curvature for the loss shear modulus curves reported in **Figure 4** causes concern for an approach that extrapolates to higher frequencies

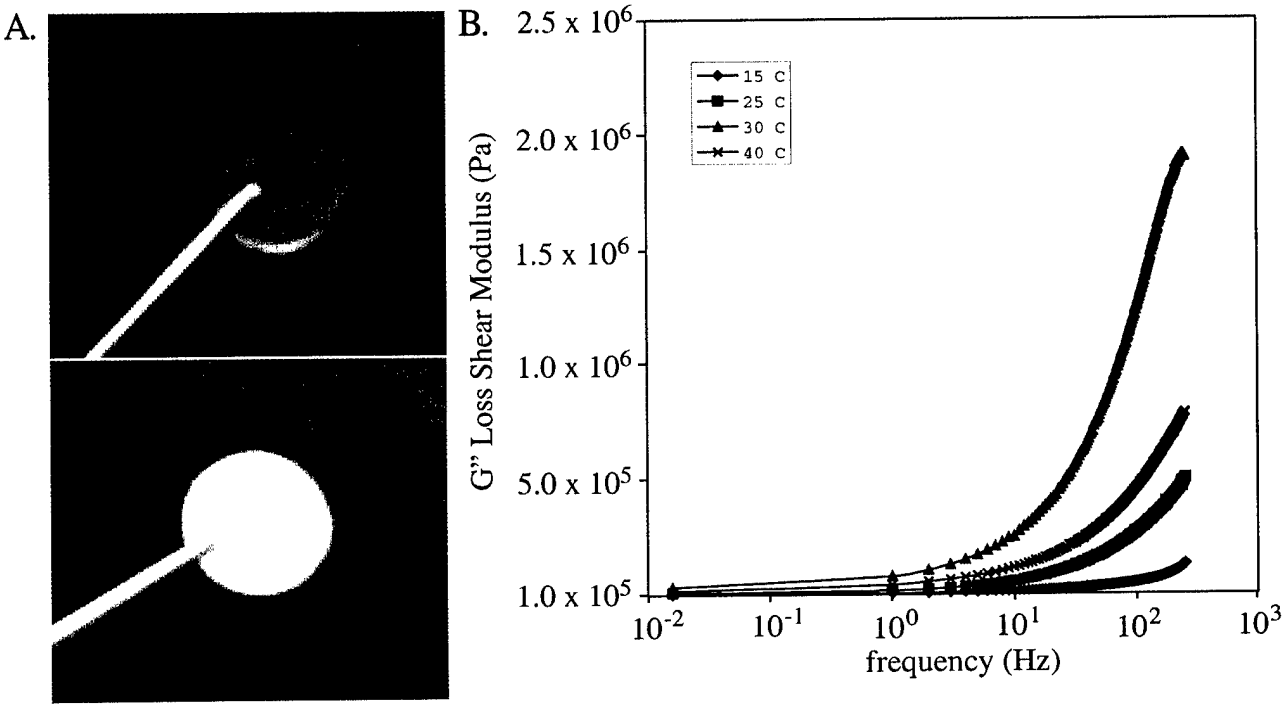

Figure 4: A. Discs of X^{20}-$(GVGIP)_{320}$. **B.** Loss shear modulus, G", vs. frequency for $(GVGIP)_{320}$

without a better understanding of the frequency dependence. Because of the correlation of loss shear modulus and loss permittivity data for polypropylene diol of **Figure 3**, loss permittivity data in the acoustic frequency range has particular significance for elastic protein-based polymers that exhibit a high temperature dependence for the loss permittivity as seen in **Figure 1B**. In fact, as shown immediately below, low frequency dielectric relaxation data provides a means more effective than computational extrapolation with which to evaluate acoustic absorption properties of elastic polymers that exhibit mechanical resonances.

Melding of loss shear modulus and loss permittivity data to evaluate acoustic absorption potential of elastic protein-based polymers:

The temperature dependence of the loss shear modulus data of **Figure 4** is quite distinctive. At 200Hz the temperature dependence is one of increasing G" on increasing the temperature from 15 to 25°C, but then the next larger G" occurs at 40°C with the value of G" at 200 Hz for the 30°C data being more than twice as large. On the other hand at 5 MHz in **Figure 1B**, the increase in intensity of the loss permittivity continues to increase on raising the temperature from 10 to 60°C.

Nonetheless, the merging of loss shear modulus, G", and loss permittivity, ε", data for the overlapping frequencies in **Figure 5** is truly remarkable. Explanation of the distinctive 40°C curve now becomes obvious. The explanation arises due to the occurrence of the temperature interval of the inverse temperature transition[8] being from 10 to 30°C. During the inverse temperature transition of hydrophobic

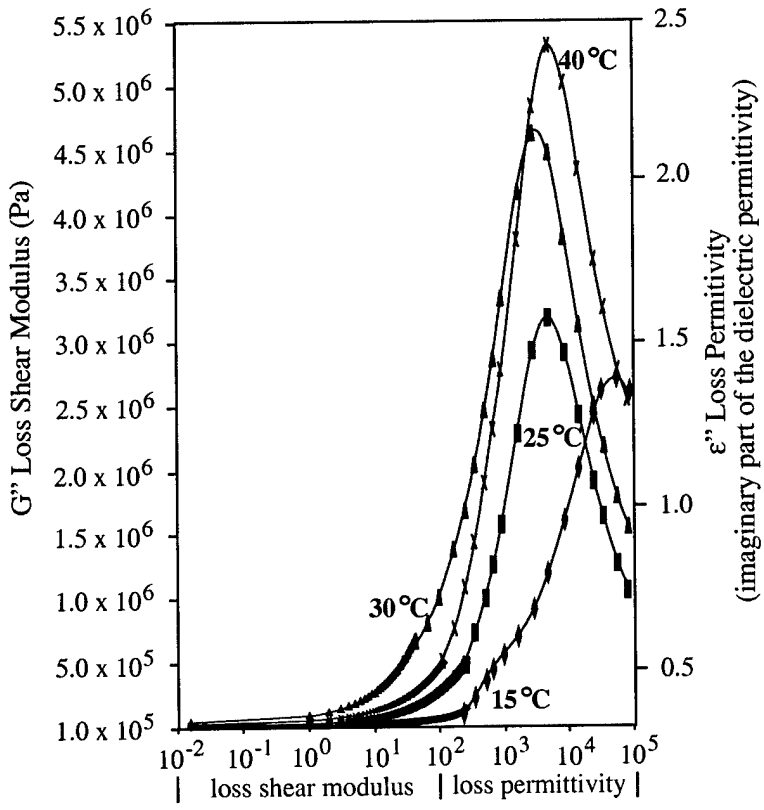

Figure 5: Melding of G" and ε" data for $(GVGIP)_{320}$

folding into the structure of **Figure 2**, the frequency maximum of the loss permittivity peak decreases as the elastic protein-based polymer folds into a more regular structure. Once the inverse temperature transition is complete, the normal increase in frequency with increase in temperature ensues.

A coarse calibration of the higher frequency loss permittivity data becomes possible by using the overlap with the loss shear modulus values. It seems reasonable to conclude that the loss shear modulus values would reach $5x10^6$ Pa or more near 3 kHz. The comparison also suggests that the intensity of the peak in **Figure 1A** would almost double on continuing from 20 to 40°C. It should also be appreciated that the composition of the elastic protein-based polymer can be chosen such that the temperature interval is below 5°C in which case the intense absorption would exist at temperatures above 5°C.

Mechanical properties of cross-linked fibers:

When utilizing the apolar-polar repulsive free energy for hydration, ΔG_{ap}, the free energy gained on ion-pairing aligns and orders cross-linking groups, E and K. This is demonstrated for the polymer pair,

Polymer	**i:**	(GVGVP GVGVP G**E**GVP GVGVP GVGVP GVGVP)$_{36}$(GVGVP)	E/0F
Polymer	**x':**	(GVGVP GVGVP G**K**GVP GVGVP GVGVP GVGVP)$_{22}$(GVGVP)	K/0F,
and for the pair,			
Polymer	**ii:**	(GVGVP GVGFP G**E**GFP GVGVP GVGVP GVGVP)$_{40}$(GVGVP)	E/2F
Polymer	**xi':**	(GVGVP GVGFP G**K**GFP GVGVP GVGVP GVGVP)$_{22}$(GVGVP)	K/2F.

Micrographs of the fibers formed and represented mechanical properties are given in **Figure 6**. Among the several experiments, values of the elastic modulus, **E**, at 20% of greater than 10^7 Pa have been obtained and break stresses greater than 1.5×10^7 Pa have also been obtained for both fiber compositions. These values are two orders of magnitude greater than obtained by means of γ irradiation cross-linking. Generally, the more hydrophobic phenylalanine (Phe, F) containing polymers gave the higher values.

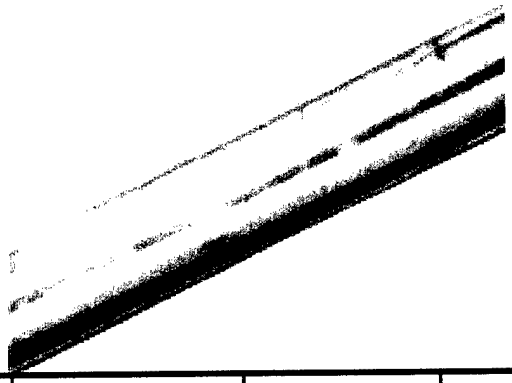

Polymer	E (Pa) at 20% Strain	Break Stress (Pa)	Break Strain (%)
ii – xi' Fiber	3.86×10^6	1.26×10^7	350

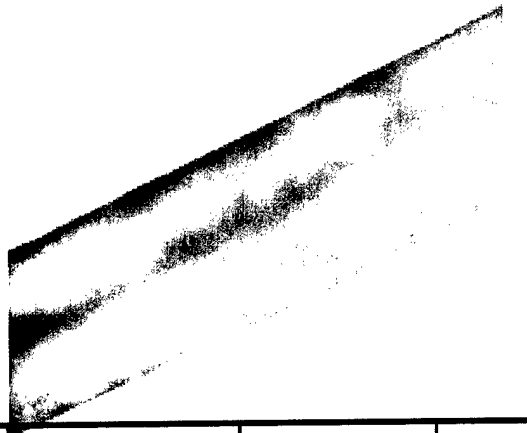

Polymer	E (Pa) at 20% Strain	Break Stress (Pa)	Break Strain (%)
i – x' Fiber	6.12×10^6	6.94×10^6	285

Figure 6: Mechanical properties of chemically cross-linked fibers.

Essential work of fracture

The stress-strain curves given in terms of the work in J/m^2 versus extension to the point of breakage is seen in **Figure 7A**. When the specific work of fracture is plotted as a function of ligament length resulting from notching each side of the elastic strip, extrapolation to the intercept gives the essential work of fracture. The results for both X^{20}–$(GVGIP)_{260}$ and X^{20}–$(GVGIP)_{320}$ are shown in **Figure 7B**. While the gene for $(GVGIP)_{260}$ indicates a chain length of 260 pentamers, the expressed protein-based polymer contained a smear of chains of lower molecular weights. In making a new monomer gene encoding for 10 pentamers, the same codons were used for the two G residues within the GVGIP pentamer but different codons for G were used between the pentamers. On multimerization a more stable higher molecular weight gene product was expressed, namely $(GVGIP)_{320}$. On 20 Mrad γ-irradiation cross-linking an elastic matrix formed with twice the essential work of fracture that was more consistent with chemically-synthesized poly(GVGIP). Thus, a tougher matrix was obtained that would be more suitable for acoustic absorption applications.

CONCLUSIONS

Elastic protein-based polymers of the (GXGXP)-type exhibit mechanical resonances that open a new vista for the development of unique acoustic absorption materials. Previously determined temperature dependent loss factor (absorption/unit volume) curves for X^{20}–$(GVGIP)_{260}$ in the 100 Hz to 10 kHz range have been dismissed as artifact in spite of the fact that exactly parallel behavior as a function of temperature is observed for a mechanical resonance of $(GVGIP)_n$ at 5 MHz by means of loss permittivity measurements. Melding of loss shear modulus and loss permittivity data confirmed the presence of an intense mechanical resonance in the acoustic absorption range for matrices of X^{20}–$(GVGIP)_{320}$. The cylindrical sample of **Figure 8** stands ready for acoustic absorption measurements by instrumentation claimed to be uniquely free of artifact.

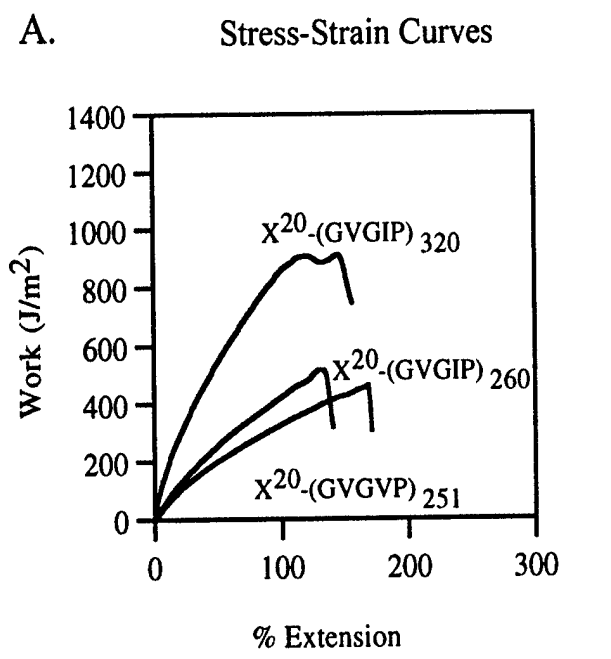

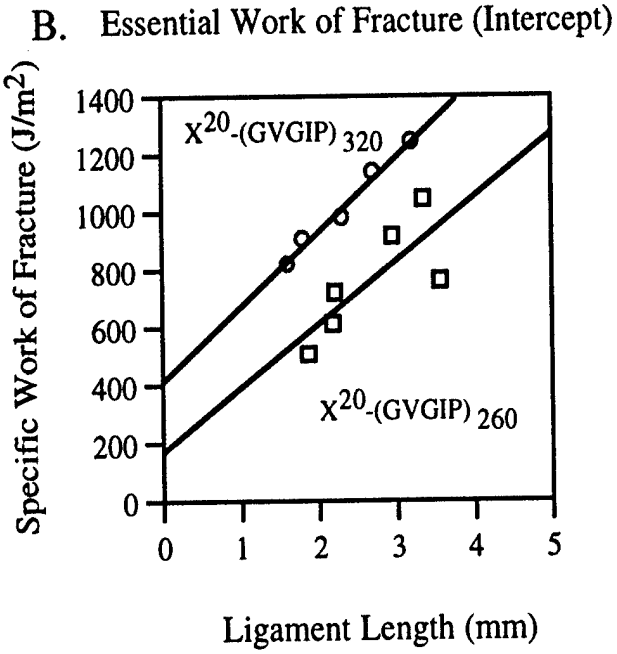

Figure 7: Essential work of fracture for X^{20}–$(GVGIP)_{260}$ and X^{20}–$(GVGIP)_{320}$.

Using an understanding of the apolar-

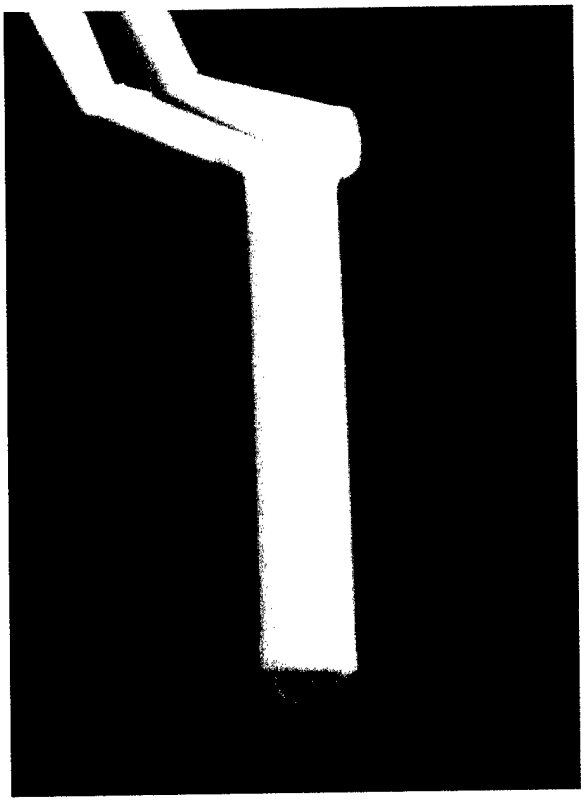

Figure 8: Cylinder of 20 Mrad γ-irradiation cross-linked $(GVGIP)_{320}$ prepared in a form suitable for acoustic absorption measurements by the "uniquely artifact free" instrumentation.

polar repulsive free energy of hydration, ΔG_{ap},[8] elastic protein-based polymers can be prepared with impressive mechanical properties of elastic moduli and break stresses up to 2×10^7 Pa and break strains of several hundred percent.

RECOMMENDATIONS

Based on the data presented in this Final Report, we respectfully recommend that the Office of Naval Research and the Navy consider elastic protein-based materials for their sound absorption needs. One possible area of application would be hearing protection. To the best of our knowledge the property of mechanical resonances with high loss factors in the acoustic absorption range, as exhibited by (GXGXP)-type protein-based elastomers, is simply not available in random chain network elastomers.

ACKNOWLEDGMENTS: The authors gratefully acknowledge the Office of Navy Research under Contract Number N00014-00-C-0178 for the support of these materials developments.

REFERENCES

1. D. W. Urry, T. Hugel, M. Seitz, H. Gaub, L. Sheiba, J. Dea, J. Xu and T. Parker, "Elastin: A Representative Ideal Protein Elastomer," Phil. Trans. R. Soc. Lond. B 357, 169-184 (2002).
2. R. Buchet, C.-H. Luan, K.U. Prasad, R.D. Harris and D.W. Urry, "Dielectric Relaxation Studies on Analogs of the Polypentapeptide of Elastin," *J. Phys. Chem.* **92**, 511-517 (1988).
3. D. W. Urry and T. M. Parker, MECHANICS OF ELASTIN: Molecular Mechanism of Biological Elasticity and its Relevance to Contraction, *J. Muscle Res. Cell Motility* **23**, 541-547, (2002); Special Issue: Mechanics of Elastic Biomolecules, Henk Granzier, Miklos Kellermayer, Wolfgang Linke, Eds.
4. C.M. Venkatachalam and D.W. Urry, "Calculation of Dipole Moment Changes Due to Peptide Librations in the Dynamic β-Spiral of the Polypentapeptide of Elastin," *Int. J. Quant. Chem.: Quant. Biol. Symp.* **12**, 15-24 (1986).
5. L. Onsager, Electric moments of molecules in liquids. *J. Am. Chem. Soc.* **58**: 1486-1493 (1936).
6. D. T. McPherson, J. Xu, and D. W. Urry, "Product Purification by Reversible Phase Transition Following *E. coli* Expression of Genes Encoding up to 251 Repeats of the Elastomeric Pentapeptide GVGVP," *Protein Expression and Purification* **7**, 51–57 (1996).
7. D.W. Urry, K. Okamoto, R.D. Harris, C.F. Hendrix and M.M. Long, "Synthetic, Cross-Linked Polypentapeptide of Tropoelastin: An Anisotropic, Fibrillar Elastomer," *Biochemistry* **15**, 4083-4089, 1976.
8. D. W. Urry, "Physical Chemistry of Biological Free Energy Transduction as Demonstrated by Elastic Protein-based Polymers," invited FEATURE ARTICLE, *J. Phys. Chem.*B, **101**, 11007-11028 (1997).
9. B. E. Read, G. D. Dean and J. C. Duncan, "Determination of dynamic moduli and loss factors." In: *Physical Methods of Chemistry,* Vol. **VII**, John Wiley & Sons (1991).
10. F. Prochazka, PhD Thesis :"Etude del'evolution des relaxations dans les gels en cours de formation, application aux polyurethanes" (1998) Université du Maine, Le Mans – France.
11. T. Nicolai, F. Prochazka, and D. Durand, "Comparison of Polymer Dynamics between Entanglements and Covalent Cross-links" *Physical Review Letters* **82**, 863-866 (1999).
12. M. Stading, M. Langton and A.-M. Hermansson, "Small and large deformation studies of protein gels."= *J. Rheol.* **39**, 1445-1450, (1995).

APPENDIX LIST:

A. D. W. Urry, T. Hugel, M. Seitz, H. Gaub, L. Sheiba, J. Dea, J. Xu and T. Parker, "Elastin: A Representative Ideal Protein Elastomer," Phil. Trans. R. Soc. Lond. B. 357, 169-184, 2002

B. D.W. Urry, T. Hugel, M. Seitz, H. Gaub, L. Sheiba, J. Dea, J. Xu, L. Hayes, T. Parker, "Ideal Protein Elasticity: The Elastin Model," Cambridge University In Press, P. Shewry and A. Bailey, Eds., in press, 2002.

C. D. W. Urry and T. M. Parker, Mechanics of Elastin: Molecular Mechanism of Biological Elasticity and its Relationship to Contraction, Special Issue: Mechanics of Elastic biomolecules, Journal of Muscle Research and Cell Motility, 23, 543-559, 2002.

THE ROYAL SOCIETY

Published online 5 March 2002

Elastin: a representative ideal protein elastomer

D. W. Urry[1,2,3*], T. Hugel[2], M. Seitz[2], H. E. Gaub[2], L. Sheiba[4], J. Dea[4], J. Xu[4] and T. Parker[3]

[1]*University of Minnesota, Twin Cities Campus, BioTechnology Institute, 1479 Gortner Avenue, St Paul, MN 55108-6106, USA*

[2]*Ludwig-Maximilians-Universität, Lehrstuhl für Angewandte Physik, Amalienstraße 54, D-80799 München, Germany*

[3]*Bioelastics Research Limited, 2800 Milan Court, Suite 386, Birmingham, AL 35211-6918, USA*

[4]*Spawar Systems Center, Code D711, San Diego, CA 92152-5001, USA*

During the last half century, identification of an ideal (predominantly entropic) protein elastomer was generally thought to require that the ideal protein elastomer be a random chain network. Here, we report two new sets of data and review previous data. The first set of new data utilizes atomic force microscopy to report single-chain force–extension curves for $(GVGVP)_{251}$ and $(GVGIP)_{260}$, and provides evidence for single-chain ideal elasticity. The second class of new data provides a direct contrast between low-frequency sound absorption (0.1–10 kHz) exhibited by random-chain network elastomers and by elastin protein-based polymers.

Earlier composition, dielectric relaxation (1–1000 MHz), thermoelasticity, molecular mechanics and dynamics calculations and thermodynamic and statistical mechanical analyses are presented, that combine with the new data to contrast with random-chain network rubbers and to detail the presence of regular non-random structural elements of the elastin-based systems that lose entropic elastomeric force upon thermal denaturation.

The data and analyses affirm an earlier contrary argument that components of elastin, the elastic protein of the mammalian elastic fibre, and purified elastin fibre itself contain dynamic, non-random, regularly repeating structures that exhibit dominantly entropic elasticity by means of a damping of internal chain dynamics on extension.

Keywords: atomic force microscopy; acoustic absorption; dielectric relaxation; thermoelasticity; entropic elasticity; β-spiral

1. INTRODUCTION

(a) *Definition of ideal or perfect elasticity*

Ideal elasticity is the property whereby the energy expended in deformation of the elastomer recovers completely on the removal of the deforming force. As the energy expended in deformation is given by the area under the force, f, versus the increase in length, ΔL, curve, a perfectly reversible force–extension curve means complete recovery on relaxation of the energy expended on deformation. Therefore, ideal elastomers exhibit perfectly reversible force–extension curves.

Perhaps our earliest perspective of the mechanism underlying ideal elasticity comes from a fundamental observation concerning rubber elasticity. In the mid-19th century, Joule and Thomson noted a quantitative correlation between the increase in temperature of the elastomer due to stretching and the increase in force due to increasing the temperature (Flory 1968). Thermodynamics provides for the analysis underlying this correlation, and the Boltzmann relationship provides the bridge between experimental thermodynamic quantities and a statistical mechanical description of molecular structures.

*Author for correspondence (durry98@aol.com).

Continuing qualitatively with the Joule and Thomson correlation, heat produces motion, and the energy represented by heat distributes into the various available degrees of freedom in the chain molecules comprising the elastomer. Accordingly, the release of heat on stretching correlates with a loss of motion. By means of statistical mechanics, the loss of motion is seen as a decrease in entropy on extension. In addition, should a solvent be essential for elasticity, this requires explicit consideration.

However, there is more to elastomeric force than entropy changes arising from changes in mobility. There is also internal energy, and a proper understanding of elasticity requires the delineation of the internal energy and entropy components of the elastomeric force. As the internal energy component of the elastic force increases, irreversible processes, such as chain breakage, become more probable. Therefore, greater durability results as elastomers become more dominantly entropic and durability becomes a feature of an ideal, or more perfect, elastomer.

(b) *Delineation of internal energy and entropy components of elastomeric force*

The delineation of internal energy and entropy components of elastomeric force can begin with the definition of

the Helmholtz free energy, A, also referred to as the maximal work function,

$$A = E - TS, \tag{1.1}$$

where E is the internal energy, T is the absolute temperature (°K), and S is the entropy for the system. The differential of the maximum work function, d A, can be written to include the work done on an elastomer by application of a force, f, over the change in length, dL, i.e.

$$\mathrm{d}A = -P\mathrm{d}V - S\mathrm{d}T + f\mathrm{d}L, \tag{1.2}$$

where P is the pressure, and V is the volume. Writing the partial differential of A in equation (1.2) with respect to length at constant V, T and composition, n, gives

$$(\partial A/\partial L)_{V,T,n} = (\partial E/\partial L)_{V,T,n} - T(\partial S/\partial L)_{V,T,n}, \tag{1.3}$$

but by equation (1.2), $(\partial A/\partial L)_{V,T,n} = f$, such that

$$f = (\partial E/\partial L)_{V,T,n} - T(\partial S/\partial L)_{V,T,n}. \tag{1.4}$$

Accordingly, the force is seen to comprise two components, an internal energy component, f_E, and an entropy component, f_S, i.e.

$$f = f_E + f_S. \tag{1.5}$$

Now it becomes useful to find an expression that will allow experimental estimation of the relative magnitude of the internal energy and entropy components of the force. Following Flory *et al.* (1960), when the functions exist and are continuous, the order of a partial differential does not matter, and it can be shown that $(\partial S/\partial L)_{V,T} = (\partial f/\partial T)_{V,L}$, such that

$$f = (\partial E/\partial L)_{V,T,n} + T(\partial f/\partial T)_{V,L,n}. \tag{1.6}$$

Interestingly, this can be rewritten as

$$f_E/f = -T(\partial \ln[f/T]/\partial T)_{V,L,n}, \tag{1.7}$$

which allows for an experimental estimate of the f_E/f ratio from the slope of a plot of $\ln(f/T)$ versus temperature under conditions of constant V, L and composition, n.

By means of an approximate correction term, the f_E/f ratio is estimated under the more usual experimental conditions of constant P, L and at equilibrium (denoted by subscript eq), e.g. with surrounding solvent, i.e.

$$f_E/f = -T(\partial \ln[f/T]/\partial T)_{P,L,\mathrm{eq}} - \beta_{\mathrm{eq}} T/[\alpha^3(V_i/V) - 1], \tag{1.8}$$

where $\beta_{\mathrm{eq}} = (\partial \ln V/\partial T)_{P,L,\mathrm{eq}}$ is the thermal expansion coefficient; α is the fractional increase in length, L/L_i, with the subscript i indicating initial length; and V_i and V are the volumes of the elastomer before and after elongation, respectively (Hoeve & Flory 1962; Dorrington & McCrum 1977). The correction term was derived under the assumption of random-chain networks with a Gaussian distribution of end-to-end chain lengths.

As we will see, a random-chain network comprised of a Gaussian distribution of end-to-end chain lengths between cross-links is neither an accurate structural description of the elastin protein nor of its simpler models. In addition, there are important solvation changes that can occur under experimental conditions. Nonetheless, the insight into the magnitude of the entropic component of the elastomeric force provided by equation (1.8), with experimental estimates of the quantities in the correction term or when neglecting the correction term altogether, is informative, but only when the temperature range for determination of the slope is chosen carefully.

(c) *Basic statistical mechanical expression for entropy*

(i) *The Boltzmann relationship*

The starting point for the statistical mechanical expressions of entropy is the Boltzmann relationship,

$$S = R\ln W, \tag{1.9}$$

R (1.987 cal deg mole^{-1}) is the gas constant, $R = Nk$, N being Avogadro's number (6.02×10^{23} mole^{-1}) and k the Boltzmann constant (1.38×10^{-16} erg deg K^{-1}), and W is the number of *a priori* equally probable states accessible to the system (Eyring *et al.* 1964). W is the volume in phase space occupied by a particular state of a molecular system. In practice, W becomes the product of partition functions for each of the degrees of freedom of the molecular system. There are $3n - k$ d.f., where n is the number of atoms in the molecule and k is the holonomic constraints on the system. In general, there are three translational and three rotational degrees of freedom, and the remainder are vibrational degrees of freedom. For large-sized molecules, the vibrational degrees of freedom also include motions of rotation (or torsional oscillations) about bonds. Due to the constraints of the elasticity measurement $k = 6$; the ends of the molecules are effectively fixed in space such that there are neither whole molecule translational nor rotational degrees of freedom.

(ii) *Fundamental expression for the change in entropy on extension*

Fortunately, when calculating entropic contributions to the elasticity, interest centres on the change in entropy on extension from a relaxed, S^r, to an extended, S^e, state of the elastomer,

$$\Delta S = (S^e - S^r) = R\ln(W^e/W^r). \tag{1.10}$$

As the change in entropy is a ratio, it becomes relatively straightforward to calculate the contribution to the change in entropy of a particular expression of motion accessible to the representation of the molecular structure under examination in its relaxed and extended states. For our purposes the β-spiral structure of the (Gly–Val–Gly–Val–Pro)$_n$, or poly(GVGVP), model of elastin is used and two different means of representing that structure are considered. The first is the enumeration of states in configuration ($\phi - \psi$ torsion angle) space within a given energy cut-off, or weighted by the Boltzmann distribution, for relaxed and extended states, and the second is to use the molecular dynamics approach to determine the change in root mean square (rms) torsional oscillations that occur on extension by the same amount as used in the enumeration of states approach. The magnitudes of the calculated entropy changes on extension obtained by each approach can then be compared.

(d) *Historical notes of proposed mechanisms for the entropic elasticity of elastin*

(i) *Classical (random chain network) theory of rubber elasticity*

During the last half of the last century, identification of ideal (dominantly entropic) protein elasticity required (by

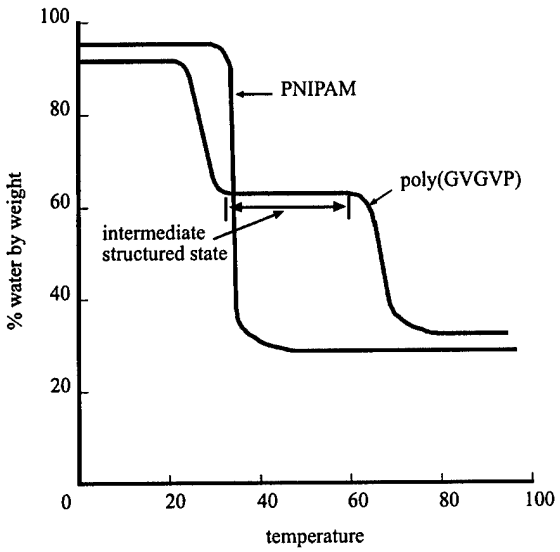

Figure 1. Plot of the percentage water by weight as a function of temperature for poly(GVGVP) showing a stable intermediate structured state of 63% water by weight between 30 °C and 60 °C, a state that slowly denatures above 60 °C to form a state containing 32% water by weight. Graph plotted from the data of Urry *et al.* (1985*b*). Amphiphilic LCST polymers such as PNIPAM, exhibit only a single, sharper transition, to what is generally considered a disordered state, with *ca.* 30% water by weight. Curve plotted from the data of Grinberg *et al.* (1999).

the recognized authorities of the period) the conclusion that the ideal elastomer comprised of random chain networks with a Gaussian distribution of end-to-end chain lengths between cross-links. For elastin, the protein of interest here, this point of view began with a paper by Hoeve & Flory (1958). This perspective became entrenched in the minds of the interested scientific community by the award, in the autumn of 1974, of the Nobel Prize to Paul Flory following reaffirmation of the random-chain network conclusion (Hoeve & Flory 1974). The message of the paper is unmistakable. In the synopsis (p. 677) it is stated, 'A network of random chains within the elastic fibres, like that in a typical rubber, is clearly indicated.' Furthermore, in fig. 1 on p. 678 of their paper there is a structural representation of the chains between cross-links with a statement in the figure legend that, 'Configurations of chains between cross-linkages are much more tortuous and irregular than shown.'

(ii) *Decrease in solvent entropy (due to hydrophobic hydration) on extension*

The purpose of the Hoeve & Flory (1974) paper, which presented no additional data, was to refute an earlier publication by Weis-Fogh & Andersen (1970), which had suggested an alternative mechanism for the elasticity of elastin. The alternative mechanism proposed that hydration of hydrophobic side chains of the protein, which become exposed to solvent on extension, would be responsible for the stretch-induced decrease in entropy, i.e. by this proposal changes in solvent entropy became the source of the entropic component of the elastomeric force.

(iii) *Damping of internal chain dynamics on extension*

Just over a decade later yet another perspective was put forward. Considering structural studies and molecular mechanics calculations of the most prominent repeating sequence of bovine elastin, $(Gly–Val–Gly–Val–Pro)_{11}$, entropic elasticity was described as arising from a decrease in available configuration space on extension (Urry *et al.* 1982). Equivalently, treating the experimentally and computationally derived regularly repeating structure from the perspective of molecular dynamics, the damping of internal chain dynamics on extension described the same decrease in entropy for the same degree of extension (Chang & Urry 1989).

In § 4, these three mechanisms are considered in more detail, following consideration of new experimental data on models of elastin together with previously published relevant data.

(e) *Inverse temperature transition behaviour of elastin and its models*

(i) *Increase in order with increase in temperature*

Filament formation on raising the temperature

When the temperature of an aqueous solution of the precursor protein, tropoelastin, is increased, the protein aggregates to form a denser viscoelastic phase, called a coacervate. When a droplet of the aqueous suspension of incipient aggregates is placed on a carbon-coated grid, negatively stained with uranyl acetate and oxalic acid at the appropriate pH, and examined under TEM, fibrils comprised of parallel-aligned filaments are observed with a 5 nm periodicity (Cox *et al.* 1974). Similar results are obtained for α-elastin, a 70 000 Da fragment of the elastic fibre (Cox *et al.* 1973), for high polymers, poly(GVGVP) and poly(GVGVAP) of repeating sequences of elastin (Volpin *et al.* 1976). Fibrils of similar dimensions have been reported for fibrous elastin itself using similar techniques (Gotte *et al.* 1974).

Crystallization of cyclic analogues on raising the temperature

Most strikingly, cyclic analogues of repeating sequences of elastin crystallize on raising the temperature (Urry *et al.* 1978; Cook *et al.* 1980) and redissolve on lowering the temperature. Without ambiguity, these polymers increase order with increase in temperature through a transition temperature range.

We refer to this phase transition as an *inverse temperature transition*. While the peptide component of this water–peptide system increases in order on increasing the temperature, ordered water molecules surrounding hydrophobic residues become less-ordered bulk water as hydrophobic groups separate from solution. Accordingly, the overall change effected by the phase transition is towards less order, in keeping with the second law of thermodynamics.

Indeed, the phase diagram for HMW polymers of repeating sequences of elastin is inverted with the soluble phase below, at lower temperature, and the insoluble phase above the binodal or coexistence line and with an inverted coexistence line, i.e. with the curvature of the coexistence line convex to the volume fraction axis

(Sciortino *et al.* 1993; Manno *et al.* 2001). Conversely, the usual circumstance for polymers is for the coexistence line to be concave to the volume fraction axis and for the polymer to be insoluble below and soluble above the coexistence line (Flory 1953).

(f) *Composition of poly(GVGVP) in water as a function of temperature*

The temperature dependence of composition of the poly(GVGVP)–water system provides a clear visualization of a water-containing, structured state at intermediate temperatures (Urry *et al.* 1985*b*). Figure 1 schematically illustrates the plot of percentage water by weight as a function of temperature. As the polymer is miscible with water in all proportions below 20 °C, the plot arbitrarily starts at *ca.* 90% water by weight near 0 °C. A rise in temperature from 20 to 30 °C causes a reversible phase separation to form a state that is 63% water by weight. The percentage water by weight of this intermediate water-retaining state remains essentially unchanged until the temperature rises above 60 °C. Then a very slow irreversible transition occurs on raising the temperature from 60 to 80 °C to form a state that is 32% water by weight. Dialysis of the polymer against 100 000 molecular weight cut-off membranes, after prolonged heating at 80 °C, resulted in a less than 1% loss of polymer. Prolonged heating did not result in chain breakage, and therefore, the slow irreversible transition was not due to chain breakage.

In figure 1, the results on poly(GVGVP) are compared to those of Grinberg *et al.* (1999) on the petroleum-based polymer, PNIPAM. This polymer shows an inverted phase diagram like that of the elastin-based polymers. Though with a composition more hydrophobic than that of poly(GVGVP), the transition for this LCST polymer occurs at a higher temperature (34 °C), is much sharper, and results directly in the formation of the state with *ca.* 30% water by weight. A reasonable description of this PNIPAM state of 30% water by weight is as a random-chain network. It is clear that poly(GVGVP) forms an intermediate, water-containing state that holds a fixed amount of water until irreversible denaturation occurs at high temperature. This state of 63% water by weight is an elementary property that simply is not consistent with the recently computed 'compact amorphous globule' for $(GVGVP)_{18}$ attributed to Li *et al.* (2000).

(i) *A structured state at intermediate temperatures for elastin-based systems*

Both the elastin fibre and α-elastin at intermediate temperatures form similar water-containing states of *ca.* 50% water by weight (Partridge *et al.* 1955; Partridge & Davis 1955; Partridge 1966, 1967). It will also be demonstrated below (see figure 8) that both cross-linked poly(GVGVP) and fibrous elastin exhibit a slow, irreversible, loss of elastic force due to prolonged exposure to temperatures above 60 °C when at fixed extension. These are further demonstrations of the slow irreversible denaturation observed in figure 1, that occurs above 60 °C, for poly(GVGVP). Furthermore, detailed dielectric relaxation studies on the elastin-based systems—fibrous elastin, α-elastin, and poly(GVGVP)—demonstrate molecular motions, relaxations, limited to localized frequency ranges (see figures 6 and 7), and these could only be the result of non-random, regularly structured, albeit dynamic, conformational states. These experimental results are not consistent with random-chain networks nor are they consistent with compact amorphous globules.

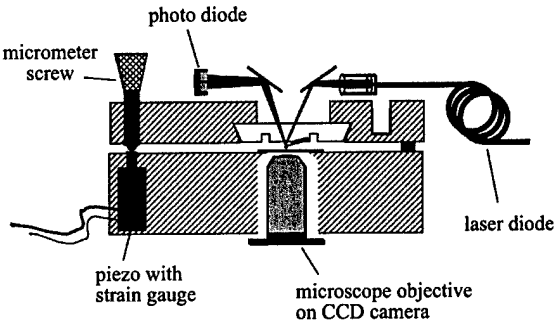

Figure 2. Schematic diagram of an AFM apparatus adapted for varying the *z*-direction to obtain force–extension curves for single chains.

2. MATERIAL AND METHODS

(a) *Preparation of elastin models*

In the native state of elastin, the precursor, tropoelastin, a protein of about 70 000 Da, occurs as the overwhelmingly dominant component (90+% by weight) of the mammalian elastic fibre. In the vascular wall, for example, the elastic fibre resides within the extracellular matrix as a structure several microns in diameter. No functional role is given to non-elastin components within the elastic fibre. During cross-linking by the enzyme, lysyl oxidase, it can be trapped within the fibre, and a fine coating of microfibres, some hundreds of nanometers in thickness, can surround the fibre. Due to the cross-linking, elastin is an insoluble material of the extracellular matrix. Efforts to isolate it, in order to define its properties, require Draconian methods. For example, refluxing in sodium hydroxide, denaturants and proteolytic enzymes are used to remove all of the surrounding matrix components. This insoluble product is called purified fibrous elastin.

Alternatively, for the study of elastin, model approaches have been used such as isolating and characterizing (i) the precursor protein, tropoelastin, which may be obtained in ill-defined intermediate states of cross-linking, (ii) the pure precursor protein prepared by microbial biosynthesis, (iii) chemical degradation products of purified fibrous elastin which have been prepared, and (iv) chemically and microbially synthesized repeating sequences found within the protein sequence as well as interesting analogues which have been prepared.

(i) *Synthesis of model systems*

Chemical synthesis

Initially, several thousand protein-based polymers were synthesized in order to determine the conformation and function of these model proteins. This involved the synthesis of oligomers and high polymers of repeating tetra-, penta-, hexa-, nona- and even decapeptides reported in the sequence of elastin. By means of chemical synthesis, many compositions could be prepared and characterized, and axioms were developed for the function of these elastic model proteins in energy conversion and for their use as biomaterials for medical and non-medical applications.

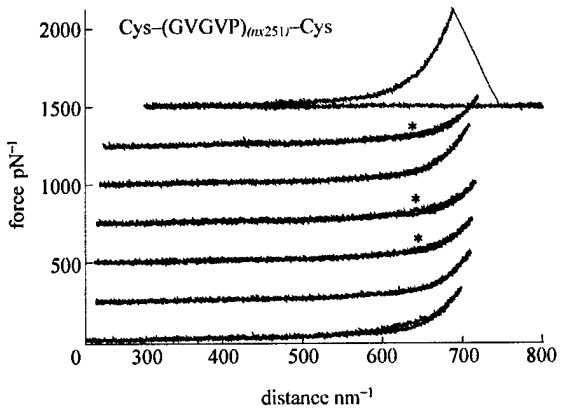

Figure 3. Single-chain force–extension curves for Cys–(GVGVP)$_{mx251}$–Cys at a temperature below the onset temperature for hydrophobic folding and assembly for this composition. The initial trace appears at the lowest position on the graph and subsequent traces of the same chain, without intervening detachment, are displaced 250 pN vertically. The second and fifth curves exhibit perfect reversibility. The curves marked by an asterisk, and the initial curve, were the result of a period of at least 30 s in the relaxed state, where one possibility is that some hydrophobic back folding occurs.

Microbial biosynthesis

Once a specific composition was identified as being of sufficient interest, it was prepared by means of recombinant DNA technology. With this approach, hundreds of grams could be prepared in a single fermentation. On the other hand, chemical synthesis at the laboratory bench would require much of a year to prepare such a quantity.

(ii) *Preparation of natural materials*

Isolation of the precursor protein, tropoelastin

Initially, the precursor protein was prepared from animals rendered copper deficient and treated with inhibitors of enzymatic cross-linking. The product was meagre in amount and a mixture of partially cross-linked and oxidized lysyl side chains. It was nonetheless helpful in determining many of the fundamental physical properties relating to structure and elastogenesis.

Preparation of tropoelastin by microbial biosynthesis

In an important development, Weiss and co-workers utilized recombinant DNA technology to prepare the precursor protein, tropoelastin, in *Escherischia coli*, which enabled the preparation of pure protein in large quantities (Vrhovski *et al.* 1997; Wu *et al.* 1999). Important aspects deduced by the model systems and by preparations of model structures derived from the elastin and from sequence knowledge have been confirmed and extended by recombinantly prepared tropoelastin.

Preparation of α-elastin

A model system useful in stepping systematically from polymers of model-repeating sequences to the natural fibrous elastin has been a chemical fragmentation product from fibrous elastin called α-elastin, prepared and chemically characterized by Partridge and co-workers (Partridge *et al.* 1955; Partridge & Davis 1955; Partridge 1966, 1967). It is a multiply cross-linked, 70 000 molecular weight fragment comprising 16 chains.

(iii) *Purification using phase transitional behaviour*

In all cases these protein-based polymers are soluble in water at a lower temperature and phase separate on raising the temperature above that for the onset of a hydrophobic folding and assembly transition. This phase separation process has been termed coacervation. It is a fundamental property of these polymers having, as they do, the proper balance of apolar (hydrophobic) and more polar residues.

(b) *Cross-linking of elastin models*

(i) *General cross-linking procedure*

Cobalt 60 γ-irradiation was used to cross-link the phase-separated, coacervate state with its interpenetrating polymer chains.

(ii) *Efforts to cross-link α-elastin*

Even though α-elastin undergoes phase separation, it does not form an elastic matrix on γ-irradiation. As a cluster of some 16 cross-linked chains, with a total molecular weight of 70 kDa, α-elastin does not cross-link by γ-irradiation because the cluster of chains of one α-elastin molecule does not interpenetrate sufficiently with surrounding molecules. This is in contrast with similar molecular weights of poly(GVGVP) which readily cross-link by γ-irradiation when in the intermediate structured state between 30 and 60 °C.

(iii) *Efforts to cross-link heat denatured poly(GVGVP)*

While the phase-separated state of poly(GVGVP) with 63% water by weight (figure 1) cross-links very effectively, the heat-denatured state obtained on prolonged heating above 60 °C does not. Even though the density of chains is twice as great for the denatured state formed above 60 °C (a state of 32% water by weight as seen in figure 1), the chains no longer interpenetrate and associate sufficiently to result in an elastic matrix on γ-irradiation. This is simply another demonstration that the intermediate state, between 30 and 60 °C, is a structured state of interpenetrating filaments rather than being globular structures with limited contact between units, as occurs with α-elastin or as would be the case for amorphous compact globules.

3. SPECIALIZED METHODOLOGIES AND ANALYSIS OF RESULTS

(a) *Single molecule force-extension curves by AFM*

(i) *Preparation of the sample for AFM*

Cleaned glass microscope slides were coated with *ca.* 30 nm of gold in a home-built evaporation chamber. Si_3N_4 AFM tips were used (Microlevers, Park Scientific Instruments, Sunnyvale, CA), also coated with gold. For the preparation of mixed self-assembled monolayers, quantities of 1 mg of the polypentapeptides and 0.5 mg of methoxy-PEG-thiol (M_W 5000) were dissolved in 1 ml Milli-Q water unless otherwise noted. A 20 μl portion of this solution was incubated on the gold-coated slide for about 30 min at 3 °C and then rinsed with Milli-Q water.

(ii) *The AFM instrument*

A detailed description of the AFM force spectroscopic technique and details of the instrumental set-up have been supplied elsewhere (Oesterhelt *et al.* 1999; Clausen-Schaumann *et al.* 2000). Briefly, the tip of a cantilever is brought into contact with molecules on the surface and then retracted, its deflection, and therefore the force, are

detected with a laser by optical lever detection (Cleveland *et al.* 1993), while the *z*-distance is controlled by a strain gauge (figure 2). The nominal spring constants of cantilevers used in the experiments were 10 mN m^{-1}. Before the first approach of the AFM tip to the surface, the spring constants of each lever were individually calibrated by measuring the amplitude of their thermal oscillations (Butt & Jaschke 1995). The sensitivity of the optical lever detection was measured by indenting the AFM tip into a hard surface. All experiments were conducted in Milli-Q water at room temperature (21 °C), unless otherwise specified.

(iii) *Obtaining the single-chain force–extension curve*

For the characterization of elastic properties, the gold-coated AFM tip was brought into contact with the polypentapeptides on the microscope slide by manual control. The AFM tip and the polymer layer were kept in contact under a contact force of several nanoNewtons for *ca.* 30 s to allow for an attachment of polypeptide chains to the tip. Usually, one or several chains adsorbed non-covalently at some position on the tip, possibly a chemical reaction between the gold-coated cantilever and the cysteine on the end of a polypentapeptide sometimes allowed for very high rupture forces. Upon retraction of the cantilever, individual polypentapeptides were stretched between the surface and the AFM tip.

Note that the first force–distance profile recorded after tip–substrate contact can be rather complex, consisting of contributions from stretching several polypentapeptides, desorption from the substrate and/or cantilever, bond rupture of short strands, as well as interchain aggregation and entanglements. Therefore, in each measurement the cantilever was first retracted from the substrate to a distance at which unspecific adhesion was no longer observed. Then, in successive retraction-approaching cycles the distance range was increased while trying to avoid contact between the tip and additional polypentapeptide strands at the substrate surface, until only one polymer strand remained between the tip and the substrate. The force–distance profile of this strand was then measured repeatedly until rupture.

(iv) *Analysis of the results*

The experimental traces were fitted by an extended WLC model (Bustamante *et al.* 1994; Odijk 1995) including linear elastic contributions arising from the stretching of bond angles and covalent bonds:

$$F\times\frac{L_P}{k_BT}=\frac{R_z}{L}-\frac{F}{K_0}+\frac{1}{4(1-R_z/L+F/K_0)^2}-\frac{1}{4}. \qquad (2.1)$$

In this expression, R_z is the measured end-to-end-distance at any given force, F, and L is the contour length of the stretched chain (polypentapeptide) under zero force ($F=0$). It should be appreciated that the WLC model entirely neglects any discrete molecular structure along the chain, and describes the polymer as a continuous rod of constant bending module. The characteristic length scale expressing the polypeptide's bending rigidity is the persistence length, L_P, which is defined as the decay length of the directional correlation along the polymer chain. Finally, the chain's extensibility upon stretching is described by the segment elasticity, K_0, which is introduced into equation (2.1) as a linear term. Hereby, K_0 can be understood as the inverse of the normalized compliance of a Hookean spring; the spring constant of the polymer chain is given by K_0/L.

This resulted in values for the persistence length L_P of $(GVGVP)_{nx251}$: $L_P=0.4$ nm in the low force regime and $L_P=0.6$ nm when fitted to higher forces, which are comparable to values measured previously for other polypeptide backbones, e.g. of proteins (Rief *et al.* 1997). The reversible traces provide evidence for single-chain ideal elasticity, i.e. any molecular processes related to the elongation and relaxation of the polypeptide chains must be fast on the time-scale of the AFM experiment. Apart from the entropic contributions at low forces below *ca.* 20 pN, which are related to the unfolding of the polymer coil ('classical conformational entropy'), it has been previously shown that ideal elastic behaviour in the high force regime may also result from enthalpic bond-angle deformations and configurational changes along the polymer backbone (Rief *et al.* 1997). As will be shown below, additional entropic, and therefore reversible elasticity, in the high forces regime can also arise from backbone torsional movements (rocking), wherein the contribution to the entropic component of the force increases with a decrease in the frequency of the oscillator. Temperature-dependent AFM measurements should allow for a proof of this finding at the single molecule level.

The small deviations from perfect reversibility in traces 3, 4 and 6 of figure 3 (marked by the asterisk) occurred when the chain was held for at least 30 s in the relaxed state. These deviations could have several origins. There could be a configurational transition, e.g. an opening of β-turns and/or hydrophobic interaction, a back folding, between different parts of the chain. The latter is favoured by the observed rate dependence of this non-equilibrium contribution.

The persistence length L_P of $(GVGIP)_{nx260}$ is difficult to determine, when intra- and/or interchain aggregation gives rise to a strong hysteresis even when located far away from the surface within two successive cycles (figure 4). It is determined to exhibit an $L_P=0.7$ nm, which might be slightly higher than with $(GVGVP)_{nx251}$, but this value lies well within the error range of *ca.* 20%. This strong aggregation of $(GVGIP)_{nx260}$ occurs at the same concentration, at which the aggregation for $(GVGVP)_{nx251}$ is much smaller. This reflects the increase in hydrophobicity due to an additional CH_2 group in GVGIP, which is the only difference with GVGVP. Unfortunately, it is not yet clear whether the aggregation is mainly due to back folding within a single chain or due to association between different chains. This is under investigation.

(v) *Comparison of AFM single-chain and macroscopic elastic moduli*

For the characterization of elastomers at the macroscopic scale, force versus elongation is plotted, but instead of being represented as an actual increase in length, as in figures 3 and 4, elongation is stated in terms of the ratio of the initial length to the extended length. Furthermore, the deformation is generally uniform so that the initial cross-sectional area, A, is used. Therefore, the Young's elastic modulus, Y, is the force, f, times the initial length, L_i, divided by the elongation, L, and the cross-section of the elastomer, that

is, $Y = fL_i/AL$. The units are N m^{-2} or dynes cm^{-2} where N m^{-2} = 10 dynes cm^{-2} and N stands for Newtons. The elastic modulus of 20 Mrad γ-irradiation cross-linked $(GVGVP)_{251}$, i.e. X^{20} $(GVGVP)_{251}$, is 1.6×10^5 N m^{-2}.

In order to utilize the data in figure 3 to obtain an estimate of the single-chain elastic modulus, estimates of the L_i/L ratio and of A are required. Initially, the total number of repeats that are being extended must be deduced. In figure 3, the WLC fit of the force–distance trace shown gives an end-to-end-distance of $L = 733$ nm, which we assume is the fully extended chain. This is too long for a chain of 251 pentamers, but appears to be too short for a chain of 753 pentamers. By elimination of chain lengths with 251 and 753 pentamers, this indicates that the structure would be $(GVGVP)_{2x251}$ giving 502 pentamers, i.e. 2510 residues with a value of 0.29 nm per residue. This is shorter than the usual value of 0.35 nm per residue, which could be due to the presence of a proline residue in every pentamer. This results from the *cis* Val–Pro peptide bond, which introduces a kink in the extended backbone for every pentamer. It should be noted, however, that if all of the β-turns were retained at rupture, the 3×251 chain length could apply with *ca.* 1 nm per pentamer, or just greater than 700 nm. This scenario was not considered because the forces for detachment can be greater than 500 pN, and retention of the β-turn was considered less likely at such forces.

It should also be noted that, in general, one cannot exclude *a priori* the possibility of polypeptides being picked up at any position along the chain due to strong unspecific adsorption. In the case of $(GVGVP)_{nx251}$, however, the simplicity and uniformity of the repeating sequence without the presence of functional groups except, at the very ends of the chain, are expected to limit *strong* unspecific adsorption. Because the polymer length estimated from the WLC fit is sufficiently close to what would be expected for 2×251 proline-containing pentamers it warrants, in our view, proceeding with this assumption.

Perhaps the most significant factor in obtaining a relevant value for the single-chain elastic modulus for comparison to the macroscopic case is the choice of the structure before elongation in order to provide an estimate of an initial length and cross-sectional area. In this regard two quite different initial lengths may be considered, one for the random coil state below the hydrophobic folding transition and another for the β-spiral structure that could only occur above the onset temperature for the hydrophobic folding transition.

Calculation of elastic modulus from AFM data assuming a random coil state for $(GVGVP)_{nx251}$

At temperatures lower than the onset temperature for the hydrophobic folding and assembly transition, the more correct representation of the unstretched single chain would be the random coil state. Based on photon correlation spectroscopic studies, the hydrodynamic diameters of disordered polymeric coils resulting from 502 pentamers (some 200 000 Da molecular weight) below the transition would be *ca.* 18 nm (San Biagio *et al.* 1988). By way of example, at a distance of 378 nm in figure 3, the L_i/L ratio would be 1 : 20. In this distance range (i.e. between 300 and 500 nm), the slope of the force curve is evaluated as 0.08 ± 0.03 pNnm^{-1}. With a slope of 0.08 ± 0.03 pN nm^{-1} from figure 3, at a distance of 378 nm from the substrate, the increase in force would be 28.8 ± 10.8 pN; i.e. upon elongation from 18 to 378 nm, the relative increase in length, $\Delta L/L_i$, would be a factor of 20, so that a force of 1.44 ± 0.54 pN is estimated for a 100% extension of the 18 nm diameter polymeric coil.

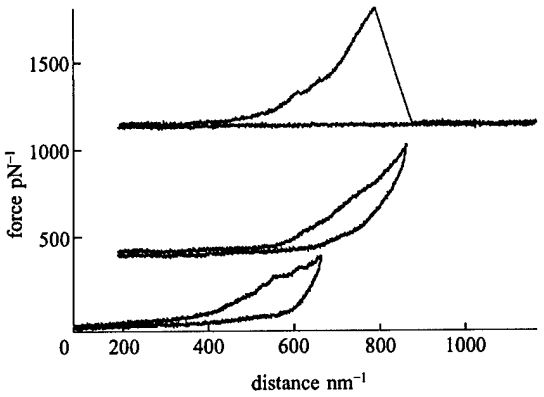

Figure 4. Single-chain force–extension curves for Cys–$(GVGIP)_{nx260}$–Cys at a temperature above the onset temperature for hydrophobic folding and assembly for this composition. In each case the energy expended in deformation is greater than that recovered on relaxation. In addition, there appears to be a complex relaxation curve.

Next, this quantity should be divided by an appropriate cross-sectional area, that is, π multiplied by the hydrodynamic radius, squared, of the random coil prior to extension of the single chain, i.e. $\pi r^2 = \pi(9\text{ nm})^2 = 254$ nm^2. Given the foregoing assumptions, the calculated single-chain elastic modulus would be $5.7(\pm 2.1) \times 10^3$ N m^{-2}. As might have been expected, without taking polymer density and cross-link density into consideration (Urry *et al.* 1984), this value is a factor of 30 from the experimental value at 37 °C for X^{20}-$(GVGVP)_{251}$ of 1.6×10^5 N m^{-2}, but more closely approximates what is expected below the transition temperature or when X^{20}-$(GVGVP)_{251}$ has been thermally denatured, as seen in figure 8*b*. Concerning polymer density, it may be noted that the density of the low-temperature random-coil state is about one-quarter that of the phase-separated state.

Calculation of elastic modulus from AFM data assuming the β-spiral structure for $(GVGVP)_{nx251}$

For comparison, it is useful to consider the structure representative of the state above the temperature of the inverse temperature for hydrophobic folding and assembly. This addresses the importance of choosing structure when converting the force–extension curve into a macroscopic elastic modulus. If the single β-spiral structure were assumed before extension with three pentamers per turn and a translation along the axis of 1 nm per turn, the length of a 502 pentamer would be *ca.* 170 nm. This means that an elongation of 100% would occur at 340 nm, and the change in force for extension of the β-spiral from 170 to 340 nm would be $170\text{ nm} \times 0.08 \pm 0.03$ pN nm^{-1} $= 13.6 \pm 5.1$ pN per β-spiral.

The next issue is an estimate of the number of β-spirals per m^2 for comparison with the cross-linked matrix from

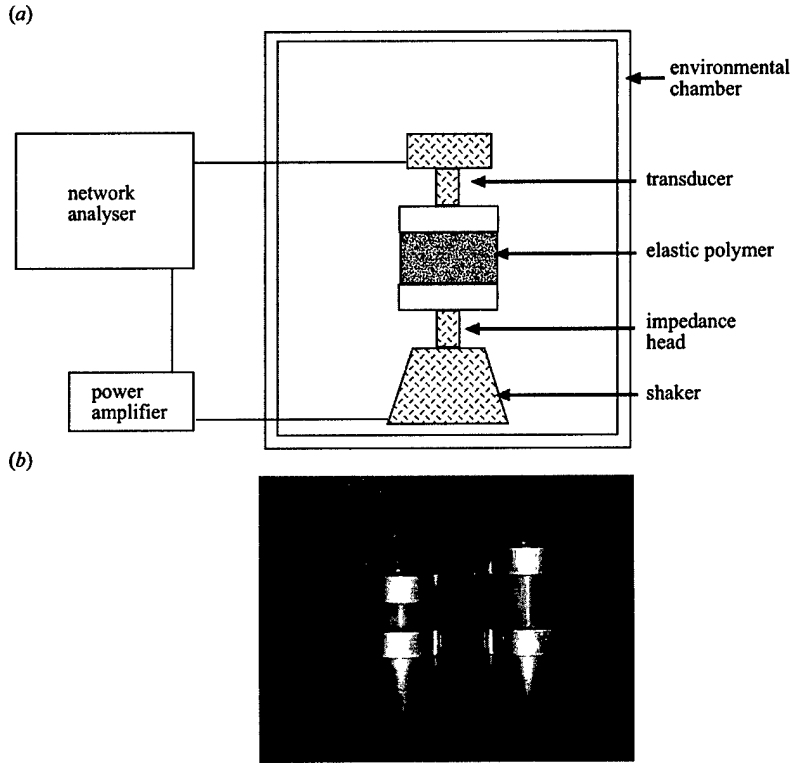

Figure 5. (*a*) Block diagram of the instrumentation used to determine the absorption per unit volume of elastic samples in the acoustic range. (*b*) Example of the use of two samples that differ in length by a factor of 2 as required to permit the analysis of Sheiba (1996) to be utilized.

which the experimental macroscopic value of 1.6×10^5 N m^{-2} is obtained. For a macroscopic state of 37% water by weight (see figure 1), an assumed density of 1.33 g cm^{-2} for the polymer, and a cross-sectional area for the β-spiral of 3.2 nm^2, the number would be *ca.* 8.7×10^{16} β-spirals m^{-2}. The single-chain elastic modulus, calculated on the basis of the β-spiral structure, would be $(13.6 \pm 5.1 \times 10^{-12}$ N per β-spiral$) \times (-8.7 \times 10^{16}$β-spirals m$^{-2}) = 1.2 \times 10^6$ N m^{-2}.

Thus, by assuming a different structure, instead of being low by a factor of 30 as was the case above for a random-coil structure, which occurs below the transition temperature, the assumption of the β-spiral structure resulted in a value for the single-chain elastic modulus that is seven and a half times larger than the macroscopic value. We note that the orientation of a random coil is not relevant in the argument relating single-chain data to macroscopic data. For the γ-irradiation cross-linked macroscopic matrix, however, the β-spirals would be randomly orientated with respect to the direction of extension. This would decrease the contribution of each β-spiral not aligned in the direction of extension. It will now be particularly interesting to obtain the elastic modulus for the twisted filament structure depicted in figure 9*f*. Work is in progress for the preparation of multistranded twisted filaments.

(b) *The acoustic absorption experiment*

(i) *Sample preparation and experimental set-up*

The polymer is prepared in the phase-separated state, i.e. the intermediate structured state with the interpenetrating chains depicted in figure 1, and 20 Mrad γ-irradiation cross-linked in the form of the desired cylindrical shape and with path lengths that differ by a factor of 2, as shown in figure 5*b*.

The Naval Research Laboratory at the Spatial Warfare Systems Center—San Diego (SSC—SD) has the capability to measure accurately the elastic properties of materials by using a broadband technique developed by Sheiba (1996). Older techniques are more cumbersome and less reliable. The frequency of measurement ranges from subsonic to *ca.* 15 kHz. The measurements are performed in air inside an environmental chamber. Figure 5 also shows the block diagram of the instrumental set-up for these measurements.

The network analyser sends sweeping signals to the shaker. The transducer (sometimes called an accelerometer) and impedance head record the velocities at the base and at the top of the sample. After recording data during this frequency sweep, a new set of data is then obtained at a new temperature setting. Commonly temperatures can range from −30° to 70 °C. The velocity record constitutes the transfer matrix. By mathematically

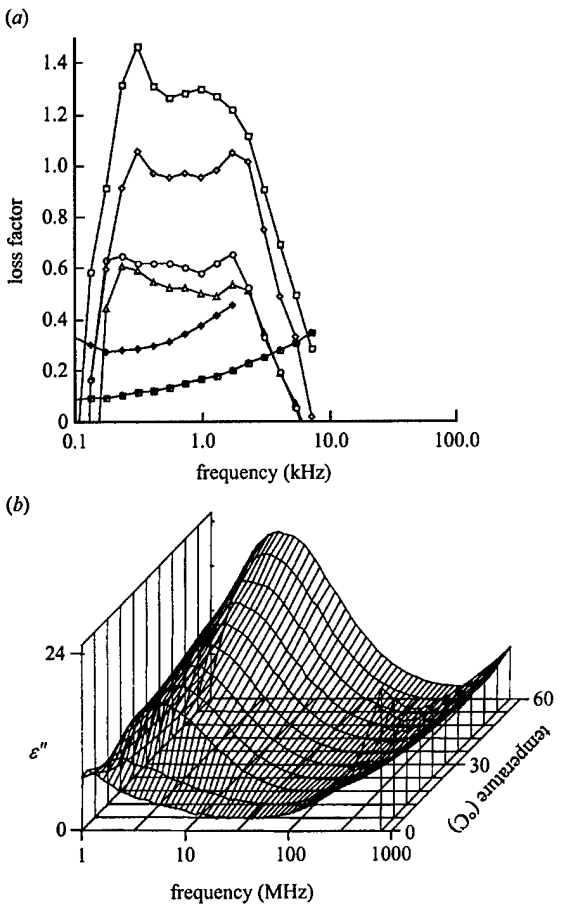

Figure 6. (*a*) Plots of the loss factor (absorption per unit volume) for a series of elastomers. Crossed squares represent the curve for natural rubber, and filled diamonds that of the structureless curve for polyurethane, which is recognized as a rubber with a high loss factor in the acoustic absorption range. The upper four curves are for 20 Mrad cross-linked $(GVGVP)_{260}$ (open squares, 20 °C; open diamonds, 10 °C; open circles, 0 °C; open triangles, −5 DC). As the temperature rises above the temperature for the inverse temperature transition of hydrophobic folding and assembly for this composition, the intensity for a localized relaxation grows dramatically. To the best of our knowledge, these model elastic protein-based polymers exhibit the greatest sound absorption for the 100–1000 Hz frequency range. This demonstrates the formation of a regular structure for $(GVGIP)_n$ in contrast to the lack of a regular structure for the classical rubbers. (*b*) The imaginary (absorptive) section of the dielectric permittivity of poly(GVGIP). The same phenomenon of increased absorption on passing through the temperature range of the inverse temperature transition is observed in the 1–100 MHz range as exhibited by the same composition in the acoustic absorption range. Reproduced, with permission, from Buchet *et al.* (1988). Such low frequency motions provide a source of entropic elasticity and low energy for the structural state of the elastic protein-based polymers.

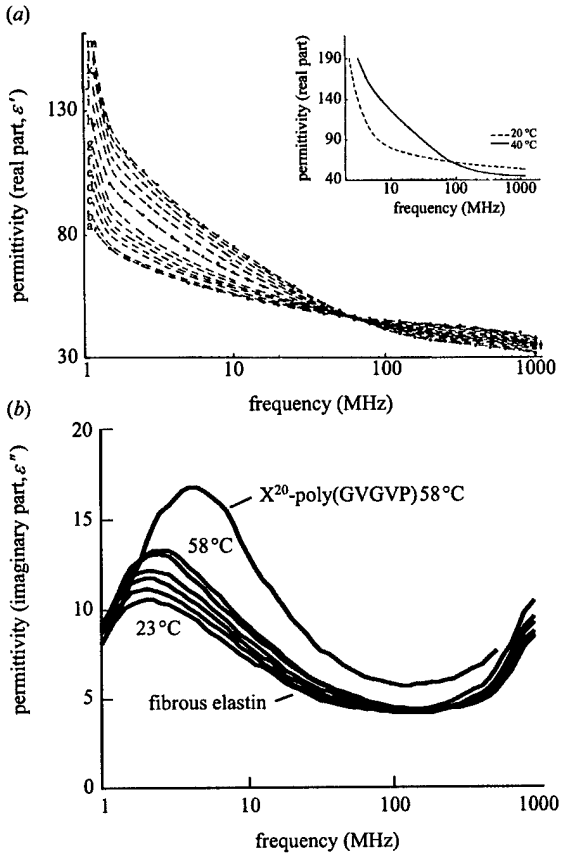

Figure 7. (*a*) The real part of the dielectric permittivity of α-elastin showing increasing relaxation intensity at *ca.* 5 MHz with increasing temperature from below to above the temperature range for the inverse temperature transition. The data for α-elastin are nearly identical to that found for the polypentapeptide of elastin, poly(GVGVP) shown in the inset for a single temperature below (20°) and one above (40°) that of the inverse temperature transition. The temperatures for the α-elastin data on the left edge of the curves listed as (a)–(m) are 68, 12.5, 20, 25, 30, 35, 40, 45, 50, 55, 60, 65 and 70 °C, respectively. This demonstrates that the same relaxation occurs in a fragment of the natural elastic fibre as has been so thoroughly characterized in the model elastic protein, poly(GVGVP). Reproduced, with permission, from Urry *et al.* (1985*a*).
(*b*) The imaginary (absorptive) part of the dielectric permittivity of natural fibrous elastin showing an increasing relaxation at *ca.* 5 MHz with increasing temperature from below (23 °C) to above (58 °C) the temperature range for the inverse temperature transition. The same relaxation is seen at 58 °C with a somewhat higher intensity and a slightly higher frequency is found for the 20 Mrad cross-linked poly(GVGVP). It seems quite evident that dynamic structured states occur in the natural elastic fibre as demonstrated for the model elastic protein-based polymer. Adapted, with permission, from Luan *et al.* (1988).

inverting the transfer matrix, it is possible to extract the complex modulus and Poisson ratio. These data provide a complete description of a material's elastic properties. Further analysis yields the shear modulus, μ, the Poisson ratio, ν, and the loss factor, η, each as a function of frequency and temperature. The loss factor, η, is the main parameter of interest. It represents the energy absorption per unit volume at a given frequency. The loss factor versus frequency and temperature were determined for several different elastic protein-based polymer compositions. The data for $(GVGIP)_{mx260}$ are given in figure 6*a*. MATHCAD 7.0 was used to perform the mathematical analysis.

(ii) *Comparison of the acoustic absorptions of (GVGIP) and natural rubber*

Natural rubber has been well characterized as a random-chain network. This means that there are no regular repeating conformational features in the polymer chain. The consequence of a random chain is a broad, slowly changing dependence on frequency of physical properties, such as absorption. Simply stated, the absence of structure means that the barrier to rotation about each bond will tend to be different. This is what is observed in figure 6*a* for natural rubber and a synthetic petroleum-based polymer, polyurethane, chosen for its relatively high loss factor in the frequency range reported.

At frequencies lower than those of the IR spectroscopic range, however, any material that exhibits a localized absorption band as a function of frequency must do so by virtue of a regular repeating structure. Interestingly, this is seen in Figure 6*a* for X^{20}-$(GVGIP)_{260}$ in the range 200 Hz to 7 kHz, and the intensity of the absorption per unit volume increases as the temperature is raised through the temperature interval of the inverse temperature transition. Acoustic absorption increases as the structure becomes more regular! Besides demonstrating the remarkable acoustic absorption property of this material, the acoustic absorption data provide an additional demonstration of the existence of a regular structure for poly(GVGIP) and for related polymers. Actually, this is simply further confirmation of earlier dielectric relaxation data, which demonstrated the development of an intense localized relaxation at *ca.* 5 MHz as the temperature was raised through the interval of the inverse temperature transition, as reviewed below.

(c) *Previous dielectric relaxation studies on elastin-related systems*

(i) *Dielectric relaxation and acoustic absorption data on the same polymer*

Figure 6*b* is a three-dimensional plot of the imaginary (absorption) part of the dielectric permittivity of poly(GVGIP) as a function of frequency and temperature. Just as for the acoustic absorption study in figure 6*a*, there is an increase in the absorption (imaginary) component of the dielectric relaxation as the temperature rises through the temperature interval of the inverse temperature transition for hydrophobic folding and assembly. Thus, the data on the elastin models can now be directly compared to α-elastin and fibrous elastin, itself. Mechanical resonances due to regularly repeating structures have now been observed both in the vicinities of 1 kHz and 5 MHz.

(ii) *Comparison of poly(GVGVP) and α-elastin*

Figure 7*a* is a graph of the real part of the dielectric permittivity as a function of temperature for α-elastin and for poly(GVGVP) in the inset. In both cases, there is development of an intense relaxation at *ca.* 5 MHz as the protein-based elastomers hydrophobically fold and assemble on increasing the temperature through the range of the inverse temperature transition. Both elastomeric molecular systems exhibit the same development of regular structure on raising the temperature through the range of the inverse temperature transition.

(iii) *Comparison of cross-linked poly(GVGVP) to fibrous elastin*

Figure 7*b* is a graph of the imaginary (absorption) part of the dielectric relaxation for purified fibrous elastin (from bovine ligamentum nuchae) as a function of temperature from 23 °C to 58 °C. Figure 7*b* also contains a plot of the same data at 58 °C for the elastomer, 20 Mrad cross-linked poly(GVGVP). While there is a small increase in mean frequency and intensity for the X^{20}-$(GVGVP)_{251}$ relaxation, it is certain that there is hydrophobic folding and assembly resulting in the formation of regular structures in the natural fibrous elastin that are similar to those of cross-linked poly(GVGVP). Incidentally, the decrease in intensity at 1 GHz for fibrous elastin reflects the loss of hydrophobic hydration as the hydrophobic folding proceeds. This is due to a dielectric relaxation at *ca.* 5 GHz, which results from hydrophobic hydration (Urry *et al.* 1997).

4. DISCUSSION

(a) *Relevance of proposed mechanisms for the entropic (ideal) elasticity of elastin*

The kernel of the classical theory of rubber elasticity originated with K. H. Meyer in 1932 which, according to Flory (1968, p. G42), can be stated as '... the orientation of the molecules of a piece of rubber when it is stretched would entail a decrease in entropy, and thus could account for the retractive force.' This was restated by Flory (1968) in terms of two subsidiary hypotheses: (i) the restoring force originates within the chain molecules by distortion of the distribution of their configurations and not from interactions between chains; and (ii) the restoring force is due 'exclusively to the *entropy* of the chain configuration'. However, is the alignment of chains really the most appropriate description of entropic elasticity? Even in the case of a bulk elastomer, might the most fundamental statement be the decrease in internal chain dynamics within each chain, which would be fundamental to the alignment of elongation? Clearly, the above-demonstrated entropic elasticity exhibited by a single chain does not arise from the alignment of many chains on extension. Rather, the observation of entropic elasticity on extension of a single chain fixed at its ends limits the source of entropy change to the damping of internal chain dynamics within the single chain. In this case entropic elasticity cannot arise from the change in relative orientation of many chain molecules.

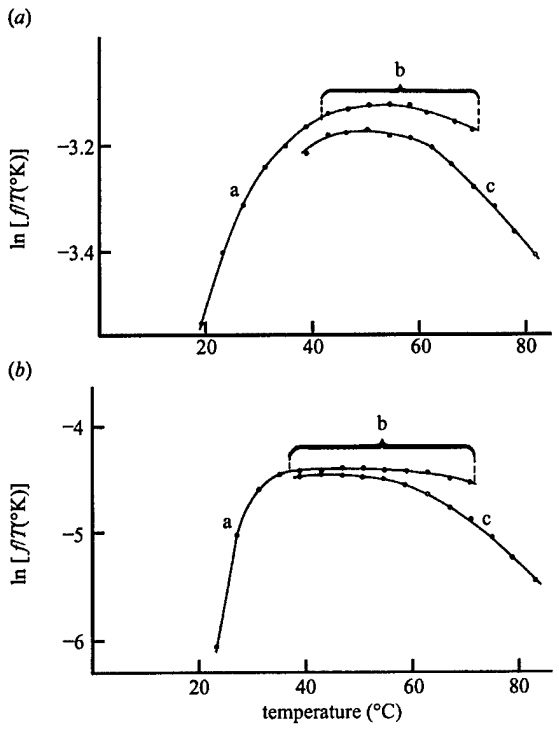

Figure 8. Thermoelasticity curves for (*a*) fibrous elastin and (*b*) 20 Mrad cross-linked poly(GVGVP). See text for discussion. Whether or not a near-zero slope, i.e. an $f_E/f << 1$, is obtained depends on the rate at which the temperature is raised. This is due to a slow denaturation at temperatures above 60 °C. (Times per data point for line segments (a), (b) and (c) are 4 h, 30 min and 4 h, respectively.) Reproduced, with permission, from Urry (1988*a*,*b*).

(i) *Relevance of the Flory random-chain network theory of entropic elasticity*

Flory's publications describe a Gaussian distribution of end-to-end chain lengths that results from a random-chain network, and they assert that the decrease in entropy due to extension, or compression, arises from distortion of the network from this most probable random distribution (Flory 1953, 1968). Hoeve & Flory (1958, 1974) concluded that the entropic elasticity of elastin arises from such a random-chain network.

There are four principal reasons why this perspective is questionable. These are (i) a limited potential for cross-links in the fixed sequence of elastin, (ii) the above spectroscopic evidence for regular, non-random, dynamic structural features in components of elastin, (iii) the above report of the occurrence of ideal reversible elasticity exhibited by a single chain of repeat sequences of elastin with calculated single-chain elastic moduli similar to the macroscopic elastic modulus, and (iv) an irreversible loss of force due to thermal denaturation when the elastomer is extended and heated at temperatures above 60 °C.

Relevance of the probability of cross-link formation to structure

In rubber, each repeating unit is a potential cross-link, and, on vulcanization, any pair of repeating units can be converted to a cross-link wherever two chain segments are sufficiently proximal. In elastin, only lysine residues form the cross-links, and yet there are only some 40 lysine residues for an elastin protein of *ca.* 800 residues, i.e. one lysine in every 20 residues. Furthermore, the lysine residues are arranged in an orderly manner along the sequence. Most commonly, four lysine residues combine to form a single cross-link, called a desmosine, and essentially all of the lysine residues in fibrous elastin have been formed into cross-links. Such cross-linking cannot be achieved within a random-chain network. The achievement of such rare cross-linkages requires elements of order (Urry 1976).

Low-frequency motions provide much entropy to chain structures

Motions that are due to rotations about backbone bonds in a chain molecule that exhibit intense relaxations limited to localized frequency intervals, that is, intense mechanical resonances, can only result from polymers containing regular, non-random, dynamic structures. For model elastin systems including purified fibrous elastin, such mechanical relaxations are observed at *ca.* 1 kHz and 5 MHz (see figures 6 and 7). As will be demonstrated below, these relaxations provide a very ample source of entropy to structured elastin systems. These contributions to entropy increase greatly as the frequency of the relaxation is lower, and they are contributions to the free energy of protein structure that have yet to be adequately treated in the current computations of low-energy protein structures. Most importantly for entropic elasticity, low-frequency motions provide an abundant and ready source of entropy decrease on extension.

Entropic elastomeric force arising from a single chain

At a fixed extension in the AFM single-chain force–extension curves of figure 3, there is a single end-to-end chain length. The entropic elastic force measured at a given extension cannot have arisen from displacement of a network of chains from a Gaussian distribution of end-to-end chain lengths nor can it arise from aligning chains in parallel. The decrease in entropy that provides the entropic restoring force in the single-chain experiment must arise from a damping of internal chain dynamics of the single chain. No other degrees of freedom can cause a decrease in chain entropy to occur. Furthermore, in order that the ends of the chain remain fixed in space, the rotation about a given bond must be compensated for by a corresponding correlated rotation about one or more additional bonds. The peptide librational mechanism of entropic elasticity, which arises so readily out of the β-spiral structure of poly(GVGVP) represents one interesting means of achieving this.

Studies of the temperature dependence of force at a fixed extension have yet to be carried out on single chains in order to determine the contribution of internal energy or the enthalpy component of the force, i.e. to determine the f_E/f ratio as given in equations (1.7) and (1.8). In respect of the internal energy or enthalpic contribution to

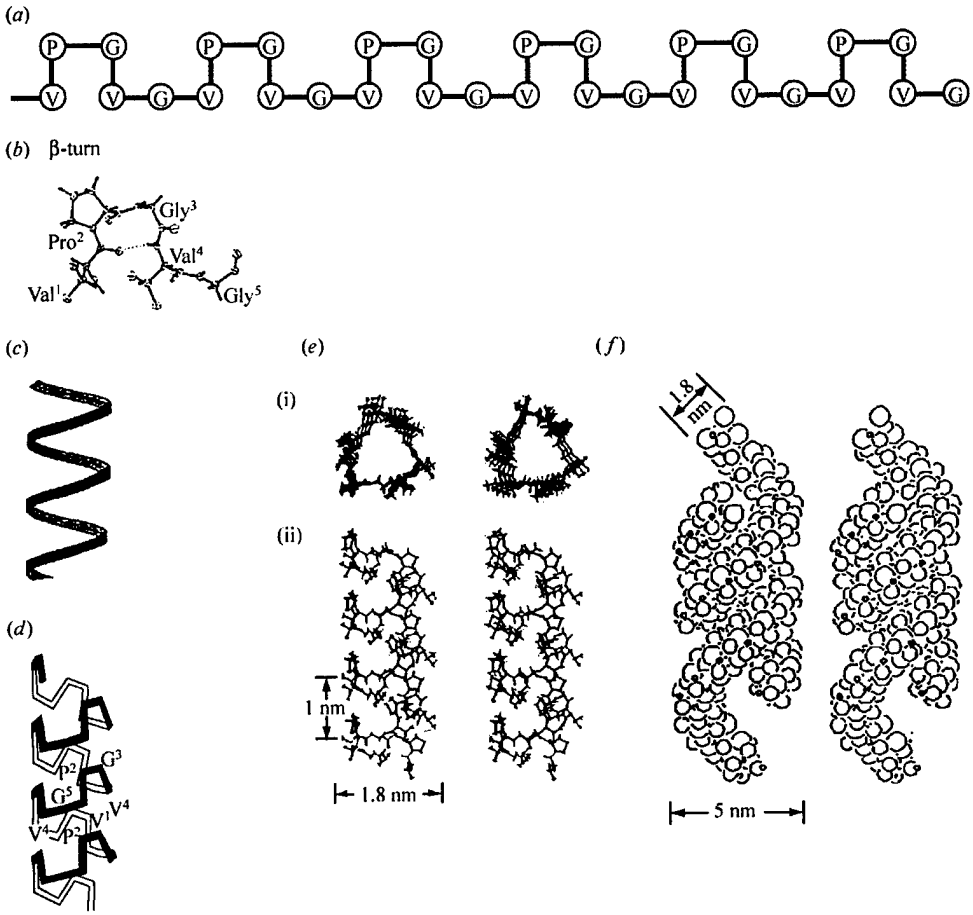

Figure 9. Description of the proposed molecular structure of poly(GVGVP). (*a*) Schematic representation of the repeating Pro-Gly-containing sequence inserting the β-turn structure, which is given in crystallographic detail in part (*b*). (*c*) Schematic helical representation of the structure that forms on raising the temperature above the inverse temperature transition. (*d*) Schematic representation of the helical structure, called a β-spiral, but with the β-turns included and functioning as spacers between turns of the helix. (*e*) Stereo pairs of the β-spiral structure in atomic detail in (i) end view and (ii) side view. (*f*) Associated β-spirals having formed multi-stranded twisted filaments, which is the more accurate description of the hydrophobically folded and assembled state.

the elastic force, these would arise reversibly without bond breakage, by strain-imposed distortions in bond lengths and bond angles. Interestingly, Young (private communication) probed the strain deformation of silk fibres (*Bombyx mori* and spider dragline) using Raman spectroscopy and observed, among other spectral changes, a shift in the 1095 cm^{-1} (wavenumber) band on extension to 3.5%. This band shift, assigned to the C–C stretch mode, represents an internal energy component to the force. Provided that the stretch is reversible with no bond breakage, it can contribute to the force of an ideal elastomer.

At high extensions, where the force resulting in bond deformations can become significant, however, distortions in bond lengths and bond angles can decrease the durability of an elastic fibre by chain rupture. In this regard, the remarkable feature of the mammalian elastic fibre is its striking durability where, in the aortic arch and descending thoracic aorta, the half-life is some 70 years during which period the elastic fibres will have undergone more than one billion stretch–relaxation cycles. This is possible due to the dominantly entropic nature of its elastic force as seen in figure 8*b* and due to uniform chain extension arising out of a regular, cross-linked structure where no single chain bears an excessive amount of the load.

Loss of elastomeric force of elastin-based systems due to thermal denaturation

In figure 1, it was noted that poly(GVGVP) exhibits a slow irreversible denaturation when held at temperatures above 60 °C. This same phenomenon is apparent in the thermoelasticity studies on fibrous elastin, as originally noted by Dorrington & McCrum (1977). In the thermoelasticity experiments illustrated in figure 8 (Urry 1988*a*,*b*), the elastomer is equilibrated at 40 °C and at that temperature is extended to 60%. At this fixed length, the temperature is lowered to *ca.* 20 °C and slowly raised

to 80 °C. The force dramatically increases as the temperature is raised through the range of the inverse temperature transition from 20 to 40 °C. Then, the force/T (°K) tends to remain nearly constant from 40 to 60 °C, especially for X^{20}–poly(GVGVP). The value of lnf/T begins to decrease above 60 °C in a time-dependent manner. When using a rate of increase of 4 °C 30 min^{-1}, 8 °C h^{-1}, there is a decrease in lnf/T, and, when the temperature is returned to 40 °C, an irreversible loss of force occurs. The decrease in force above 60 °C is more dramatic on raising the temperature more slowly, e.g. when raising the temperature at a rate of 1 °C h^{-1}. When the temperature maintained above 60 °C for a longer interval irreversible thermal denaturation is seen most dramatically. Furthermore, a plot of ln(elastic modulus) versus time at 80 °C is linear, providing evidence of a first order process (Urry 1988*a*,*b*). Interestingly, while heating above 60 °C decreases force, it also shortens the length at which zero force is obtained, as is to be expected when a filamentous, β-spiral-like structure becomes randomized by thermal denaturation.

As discussed in relation to equations (1.7) and (1.8), a slope of zero for plots like those in figure 8 would mean an ideal (entirely entropic) elastomer. As clearly seen for X^{20}–poly(GVGVP) in the 40–60 °C temperature range, when data are collected at the rate of 30 min per data point, a near-zero slope is obtained. Commonly, an f_E/f ratio of 0.1 is obtained for X^{20}–poly(GVGVP) (Luan *et al.* 1989). Because of the steep positive slope between 20 and 40 °C, due to the hydrophobic folding and assembly of the inverse temperature transition, and because of the slow irreversible thermal denaturation above 60 °C, the slope, obtained in the thermoelasticity experiment from which the entropic contribution is estimated, depends on the rate at which the data are collected and the temperature interval over which they are collected.

A steep rise in force in the 20–40 °C temperature interval for fibrous elastin in figure 8*a*, although less steep than that seen in figure 8*b* for X^{20}–poly(GVGVP), demonstrates the effect of the inverse temperature transition within elastin itself. More dramatic for fibrous elastin is the loss of elastomeric force on raising the temperature above 60 °C. This finding, of a slow loss of force at elevated temperature, would not have been so apparent if the time had been limited to a single day to perform the experiment (without the advantage of computerized equipment), as was the case when Hoeve & Flory (1958) carried out their original study on fibrous elastin. For the thermoelasticity study of fibrous elastin shown in figure 8, however, the rate of loss of force at elevated temperature is even greater than for X^{20}–poly(GVGVP).

Additionally, the plot of ln(elastic modulus) versus time for fibrous elastin maintained at 80 °C, as determined by a stress–strain curve every 24 h, is a straight line with a half-life of *ca.* 10 days (Urry 1988*b*). Another important feature of the data for determining half-life is that the length at which zero force is obtained decreases with time at 80 °C. Remarkably, this means that the loss of force in figure 8, and the progressive loss of elastic modulus exhibited by a series of stress–strain curves after heating for 24 h at 80 °C, are not due to structural rearrangement to an extended state under load. Additionally, it cannot be due to slipping of the sample in the grip. Instead, extended time-periods at a high temperature result in a denaturation, which entails a randomization from linear filamentous structures towards denatured random-coil structures. This has an analogy to the loss of percentage water by weight for time above 60 °C in figure 1.

Figure 8 clearly displays, in the thermoelasticity data of elastin-based systems, in the half-life studies for the elastic modulus at 80 °C, and in the structural change above 60 °C in figure 1, a slow thermal denaturation of protein-based elastomers. As random-chain networks do not exhibit thermal denaturation, these elastin-based systems cannot properly be described as random-chain networks. Thus, the evidence is clear and abundant; elastin-based systems contain regular repeating conformations and those ordered structures denature.

(ii) *Relevance of solvent entropy changes as a source of entropic elastic force*

Effect of removing solvent entropy change during the inverse temperature transition

The change in solvent entropy is fundamental to the occurrence of an inverse temperature transition. This transition has been extensively utilized to perform the family of energy conversions that sustain living organisms (Urry 1993, 1997), and therefore the inverse temperature transition is extensively characterized. One approach to testing whether the change in solvent entropy contributes to the elastomeric force is to utilize an approach due to Flory, that is, to reduce the heat of the inverse temperature transition to near zero by an appropriate solvent mixture. Hoeve & Flory (1958) used a mixture of 30% ethylene glycol by weight in water in their thermoelasticity study that deduced a dominant entropic elastic force for fibrous elastin. When Luan *et al.* (1989) compared the thermoelasticity-derived f_E/f ratio of X^{20}–poly(GVGVP) in water and in 30% ethylene glycol, the values were the same, 0.1. Based on the approximations of equations (1.7) and (1.8), X^{20}–poly(GVGVP) is a dominantly entropic elastomer in both solvent systems. The effect of adding the ethylene glycol is to reduce the heat of the transition to near zero. Now, since the entropy of the desolvation process is the heat of the transition divided by the temperature of the transition, $\Delta H_t/T_t$, the solvent entropy change would be approaching zero, and yet the solvent mixture, instead of reducing the elastomeric force, remarkably, did the opposite and resulted in a substantial increase in force. The conclusion is that there is no experimental basis for believing that solvent entropy change contributed to elastomeric force.

The polymer chains bear the force; solvation changes alter the fraction of chain segments that sustain the force?

The force of deformation must be borne by the chains; it cannot be borne by the solvent. At a fixed length, raising the temperature of a band of elastomer from below to above the temperature of the inverse temperature transition increases the force. Alternatively, increasing the chemical potential to lower the transition temperature from above to below the operating temperature at a fixed length causes an increase in the elastomeric force (Urry 1997; Urry *et al.* 1988*a*,*b*). These results are due to an increase in hydrophobic folding and assembly of the chains. As this is the case at a fixed length, the smaller fraction of a chain's length, which is not folded, must

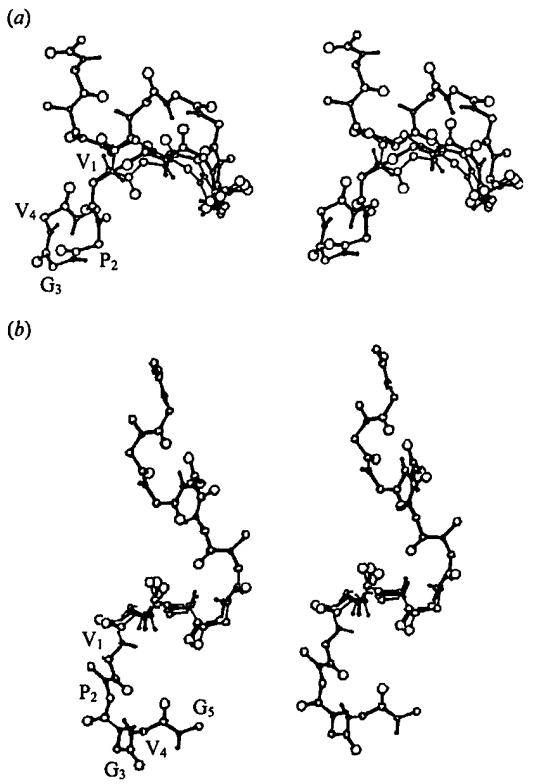

Figure 10. Stereo view of the torsional oscillations possible within a 2 kcal mol^{-1} residue cut-off energy for the central pentamer of one turn (three pentamers) of the β-spiral structure of poly(GVGVP) (*a*) in the relaxed state and (*b*) in the 130% extended state. See text for discussion. Reproduced, with permission, partly from Urry *et al.* (1982) and the remainder from Urry *et al.* (1985*c*).

necessarily be further extended. Accordingly, in order to maintain a fixed length, the unfolded segments must be further extended. This provides for the increase in entropic elastic force by means of a decrease in configurational entropy.

(iii) *Entropic elasticity due to damping of internal chain dynamic on extension*

Molecular structure of poly(GVGVP)

In order to understand the concept of the damping of internal chain dynamics on extension, the structure given in figure 9 is helpful. The Pro–Gly-containing elastomeric sequential polypeptides exhibit a repeating β-turn structure as schematically shown in figure 9*a*, and the β-turn is given in crystallographic detail in figure 9*b*. A rise in the temperature of the inverse temperature transition results in the optimization of intra- and intermolecular hydrophobic association. Intramolecularly, this results in a helical structure called a β-spiral, which is shown schematically as a helix in figure 9*c*, in more detail, with β-turns schematically shown as spacers between turns of the helix, in figure 9*d*, and in atomic stereo detail in figure 9*e*. Intermolecularly, the β-spirals associate to form multistranded twisted filaments, as depicted in figure 9*f*. Because there is water within the β-spiral, and as a result of the β-turns functioning as spacers, the peptide segments connecting β-turns are free to undergo large amplitude torsional oscillations.

Effect of extension on the amplitude of the torsional oscillations and on chain entropy

The magnitude of the torsional (dihedral angle) excursions for a single pentamer sandwiched within a turn of β-spiral (three pentamers) for a 1.5 kcal mol^{-1} residue cut-off energy is shown in figure 10*a* when using the molecular mechanics calculations of the Scheraga approach (Momany *et al.* 1975). Dihedral angle oscillations of 160° are possible. The effect of a 130% extension of the β-spiral pitch, shown in figure 10*b*, is a dramatic decrease in the amplitude of the torsional oscillations allowed within a 1.5 kcal mol^{-1} residue cut-off energy. Using an enumeration of states approach with each change of 5° in any single torsion angle counted as a new state, the decrease in numbers of states for a 0.6 kcal mol^{-1} residue cut-off energy (i.e. within an energy cut-off of RT) is from a W^r of 342 to a W^e of 24. Using equation (1.10), this gives a value for ΔS of -5.28 cal mol^{-1} deg^{-1} per pentamer. If the Boltzmann summation over all energies is used, the value is -5.06 cal mol^{-1} deg^{-1} per pentamer (Urry *et al.* 1985*c*).

Alternatively, when using the molecular dynamics approach of Karplus, the expression becomes

$$\Delta S = R \ln[\Pi_i \Delta\phi_i^e \Delta\psi_i^e / \Pi_i \Delta\phi_i^r \Delta\psi_i^r], \tag{3.1}$$

where the product Π_i is over the rms torsion angle fluctuations $\Delta\phi_i^e$ and $\Delta\psi_i^e$ for the extended state divided by the product of the rms torsion angle fluctuations $\Delta\phi_i^r$ and $\Delta\psi_i^r$ for the relaxed state as obtained from the molecular dynamics trajectories for the relaxed and 130% extended states. The calculated decrease in entropy was -5.5 cal mol^{-1} deg^{-1} per pentamer for the 130% extension (Chang & Urry 1989). Whether the calculation of entropy is by means of an enumeration of states in ψ–ϕ configuration space or the amplitude of the torsional oscillations in a molecular dynamic simulation, the calculated entropy change for a 130% extension is the same.

Calculation of contribution of force due to decrease in freedom of motion on extension

From equations (1.4) and (1.5) we have

$$f_S = T(\partial S/\partial L)_{V,T}. \tag{3.2}$$

At physiological temperatures, 310 K, and for an extension from 0.35 to 0.8 nm for a pentamer within the β-spiral structure of figure 9*e* with a calculated decrease in entropy of 5 cal mol^{-1} deg^{-1} per pentamer, the calculated value for the entropic contribution to the elastomeric force is 24 pN for a single chain of β-spiral.

To put this in terms of an elastic modulus in units of N m^{-2}, it is necessary to estimate the number of β-spirals per m^2. From figure 1, the functional state is 37% peptide by weight. Taking the density of the peptide to be 1.33 g cm^{-3}, and a cross-sectional area of 3.2 nm^2 per β-spiral, there would be *ca.* 8.7×10^{16} parallel-aligned β-spirals per m^2. The calculated result is 2×10^6 N m^{-2}, which is an order of magnitude larger than the

experimental value of 1.6×10^5 N m^{-2} for 20 Mrad cross-linked $(GVGVP)_{251}$.

Several obvious factors can be considered, that would contribute to a higher calculated value for the elastic modulus of the isolated β-spiral than for the experimental elastic modulus of the cross-linked matrix. First, in the cross-linked matrix the β-spirals would be randomly orientated with respect to the direction of extension. Second, the β-spirals occur as part of a multistranded twisted filament as shown in figure 9*f*, which would tend to dampen the torsional oscillations within the triple-stranded filament and thereby result in a lower entropy change on extension. Thus, it would seem that the damping of internal chain dynamics on extension provides abundant entropic restoring force in elastin-based systems. Furthermore, given the entropic elasticity of single chains demonstrated by the AFM single-chain force–extension curves, damping of internal chain dynamics on extension should be considered, in general, as a potential fundamental source for the development of entropic elastic force in chain molecules.

(iv) *Dependence of entropy and structural free energy on oscillator frequency*

One final point for consideration in this report is the significance of the occurrence of intense low-frequency mechanical motions in elastin-based systems. The insight comes from the expression for the dependence of entropy on oscillator frequency. From the expression for the partition function of the harmonic oscillator (Dauber *et al.* 1981), it is seen that the slope for the frequency dependence of entropy is –4.6 EU $\log\nu_i^{-1}$. The extrapolation of the harmonic oscillator treatment to low-frequency torsional oscillations is surely not quantitative, but it is nonetheless informative. While the contribution of a lower classical vibration frequency is of the order of 5 cal mol^{-1} deg^{-1} (EU), giving a Gibbs free energy of 1.5 kcal mol^{-1} at 298 K, the contribution of the 5 MHz relaxation, seen in figures 6 and 7, would approach 30 cal mol^{-1} deg^{-1} or 9 kcal mol^{-1}, and that for the mechanical resonance at *ca.* 1 kHz, reported in figure 6*a*, would approach 47 cal mol^{-1} deg^{-1} or 14 kcal mol^{-1}. From this it should be apparent that these relaxations are fundamental in providing for the entropic elasticity of elastin-based systems. On a more general note, computations of protein structure that do not include these important low-frequency contributions to the free energy would seem to be limited in their treatment of the structure–function issue.

The work was supported, in part, by the Office of Naval Research under contract numbers N00014-00-C-0178 and N00014-00-C-0404.

REFERENCES

Buchet, R., Luan, C.-H., Prasad, K. U., Harris, R. D. & Urry, D. W. 1988 Dielectric relaxation studies on analogs of the polypentapeptide of elastin. *J. Phys. Chem.* **92**, 511–517.

Bustamante, C., Marko, J. F., Siggia, E. D. & Smith, S. 1994 Entropic elasticity of lambda-phage DNA. *Science* **265**, 1599–1600.

Butt, H. J. & Jaschke, M. 1995 Calculation of thermal noise in atomic force microscopy. *Nanotechnology* **6**, 1–7.

Chang, D. K. & Urry, D. W. 1989 Polypentapeptide of elastin: damping of internal chain dynamics on extension. *J. Comput. Chem.* **10**, 850–855.

Clausen-Schaumann, H., Rief, M., Tolksdorf, C. & Gaub, H. E. 2000 Mechanical stability of single DNA molecules. *Biophys. J.* **78**, 1997–2007.

Cleveland, J. P., Manne, S., Bocek, D. & Hansma, P. K. 1993 A nondestructive method for determining the spring constant of cantilevers for scanning force microscopy. *Rev. Sci. Instrum.* **64**, 403–405.

Cook, W. J., Einspahr, H. M., Trapane, T. L., Urry, D. W. & Bugg, C. E. 1980 Crystal structure and conformation of the cyclic trimer of a repeat pentapeptide of elastin, cyclo-(L-valyl-L-prolylglycyl-L-valylglycyl)$_3$. *J. Am. Chem. Soc.* **102**, 5502–5505.

Cox, B. A., Starcher, B. C. & Urry, D. W. 1973 Coacervation of α-elastin results in fiber formation. *Biochim. Biophys. Acta* **317**, 209–213.

Cox, B. A., Starcher, B. C. & Urry, D. W. 1974 Coacervation of tropoelastin results in fiber formation. *J. Biol. Chem.* **249**, 997–998.

Dauber, P., Goodman, M., Hagler, A. T., Osguthorpe, D., Sharon, R. & Stern, P. 1981 In *ACS Symp. Ser. No. 173. Suypercomputers in chemistry* (ed. P. Lykos & I. Shavitt), pp. 161–191. Washington, DC: American Chemical Society.

Dorrington, K. L. & McCrum, N. G. 1977 Elastin as a rubber. *Biopolymers* **16**, 1201–1222.

Eyring, H., Henderson, D., Stover, B. J. & Eyring, E. M. 1964 *Statistical mechanics and dynamics*. New York: Wiley.

Flory, P. J. 1953 *Principles of polymer chemistry*. Ithaca, NY: Cornell University Press.

Flory, P. J. 1968 Molecular interpretation of rubber elasticity. *Rubber Chem. Technol.* **41**, G41–G48.

Flory, P. J., Ciferri, A. & Hoeve, C. A. J. 1960 The thermodynamic analysis of thermoelastic measurements on high elastic materials. *J. Polymer Sci.* **XLV**, 235–236.

Gotte, L., Giro, G., Volpin, D. & Horne, R. W. 1974 The ultrastructural organization of elastin. *J. Ultrastruct. Res.* **46**, 23–33.

Grinberg, N. V., Dubovik, A. S., Grinberg, V. Y., Kuznetsov, D. V., Makhaeva, E. E., Grosberg, A. U. & Tanaka, T. 1999 Studies of the thermal volume transition of poly(N-isopropylacrylamide) hydrogels by high sensitivity differential scanning microcalorimetry. 1. Dynamic effects. *Macromolecules* **32**, 1471–1475.

Hoeve, C. A. J. & Flory, P. J. 1958 The elastic properties of elastin. *J. Am. Chem. Soc.* **80**, 6523–6526.

Hoeve, C. A. J. & Flory, P. J. 1962 Elasticity of crosslinked amorphous polymers in swelling equilibrium with diluents. *J. Polymer Sci.* **60**, 155–164.

Hoeve, C. A. J. & Flory, P. J. 1974 Elastic properties of elastin. *Biopolymers* **13**, 677–686.

Li, B., Alonso, D. O. V. & Daggett, V. 2000 The molecular basis for the inverse temperature transition of elastin. *J. Mol. Biol.* **305**, 581–592.

Luan, C.-H., Harris, R. D. & Urry, D. W. 1988 Dielectric relaxation studies on bovine ligamentum nuchae. *Biopolymers* **27**, 1787–1793.

Luan, C.-H., Jaggard, J., Harris, R. D. & Urry, D. W. 1989 On the source of entropic elastomeric force in polypeptides and proteins: backbone configurational vs side chain solvational entropy. *Int. J. Quant. Chem. Quant. Biol. Symp.* **16**, 235–244.

Manno, M., Emanuele, A., Martorana, V., San Biagio, P. L., Bulone, D., Palma-Vitorelli, M. B., McPherson, D. T., Xu, J., Parker, T. M. & Urry, D. W. 2001 Interaction of processes on different time scales in a bioelastomer capable of performing energy conversion. *Biopolymers* **59**, 51–64.

Odijk, T. 1995 Stiff chains and filaments under tension. *Macromolecules,* **28,** 7016–7018.

Oesterhelt, F., Rief, M. & Gaub, H. E. 1999 Single molecule force spectroscopy by AFM indicates helical structure of poly(ethylene-glycol) in water. *New J. Phys.* **1,** 6.

Partridge, S. M. 1966 Biosynthesis and nature of elastin structures. *Federation Proc.* **25,** 1023–1029.

Partridge, S. M. 1967 Diffusion of solutes in elastin fibers. *Biochim. Biophys. Acta* **140,** 132–141.

Partridge, S. M. & Davis, H. F. 1955 The chemistry of connective tissues. II. Composition of soluble proteins derived from elastin. *Biochem. J.* **61,** 21–30.

Partridge, S. M., Davis, H. F. & Adair, G. S. 1955 The chemistry of connective tissues. II. Soluble proteins derived from partial hydrolysis of elastin. *Biochem. J.* **61,** 11–21.

Rief, M., Oesterhelt, F., Heymann, B. & Gaub, H. E. 1997 Single molecule force spectroscopy on polysaccharides by atomic force microscopy science. *Science* **275,** 1295–1297.

San Biagio, P. L., Madonia, F., Trapane, T. L. & Urry, D. W. 1988 Overlap of elastomeric polypeptide coils in solution required for single phase initiation of elastogenesis. *Chem. Phys. Lett.* **145,** 571–574.

Sciortino, F. K., Prasad, K. U., Urry, D. W. & Palma, M. U. 1993 Self-assembly of bioelastomeric structures from solutions: mean field critical behavior and Flory–Huggins free-energy of interaction. *Biopolymers* **33,** 743–752.

Sheiba, L. 1996 Broad band method and apparatus for the precise measurement of the complex modulus of viscoelastic materials. US patent 08/645,878, pending.

Urry, D. W. 1976 On the molecular mechanisms of elastin coacervation and coacervate calcification. *Farad. Discuss. Chem. Soc.* **61,** 205–212.

Urry, D. W. 1988*a* Entropic elastic processes in protein mechanisms. I. Elastic structure due to an inverse temperature transition and elasticity due to internal chain dynamics. *J. Protein Chem.* **7,** 1–34.

Urry, D. W. 1988*b* Entropic elastic processes in protein mechanism. II. Simple (passive) and coupled (active) development of elastic forces. *J. Protein Chem.* **7,** 81–114.

Urry, D. W. 1993 Molecular machines: how motion and other functions of living organisms can result from reversible chemical changes. *Angew. Chem.* **105,** 859–883 [in German]; *Angew. Chem. Int. Edn* **32,** 819–841 [in English].

Urry, D. W. 1997 Physical chemistry of biological free energy transduction as demonstrated by elastic protein-based polymers. *J. Phys. Chem.* B **101,** 11 007–11 028.

Urry, D. W., Long, M. M. & Sugano, H. 1978 Cyclic analog of elastin polyhexapeptide exhibits an inverse temperature transition leading to crystallization. *J. Biol. Chem.* **253,** 6301–6302.

Urry, D. W., Venkatachalam, C. M., Long M. M. & Prasad, K. U. 1982 Dynamic β-spirals and a librational entropy mechanism of elasticity. In *Conformation in biology,* G. N., Ramachandran Festschrift vol. (ed. R. Srinivasan & R. H. Sarma), pp. 11–27. Guilderland, NY: Adenine Press.

Urry, D. W., Wood, S. A., Harris, R. D. & Prasad, K. U. 1984 Polypentapeptide of elastin as an elastomeric biomaterial. In *Polymers as biomaterials* (ed. S. W. Shalaby, T. Horbett, A. S. Hoffman & B. Ratner), pp. 17–32. New York: Plenum Press.

Urry, D. W., Henze, R., Redington, P., Long, M. M. & Prasad, K. U. 1985*a* Temperature dependence of dielectric relaxations in α-elastin coacervate: evidence for a peptide librational mode. *Biochem. Biophys. Res. Commun.* **128,** 1000–1006.

Urry, D. W., Trapane, T. L. & Prasad, K. U. 1985*b* Phase-structure transitions of the elastin polypentapeptide–water system within the framework of composition–temperature studies. *Biopolymers* **24,** 2345–2356.

Urry, D. W., Venkatachalam, C. M., Wood, S. A. & Prasad, K. U. 1985*c* Molecular structures and librational processes in sequential polypeptides: from ion channel mechanisms to bioelastomers. In *Structure and motion: membranes, nucleic acids and proteins* (ed. E. Clementi, G. Corongiu, M. H. Sarma & R. H. Sarma), pp. 185–203. Guilderland, NY: Adenine Press.

Urry, D. W., Haynes, B., Zhang, H., Harris, R. D. & Prasad, K. U. 1988*a* Mechanochemical coupling in synthetic polypeptides by modulation of an inverse temperature transition. *Proc. Natl Acad. Sci. USA* **85,** 3407–3411.

Urry, D. W., Harris, R. D. & Prasad, K. U. 1988*b* Chemical potential driven contraction and relaxation by ionic strength modulation of an inverse temperature transition. *J. Am. Chem. Soc.* **110,** 3303–3305.

Urry, D. W., Peng, S. Q., Xu, J. & McPherson, D. T. 1997 Characterization of waters of hydrophobic hydration by microwave dielectric relaxation. *J. Am. Chem. Soc.* **119,** 1161–1162.

Vrhovski, B., Jensen, S. & Weiss, A. S. 1997 Coacervation characteristics of recombinant human tropoelastin. *Eur. J. Biochem.* **250,** 92–98.

Volpin, D., Urry, D. W., Pasquali-Ronchetti, I. & Gotte, L. 1976 Studies by electron microscopy on the structure of coacervates of synthetic polypeptides of tropoelastin. *Micron* **7,** 193–198.

Weis-Fogh, T. & Andersen, S. O. 1970 New molecular model for the long-range elasticity of elastin. *Nature* **227,** 718–721.

Wu, W. J., Vrhovski, B. & Weiss, A. S. 1999 Glycosaminoglycans mediate the coacervation of human tropoelastin through dominant charge interactions involving lysine side chains. *J. Biol. Chem.* **274,** 21 719–21 724.

Appendix B

To Appear In "Elastomeric Proteins", Cambridge University Press, P. Shewry and A. Bailey, Eds., (in press) 2002

IDEAL PROTEIN ELASTICITY: THE ELASTIN MODELS

D. W. Urry[1,2,4], T. Hugel[2], M. Seitz[2], H. Gaub[2], L. Sheiba[3], J. Dea[3], J. Xu[4], L. Hayes[4], F. Prochazka[1], T. Parker[4]

[1]University of Minnesota, Twin Cities Campus, BioTechnology Institute, 1479 Gortner Avenue, St. Paul, MN 55108-6106, USA.

[2]Ludwig-Maximilians-Universität, Lehrstuhl für Angewandte Physik, Amalienstraße 54, D-80799 München, Germany.

[3]SPAWAR SYSTEMS CENTER, Code D711, San Diego, CA 92152-5001, USA.

[4]Bioelastics Research Ltd., 2800 Milan Court, Suite 386, Birmingham, AL, 35211-6918, USA.

Key words: AFM(force-extension mode), acoustic absorption, dielectric relaxation, thermoelasticity, entropic elasticity, β-spiral, internal chain dynamics

Running Title: Elastin: an ideal elastomer

ABSTRACT

During the last half century, identification of an ideal (predominantly entropic) protein elastomer was generally thought to require that the ideal protein elastomer be a random chain network. Here, we report two new sets of data and review previous data. The first set of new data utilizes atomic force microscopy to report single-chain force-extension curves for $(GVGVP)_{251}$ and $(GVGIP)_{260}$, and provides evidence for single-chain ideal elasticity. The second class of new data provides direct contrast between low frequency sound absorption (0.1 to 10 kHz) exhibited by random chain network elastomers and by elastin protein-based polymers.

Earlier composition, dielectric relaxation (1 to 1000 MHz), thermoelasticity, molecular mechanics and dynamics calculations and thermodynamic and statistical mechanical analyses are presented that combine with the new data to contrast with random chain network rubbers and to detail the presence of regular non-random structural elements of the elastin-based systems that lose entropic elastomeric force on thermal denaturation.

The data, analyses and calculations affirm an earlier contrary argument that components of elastin, the elastic protein of the mammalian elastic fiber, and purified elastin fiber itself contain dynamic, nonrandom, regularly repeating structures that exhibit dominantly entropic elasticity by means of a damping of internal chain dynamics on extension.

1. Introduction

1.1 Definition of ideal or perfect elasticity

Ideal elasticity is the property whereby the energy expended in deformation of the elastomer is completely recovered on removal of the deforming force. Since the energy expended in deformation is given by the area under the force, f, versus increase in length, ΔL, curve, a perfectly reversible force-extension curve means complete recovery on relaxation of the energy expended on deformation. Therefore, ideal elastomers exhibit perfectly reversible force-extension curves.

Perhaps our earliest perspective of the mechanism underlying ideal elasticity comes from a fundamental observation concerning rubber elasticity. In the mid nineteenth century, Joule and Thomson noted a quantitative correlation between the increase in temperature of the elastomer due to stretching and the increase in force due to increasing the temperature (Flory 1968). Thermodynamics provides for the analysis underlying this correlation, and the Boltzmann relation provides the bridge between experimental thermodynamic quantities and statistical mechanical description of molecular structures.

Continuing qualitatively with the Joule and Thomson correlation, heat produces motion, and the energy represented by heat distributes into the various available degrees of freedom in the chain molecules comprising the elastomer. Accordingly, the release of heat on stretching correlates with a loss of motion. By means of statistical mechanics, the loss of motion is seen as a decrease in entropy on extension. In addition, should solvent be essential for elasticity, this requires explicit consideration.

But there is more to elastomeric force than entropy changes arising from changes in mobility. There is also internal energy, and a proper understanding of elasticity requires delineation of internal energy and entropy components of the elastomeric force. As the internal energy component of the elastic force increases, irreversible processes such as chain breakage become

more probable. So greater durability results as elastomers become more dominantly entropic and durability becomes a feature of an ideal or more perfect elastomer.

1.2 Delineation of internal energy and entropy components of elastomeric force

Delineation of internal energy and entropy components of elastomeric force can begin with the definition of the Helmholtz free energy, A, also referred to as the maximal work function,

$$A \equiv E - TS, \tag{1}$$

where E is the internal energy, T is the absolute temperature (degrees K), and S is the entropy for the system. The differential of the maximum work function, dA, can be written to include the work done on an elastomer by application of a force, f, over the change in length, dL, i.e.,

$$dA = -PdV - SdT + fdL \tag{2}$$

where P is the pressure, and V is the volume. Writing the partial differential of A in Eq. (1) with respect to length at constant V, T and composition, n, gives

$$(\partial A/\partial L)_{V,T,n} = (\partial E/\partial L)_{V,T,n} - T(\partial S/\partial L)_{V,T,n}, \tag{3}$$

but by Eq. (2), $(\partial A/\partial L)_{V,T,n} = f$, such that

$$f = (\partial E/\partial L)_{V,T,n} - T(\partial S/\partial L)_{V,T,n}. \tag{4}$$

Accordingly, the force is seen to be comprised of two components, an internal energy component, f_E, and an entropy component, f_S, i.e.,

$$f = f_E + f_S. \tag{5}$$

Now it becomes useful to find an expression that will allow experimental estimation of the relative magnitude of the internal energy and entropy components of the force. Following Flory et al (1960), when the functions exist and are continuous, the order of a partial differential does not matter, and it can be shown that $(\partial S/\partial L)_{V,T} = (\partial f/\partial T)_{V,L}$, such that,

$$f = (\partial E/\partial L)_{V,T,n} + T(\partial f/\partial T)_{V,L,n}. \tag{6}$$

Interestingly, this can be rewritten as

$$f_E/f = -T(\partial \ln[f/T]/\partial T)_{V,L,n}, \tag{7}$$

which allows for an experimental estimate of the f_E/f ratio from the slope of a plot of ln(f/T) versus temperature under conditions of constant V, L and composition, n.

By means of an approximate correction term, the f_E/f ratio can be estimated under more usual experimental conditions of constant P, L and at equilibrium, e.g., with surrounding solvent, i.e.,

$$f_E/f = -T(\partial \ln[f/T]/\partial T)_{P,L,eq}, - \beta_{eq} T/[\alpha^3(V_i/V) - 1] \qquad (8)$$

where $\beta_{eq} = (\partial \ln V/\partial T)_{P,L,eq}$ is the thermal expansion coefficient; α is the fractional increase in length, L/L_i, with the subscript i indicating initial length; and V_i and V are the volumes of the elastomer before and after elongation, respectively (Dorrington & McCrum 1977; Hoeve and Flory 1962). The correction term was derived under the assumption of random chain networks with a Gaussian distribution of end-to-end chain lengths.

As we will see, a random chain network comprised of a Gaussian distribution of end-to-end chain lengths between cross-links is not an accurate structural description of the elastin protein nor of its simpler models. Also, there are important solvation changes that can occur under experimental conditions. Nonetheless, the insight into the magnitude of the entropic component of the elastomeric force provided by Eq. (8), with experimental estimates of the quantities in the correction term or when neglecting the correction term altogether, is informative, but only when the temperature range for determination of slope is judiciously chosen.

1.3 Basic statistical mechanical expression for entropy

1.3.1 The Boltzmann relation

The starting point for the statistical mechanical expressions of entropy is the Boltzmann relation,

$$S = R \ln W \qquad (9)$$

R (1.987 cal/degree-mole) is the gas constant, R = Nk, with N being Avogadro's number (6.02 x 10^{23} /mole) and k the Boltzmann constant (1.38 x 10^{-16} erg/degree K), and W is the number of *a priori* equally probable states accessible to the system (Eyring et al 1964). W is the volume in

phase space occupied by a particular state of a molecular system. In practice, W becomes the product of partition functions for each of the degrees of freedom of the molecular system. There are 3n - k degrees of freedom where n is the number of atoms in the molecule and k are the holonomic constraints on the system. In general, there are three translational and three rotational degrees of freedom, and the remaining are vibrational degrees of freedom. For large enough molecules, the vibrational degrees of freedom also include motions of rotation (or torsional oscillations) about bonds. Due to the constraints of the elasticity measurement k is 6; the ends of the molecules are effectively fixed in space such that there are neither translational nor whole molecule rotational degrees of freedom.

1.3.2 Fundamental expression for the change in entropy on extension

Fortunately, when calculating entropic contributions to the elasticity, interest centers on the change in entropy on extension from a relaxed, S^r, to an extended, S^e, state of the elastomer,

$$\Delta S = (S^e - S^r) = R\ln(W^e/W^r). \qquad (10)$$

Since the change in entropy is a ratio, it becomes relatively straight-forward to calculate the contribution to the change in entropy of a particular expression of motion accessible to the representation of the molecular structure to be examined in its relaxed and extended states. For our purposes the β-spiral structure of the $(Gly\text{-}Val\text{-}Gly\text{-}Val\text{-}Pro)_n$, or poly(GVGVP), model of elastin is used and two different means of representing that structure are considered. The first is the enumeration of states in configuration (ϕ-ψ torsion angle) space within a given energy cut-off for relaxed and extended states, and the second is to use the molecular dynamics approach to determine the change in rms torsional oscillations that occur on extension by the same amount as used in the enumeration of states approach. The magnitudes of the calculated entropy changes on extension obtained by each approach can then be compared.

1.4 Historical notes of proposed mechanisms for protein entropic elasticity

1.4.1 Classical (random chain network) theory of rubber elasticity

During the last half of the last century, identification of ideal (dominantly entropic) protein elasticity required, by the recognized authorities of the period, the conclusion that the ideal elastomer was comprised of random chain networks with a Gaussian distribution of end-to-end chain lengths between cross-links. For elastin, the protein of interest here, this point of view began with a paper by Hoeve and Flory, (1958). This perspective became entrenched in the minds of the interested scientific community by the award in the Fall of 1974 of the Nobel Prize to Paul Flory following reaffirmation of the random chain network conclusion (Hoeve and Flory 1974). The message of the paper is unmistakable. In the Synopsis it is stated, "*A network of random chains within the elastic fibers, like that in a typical rubber, is clearly indicated.*" Furthermore, in Figure 1 of their paper is a structural representation of the chains between cross-links with a statement in the figure legend that, "*Configurations of chains between cross-linkages are much more tortuous and irregular than shown.*"

1.4.2 Decrease in solvent entropy on extension

The purpose of the 1974 Hoeve and Flory paper, which presented no additional data, was to refute an earlier publication by Weis-Fogh and Anderson (1970), who had suggested an alternate mechanism for the elasticity of elastin. The alternate mechanism proposed that hydration of hydrophobic side chains of the protein that become exposed to solvent on extension would be responsible for the stretch-induced decrease in entropy, that is, by this proposal changes in solvent entropy became the source of the entropic component of the elastomeric force.

1.4.3 Damping of internal chain dynamics on extension

Just over a decade later yet another perspective was put forward. Considering structural studies and molecular mechanics calculations of the most prominent repeating sequence of bovine elastin, $(Gly\text{-}Val\text{-}Gly\text{-}Val\text{-}Pro)_{11}$, entropic elasticity was described as arising from a decrease in available configuration space on extension (Urry et al 1982). Equivalently, treating

the experimentally and computationally derived regularly repeating structure from the perspective of molecular dynamics, the damping of internal chain dynamics on extension described the same decrease in entropy for the same degree of extension (Chang & Urry 1989).

In the Discussion section below, these three mechanisms will be considered in more detail, following consideration of new experimental data on models of elastin along with previously published relevant data.

1.5 Inverse Temperature Transition Behavior of Elastin and its Models

1.5.1 Increase in order with increase in temperature

1.5.1.1 *Filament Formation on Raising the Temperature:* When the temperature of an aqueous solution of the precursor protein, tropoelastin, is increased, the protein aggregates to form a more-dense viscoelastic phase, called a coacervate. When a droplet of the aqueous suspension of incipient aggregates is placed on a carbon coated grid, negatively stained with uranyl acetate and oxalic acid at the appropriate pH, and examined in the transmission electron microscope, fibrils comprised of parallel aligned filaments are observed with a 5 nm periodicity (Cox et al 1974). Similar results are obtained for α-elastin, a 70,000 Da fragment of the elastic fiber (Cox et al 1973) and for high polymers, poly(GVGVP) and poly(GVGVAP), of repeating sequences of elastin (Volpin et al 1976). Fibrils of similar dimensions have been reported for fibrous elastin itself using similar techniques (Gotte et al 1974).

1.5.1.2 *Crystallization of Cyclic Analogues on Raising the Temperature of the inverse temperature transition:* Most strikingly, cyclic analogues of repeating sequences of elastin crystallize on raising the temperature (Urry et al 1978; Cook et al 1980) and redissolve on lowering the temperature. Without ambiguity, these polymers increase order with increase in temperature through a transition temperature range.

We refer to this phase transition as an *inverse temperature transition.* While the peptide component of this water-peptide system increases in order on increasing the temperature, ordered water molecules surrounding hydrophobic residues become less ordered bulk water as hydrophobic groups separate from solution. Accordingly, the overall change effected by the phase transition is to less order in keeping with the second law of thermodynamics.

Indeed the phase diagram for high molecular weight polymers of repeating sequences of elastin is inverted with the soluble phase below, at lower temperature, and the insoluble phase above the binodal or coexistence line and with an inverted coexistence line, i.e., with the curvature of the coexistence line convex to the volume fraction axis (Sciortino et al 1993; Manno et al 2001). On the other hand, the usual circumstance for polymers is for the coexistence line to be concave to the volume fraction axis and for the polymer to be insoluble below and soluble above the coexistence line (Flory 1953).

1.5.2 Composition of poly(GVGVP) in water as a function of temperature

The temperature dependence of composition of the poly(GVGVP)-water system provides a clear visualization of a water-containing, structured state at intermediate temperatures (Urry et al 1985b). A plot of percent water by weight as a function of temperature is schematically shown in Figure 1. As the polymer is miscible with water in all proportions below 20°C, the plot arbitrarily starts at about 90% water by weight near 0°C. On raising the temperature from 20 to 30°C, there occurs a reversible phase separation to form a state that is 63% water by weight. The percent water by weight of this intermediate water-retaining state remains essentially unchanged until the temperature is raised above 60°C. Then a very slow irreversible transition occurs on raising the temperature from 60 to 80°C to form a state that is 32% water by weight. Dialysis of the polymer against 100,000 Da cut-off membranes, after the prolonged heating at 80°C, resulted in less than 0.1% loss of polymer, that is, prolonged heating did not result in chain breakage.

The results on poly(GVGVP) are compared in Figure 1 to those of Grinberg et al (1999) on the petroleum-based polymer, poly(N-isopropylacrylamide), (PNIPAM). This polymer shows an inverted phase diagram like that of the elastin-based polymers. Though with a composition more hydrophobic than that of poly(GVGVP), the transition for this LCST (lower critical solution temperature) polymer occurs at a higher temperature (34°C), is much sharper, and directly results in the formation of the state with approximately 30% water by weight. This PNIPAM state of 30% water by weight may reasonably be described as a random chain network. It is clear that poly(GVGVP) forms an intermediate, water containing state that holds a fixed amount of water until irreversible denaturation occurs at high temperature. This state of 63% water by weight is an elementary property that simply is not consistent with the recently computed "compact amorphous globule" for $(GVGVP)_{18}$ due to Li et al (2000).

1.5.3 A structured state at intermediate temperatures for elastin-based systems

Both the elastin fiber and α-elastin at intermediate temperatures form similar water-containing states of about 50% water by weight (Partridge et al 1955; Partridge & Davis 1955; Partridge 1966, 1967). It will also be shown below (see Figure 9) that both cross-linked poly(GVGVP) and fibrous elastin exhibit a slow, irreversible, loss of elastic force when at fixed extension after prolonged exposure to temperatures above 60°C. These are further demonstrations of the slow irreversible denaturation observed in Figure 1 above 60°C for poly(GVGVP). Furthermore, detailed dielectric relaxation studies on the elastin-based systems – fibrous elastin, α-elastin, and poly(GVGVP) – demonstrate molecular motions, relaxations, limited to localized frequency ranges (See Figures 6, 7 and 8), and these could only be the result of non-random, regularly structured, albeit dynamic conformational states. These experimental results are consistent with neither random chain networks nor compact amorphous globules.

2. MATERIALS

2.1 Preparation of elastin models

In its native state elastin, a protein of about 70,000 Da, occurs as the overwhelming dominant component (90+% by weight) of the mammalian elastic fiber, which resides within the extracellular matrix, for example, as a structure several microns in diameter in the vascular wall. Non-elastin components are trapped enzymatic protein involved in the cross-linking and a fine fibrillar coating of some hundreds of nanometer thickness. The elastic fiber is a substantially cross-linked, insoluble material of the extracellular matrix. Efforts to isolate it for purposes of defining its properties require draconian methods, for example, refluxing in sodium hydroxide, to remove all of the surrounding matrix components. This product is called purified fibrous elastin. Alternatively, model approaches are used such as isolating and characterizing (1) the precursor protein, tropoelastin, which may be obtained in ill-defined intermediate states of cross-linking, (2) the pure precursor protein prepared by microbial biosynthesis, (3) chemical degradation products of purified fibrous elastin, and (4) chemically and microbially synthesized repeating sequences found within the protein sequence as well as interesting analogues.

2.1.1 Synthesis of model systems

2.1.1.1 *Chemical Synthesis*: Initially several thousand protein-based polymers were synthesized in order to determine the conformation and function of these model proteins. This involved the synthesis of oligomers and high polymers of repeating tetra-, penta-, hexa-, nona- and even decapeptides reported in the sequence of elastin. By means of chemical synthesis, many compositions could be prepared and characterized, and axioms were developed for the function of these elastic model proteins in energy conversion and for their use as biomaterials for medical and non-medical applications.

2.1.1.2 *Microbial Biosynthesis* Once a specific composition was identified as being of sufficient interest, it was prepared by means of recombinant DNA technology where hundreds of grams could be prepared in a single fermentation that by means of bench chemical synthesis would require much of a year to prepare.

2.1.2 Preparation of natural materials

2.1.2.1 *Isolation of the precursor protein, tropoelastin*: Initially, the precursor protein was prepared from animals made copper deficient and treated with inhibitors of enzymatic cross-linking. The product was meager in amount and a mixture of partially cross-linked and oxidized lysyl side chains. It was nonetheless helpful in determining many of the fundamental physical properties relating to structure and elastogenesis.

2.1.2.2 *Preparation of tropoelastin by microbial biosynthesis* In an important development, Weiss and coworkers utilized recombinant DNA technology to prepare the precursor protein, tropoelastin, in E. coli, which allowed preparation of pure protein in large quantities (Vrhovski et al 1997; Wu et al 1999). Important aspects deduced by the model systems and by preparations of model structures derived from the elastin and from knowledge of sequence have been confirmed and extended by recombinantly prepared tropoelastin.

2.1.2.3 *Preparation of α-elastin* A model system useful in stepping systematically from polymers of model repeating sequences to the natural fibrous elastin has been a chemical fragmentation product from fibrous elastin called α-elastin. It is a 70,000 molecular weight fragment comprised of 16 cross-linked chains (Partridge et al 1955; Partridge & Davis 1955; Partridge 1966, 1967).

2.1.3 Purification using phase transitional behavior

In all cases these protein-based polymers are soluble in water at a lower temperature and phase separate on raising the temperature above that for the onset of a hydrophobic folding and assembly transition. This phase separation process has been called coacervation. It is a fundamental property of these polymers with the correct balance of apolar and more polar residues.

2.2 Cross-linking of elastin models

2.2.1 General cross-linking procedure

Cobalt 60 γ-irradiation has been used to cross-link the phase separated, coacervated and structured state of the elastic protein-based polymers with interpenetrating polymer chains. The effective cross-linking doses have ranged from 6 to 30 Mrads (million radiation absorbed dose) with 20 Mrads chosen as the usual circumstance for the elastic model proteins.

2.2.2 Efforts to cross-link α-elastin

Even though α-elastin undergoes phase separation, it does not form an elastic matrix on γ-irradiation. As a cluster of some 16 cross-linked chains of a total of 70 kDa molecular weight it does not cross-link because there are no chains of sufficient length to interpenetrate.

2.2.3 Efforts to cross-link heat denatured poly(GVGVP)

While the phase separated state of poly(GVGVP) with 63% water by weight (Figure 1) cross-links very effectively, the heat denatured state obtained on prolonged heating above 60°C does not. Even though the density of chains is twice as great for the denatured state formed above

60°C (a state of 32% water by weight as seen in Figure 1), the chains no longer form the intermediate structured state of Figure 1 and the chains no longer sufficiently interpenetrate to result in an elastic matrix on γ-irradiation. This is simply another demonstration that the intermediate between 30 and 60°C is a structured state of interpenetrating chains and filaments.

3. Specialized methodologies and analysis of results

3.1 Atomic Force Microscopy (AFM) in the force-extension mode

3.1.1 Preparation of the sample for AFM

Glass microscope slides were cleaned and coated with about 30 nm of gold in a home built machine. Si_3N_4 AFM tips were used (Microlevers, Park Scientific Instruments, Sunnyvale, CA), and also coated with gold. Quantities of 1 mg of the polypentapeptides and 0.5 mg methoxy-PEG-thiol (M_w 5000) were dissolved in 1 ml Milli-Q water unless otherwise noted. 20 μl of this solution were incubated on the gold coated slide for about 30 min at 3°C and then rinsed with Milli-Q water.

3.1.2 The AFM Instrument

A detailed description of the AFM force spectroscopic technique and details of the instrumental set-up have been given elsewhere (Oesterhelt et al 1999; Clausen-Schaumann et al 2000). Briefly, the tip of a cantilever is brought into contact with molecules on the surface and then retracted, its deflection – and therefore the force – are detected with a laser by optical lever detection (Cleveland et al 1993), while the z-distance is controlled by a strain gauge (Figure 2). The nominal spring constants of cantilevers used in the experiments were 10 mN/m. Prior to the first approach of the AFM tip to the surface, the spring constants of each lever were individually

calibrated by measuring the amplitude of its thermal oscillations (Butt & Jaschke 1995). The sensitivity of the optical lever detection was measured by indenting the AFM tip into a hard surface. All experiments were conducted in Milli-Q water at room temperature (21°C), unless otherwise specified.

3.1.3 Obtaining the single-chain force-extension curve

For the characterization of elastic properties, the gold-coated AFM tip was brought into contact with the polypentapeptides on the microscope slide by manual control. The AFM tip and the polymer layer were kept in contact under a contact force of several nanoNewton (nN) for approximately 30 seconds to allow for an attachment of the chain to the tip. Usually the chain adsorbed non-covalently at some position on the tip, maybe sometimes a chemical reaction between the gold-coated cantilever and the cysteine on the end of a polypentapeptide allowed for really high rupture forces. Upon retraction of the cantilever, individual polypentapeptides were stretched between the surface and the AFM tip.

Note that the first force-distance profile recorded after tip-substrate contact can be rather complex, consisting of contributions from stretching several polypentapeptides, desorption from the substrate and/or cantilever, bond rupture of short strands, as well as interchain aggregation and entanglements. Therefore, in each measurement the cantilever was first retracted from the substrate to a distance at which unspecific adhesion was no longer observed. Then, in successive retraction-approaching cycles the distance range is increased while trying to avoid contact between the tip and additional polypentapeptide strands at the substrate surface, until only one polymer strand remained between tip and substrate. The force-distance profile of this strand was then measured repeatedly until rupture.

3.1.4 Analysis of the results

The experimental traces were fit by an extended wormlike chain (WLC) model including linear elastic contributions arising from the stretching of bond angles and covalent bonds:

$$F \cdot \frac{L_P}{k_B T} = \frac{R_z}{L} - \frac{F}{K_o} + \frac{1}{4(1 - R_z / L + F / K_o)^2} - \frac{1}{4} \qquad (11)$$

In this expression, R_z is the measured end-to-end-distance at any given force, F, and L is the contour length of the stretched chain (polypentapeptide) under zero force (F = 0). The peptides bending rigidity is expressed by the chain's persistence length, L_P. Finally, the chain's extensibility upon stretching is described by the segment elasticity, K_o, which is introduced into Eq. (9) as a linear term (hereby, K_o can be understood as the inverse of the normalized compliance of a Hookean spring; the spring constant of the polymer chain is given by K_o/L). (It should be appreciated that the WLC model is not modeled at the molecular structure level but rather is based on more macroscopic considerations.)

This resulted in values for the persistence length Lp of $(GVGVP)_{nx251}$: Lp = 0.4 nm in the low force regime and Lp = 0.6 nm when fitted to higher forces. The reversible traces provide evidence for single chain ideal elasticity (entropic and therefore reversible – most probably from backbone torsional movements (rocking), wherein the contribution to the entropic component of the force increases with decrease in the frequency of the oscillation). The small deviations from perfect reversibility in traces 2, 3 and 5 of Figure 3 occurred when the chain was held at least 30 s in the relaxed state. These deviations could have several origins. There could be a *configurational transition, e.g., an opening of* β*-turns* and/or hydrophobic interaction, a backfolding, between different parts of the chain. The latter is favored by the observed rate dependence of this non-equilibrium contribution.

The persistence length Lp of $(GVGIP)_{nx260}$ is difficult to determine, when intra and/or inter chain aggregation gives rise to a strong hysteresis even when being far away from the surface within two successive cycles (Figure 4). It is determined to exhibit an Lp = 0.7 nm, which might be a little higher than with $(GVGVP)_{nx251}$, but this value lies well within the error range of about

20 %. This strong aggregation of $(GVGIP)_{nx260}$ happens at the same concentration, at which the aggregation for $(GVGVP)_{nx251}$ is much smaller. This reflects the increase in hydrophobicity due to an additional CH_2 group in GVGIP, which is the only difference with GVGVP. Unfortunately, it is not yet clear, whether the aggregation is mainly due to backfolding within a single chain or due to association between different chains. This is under investigation.

3.1.5 Comparison of AFM single-chain and macroscopic elastic moduli

For the characterization of elastomers at the macroscopic scale, force is plotted versus elongation, but instead of being given as actual increase in length as in Figures 3 and 4, elongation is given in terms of the ratio of the initial length to the extended length. Furthermore, the deformation is generally uniform so that the initial cross-sectional area, A, is used. So the Young's elastic modulus, Y, is the force, f, times the initial length, L_i, divided by the elongation, L, and the cross section of the elastomer, that is, $Y = fL_i /AL$. The units are N/m^2 or $dynes/cm^2$ where $N/m^2 = 10$ $dynes/cm^2$ and N stands for Newtons. The elastic modulus of 20 Mrad γ-irradiation cross-linked $(GVGVP)_{251}$, i.e., X^{20}-$(GVGVP)_{251}$, is 1.6×10^5 N/m^2.

In order to utilize the data in Figure 3 to obtain an estimate of single chain elastic modulus, estimates of the L_i /L ratio and of A are required. Initially, the total number of repeats being extended must be deduced. In Figure 3, the length to rupture is just greater than 700 nm, which we take to be the fully extended chain. This is too long for a chain of 251 pentamers, but appears to be too short for a chain of 753 pentamers. By elimination of chain lengths with 251 and 753 pentamers, this indicates that the structure would be $(GVGVP)_{2x251}$ giving 502 pentamers, i.e., 2510 residues with a value of 0.29 nm per residue. This is shorter than the usual value of 0.35 nm per residue due to the presence of a proline residue in every pentamer. This is considered to be due to the cis Val-Pro peptide bond, which introduces a kink in the extended backbone for every pentamer. It should be noted, however, that if all of the β-turns were retained at rupture, the 3x251 chain length could apply with approximately 1 nm per pentamer, or just greater than

700 nm. This was not considered because the forces for detachment can be greater than 500 pN, and retention of the β-turn was considered less likely at such forces.

Perhaps the most significant factor in obtaining a relevant value for the single chain elastic modulus is the choice of the structure before elongation in order to provide an estimate of an initial length and cross sectional area. In this regard two quite different initial lengths may be considered, one for the random coil state below the hydrophobic folding transition and another for the β-spiral structure that could only occur above the onset temperature for the hydrophobic folding transition.

3.1.5.1 *Calculation of elastic modulus from AFM data assuming a random coil state for* $(GVGVP)_{nx251}$ At temperatures lower than the onset temperature for the hydrophobic folding and assembly transition, the more correct representation of the unstretched single chain would be the random coil state. Based on photon correlation spectroscopic studies, the hydrodynamic diameters of disordered polymeric coils resulting from 502 pentamers (some 200,000 Da molecular weight) below the transition would be about 18 nm (San Biagio et al 1988). By way of example, at a distance of 378 nm in Figure 3, the L_i /L ratio would be 1/20. With a slope of 0.1 pN/nm from Figure 3, at a distance of 378 nm from the substrate the increase in force would be 36 pN, i.e., due to elongation from 18 to 378 nm, and the change in length, ΔL, would be a factor of 20 or a slope of 1.8 pN for a 100% extension. Next this quantity should be divided by an appropriate cross sectional area, that is, π times the hydrodynamic radius squared of the random coil prior to extension of the single chain, i.e., $\pi r^2 = \pi(9\text{ nm})^2 = 254\text{ nm}^2$. Given the foregoing assumptions, the calculated single chain elastic modulus would be 7×10^4 N/m^2. Somewhat surprisingly, even without taking cross-link density into consideration (Urry et al 1984), this value is only a factor of two from the experimental value at 37°C for X^{20}-$(GVGVP)_{251}$ of 1.6×10^5 N/m^2.

3.1.5.2 *Calculation of elastic modulus from AFM data assuming a single chain β-spiral structure for* $(GVGVP)_{nx251}$ For comparison it is useful to consider the structure representative of the state above the temperature of the inverse temperature for hydrophobic folding and assembly. If the single β-spiral structure were assumed before extension with three pentamers per turn and a translation along the axis of 1 nm per turn, the length of a 502 mer would be about 170 nm. This means that an elongation of 200% would occur at 510 nm. With this information and a cross-sectional area of the β-spiral structure of about 2.5 nm^2, the reversible curves in Figure 3 with a slope of 0.1 pN/nm would indicate an elastic modulus of about 7×10^6 N/m^2. This is a factor of 100 greater than that obtained under the assumption of a random coil. It will indeed be interesting to determine the elastic modulus of the fundamental filament, once synthetically prepared, which is thought to be a triple stranded twisted filament, as depicted below in Figure 9F.

3.2 The acoustic absorption experiment

3.2.1 Sample preparation and experimental set-up

The polymer is prepared in the phase separated state, i.e., the intermediate structured state of Figure 1, and 20 Mrad γ-irradiation cross-linked in the form of the desired cylindrical shape and with path lengths that differ by a factor of two, as shown in the lower part of Figure 5.

The Naval Research Laboratory at SSC-SD has the capability to measure very accurately the elastic properties of materials by using a broadband technique developed by Sheiba (1996). The technique is under US Patent Pending. Older techniques are more cumbersome and less reliable. The frequency of measurement ranges from sub-sonic to about 15 kHz. The measurements are performed in air inside an environmental chamber. Figure 5 also shows the block diagram of the instrumental set-up for these measurements.

The network analyzer sends sweeping signals to the shaker. The transducer (sometimes called an accelerometer) and impedance head record the velocities at the base and at the top of the sample. After recording data during this frequency sweep, a new set of data is then obtained at a new temperature setting. Commonly temperatures can range from –30° to +70°C. The velocity record constitutes the transfer matrix. By mathematically inverting the transfer matrix, it is possible to extract the complex modulus and Poisson ratio. These data provide a complete description of a material's elastic properties. Further analysis yields the shear modulus, μ, the Poisson ratio, ν, and the loss factor, η, each as a function of frequency and temperature. The loss factor, η, is the main parameter of interest. It represents the energy absorption per unit volume at a given frequency. The loss factor versus frequency and temperature were found for several different elastic protein-based polymer compositions. The data for $(GVGIP)_{nx260}$ is given in Figure 6A. MATHCAD 7.0 was used to perform the mathematical analysis.

3.2.2 Comparison of the acoustic absorptions of (GVGIP) and natural rubber

Natural rubber is well characterized as a random chain network. This means that there are no regular repeating conformational features in the polymer chain. The consequence of a random chain is a broad, slowly changing dependence on frequency of physical properties, such as absorption. Simply stated the absence of structure means that the barrier to rotation about each bond will tend to be different. This is what is observed in Figure 6A for natural rubber and a synthetic petroleum-based polymer, polyurethane, chosen for its relatively high loss factor in the frequency range reported.

On the other hand at frequencies lower than those of the infrared spectroscopic range, any material that exhibits a localized absorption band as a function of frequency must do so by virtue of a regular repeating structure. Interestingly, this is seen in Figure 6A for X^{20}-$(GVGIP)_{260}$ in the range of 200 Hz to 7 kHz, and it is seen that the intensity of the absorption per unit volume increases as the temperature is raised through the temperature interval of the inverse temperature

transition. Besides demonstrating the remarkable acoustic absorption property of this material, the acoustic absorption data provide additional demonstration of the existence of a regular structure for poly(GVGIP) and for related polymers. Actually, this is simply further confirmation of earlier dielectric relaxation data, which demonstrated the development of intense localized relaxations near 5 MHz as the temperature is raised through the interval of the inverse temperature transition, as reviewed below.

3.3 Dielectric Relaxation Studies on Elastin-Related Systems

3.3.1 Dielectric relaxation and acoustic absorption data for $(GVGIP)_n$ over the frequency range, 0.1 to 100 kHz.

In the acoustic absorption measurement of Figure 6A, an oscillating compressional wave activates the mechanical relaxation in the vicinity of one kHz, and the relaxation requires reorientation of peptide moieties in order for the polypentapeptide to respond to the acoustical frequency of the vibrational wave. As peptide moieties have very large dipole moments, poly(GVGIP) could be expected to function as a transducer in which the acoustically activated mechanical relaxation would be transduced into a dielectric relaxation signal of the same frequency. The experimental equipment to demonstrate this free energy transduction has yet to be designed.

The existence of the acoustic absorption, however, indicates that a dielectric relaxation should be observed in a not too distant frequency range. An exact overlap is not expected in the two different experiments because in the dielectric relaxation experiment that alternates positive and negative charge on a pair of plates directly drives the peptide reorientation, and the particular repeating structure determines the frequency range and intensity of the relaxation. On the other hand, in the acoustically driven relaxation the peptide reorientations are a secondary result that is required in order for the repeating structure to respond to the hammering frequency of the acoustic wave. Of course, the fact that a mechanical resonance grows in intensity as the inverse

temperature transition progresses requires progressive formation of a regular repeating structural feature on raising the temperature.

It is to be expected, therefore, that a dielectric relaxation be observed in the frequency range of 0.1 to 100 kHz as reported in Figure 6B, which plots the imaginary (absorption) part of the dielectric permittivity of poly(GVGIP) as a function of temperature. Just as for the acoustic absorption study in Figure 6A, there is an increase in the absorption (imaginary) component of the dielectric relaxation as the temperature is raised through the temperature interval of the inverse temperature transition for hydrophobic folding and assembly. Interestingly intensity of the relaxation continues to grow above 20 to 40°C suggesting that an acoustic absorption even more intense than reported in Figure 6A might be expected.

3.3.2 A related dielectric relaxation (mechanical resonance) near 5 MHz for poly(GVGIP).

For poly(GVGIP) in the frequency range of 1 MHz to 1000 MHz and over the temperature range of 0 to 60°C, the real part of the dielectric permittivity is given in Figure 7A and the imaginary (absorption) part in Figure 7B. As with the data in the 1 kHz range of Figure 6, there is an increase in regular structure as the temperature is raised from below to above the inverse temperature transition. This type of data was used more than a decade ago to demonstrate the formation of regular structure; it is equally valid today, and it is what allowed anticipation of the data recently obtained in Figure 6, that is, anticipation of the remarkable acoustic absorption properties of these materials. This successful trail of proposed structural regularity, testing of the proposal, and predicting of additional properties continues unbroken for much of two decades.

The predictive success and usefulness of a perspective is the truest test of its validity. The perspectives of disorder and randomness have given rise to no such progress. On the other hand the perspective of a regular dynamic structure has led to properties such as numerous free energy transductions otherwise unimaginable. Now, the data on the elastin models can be directly

compared to α-elastin and fibrous elastin, itself. Mechanical resonances due to regularly repeating structures are observed both in the vicinities of 1 kHz and of 5 MHz.

3.3.3 Comparison of poly(GVGVP) and α-elastin

Plotted in Figure 8A is the real part of the dielectric permittivity as a function of temperature for α-elastin and for poly(GVGVP) in the inset (Urry et al, 1985a). In both cases, there is the development of an intense relaxation near 5 MHz as the protein-based elastomers hydrophobically fold and assemble on increasing the temperature through the range of the inverse temperature transition. Both elastomeric molecular systems exhibit the same development of regular structure on raising the temperature through the range of the inverse temperature transition.

3.3.4 Comparison of cross-linked poly(GVGVP) to fibrous elastin

In Figure 8B is plotted the imaginary (absorption) part of the dielectric relaxation for purified natural fibrous elastin (from bovine ligamentum nuchae) as a function of temperature from 23 to 58°C (Luan et al 1988). Also, in Figure 8B is plotted the same data at 58°C for the elastomer, 20 Mrad cross-linked poly(GVGVP). While there is a small increase in mean frequency for the X^{20}-$(GVGVP)_{251}$ relaxation in Figure 8B as in Figure 8A, it is unmistakable that there is hydrophobic folding and assembly resulting in the formation of regular, dynamic, non-random structures in the natural fibrous elastin that are similar to those of cross-linked poly(GVGVP) and poly(GVGIP). Incidentally, the decrease in intensity at 1 GHz for fibrous elastin in Figure 8A for α-elastin and in Figure 8B for fibrous elastin reflects the loss of hydrophobic hydration as the hydrophobic folding proceeds. This is due to a dielectric relaxation near 5 GHz, which arises from hydrophobic hydration (Urry et al 1997).

To be brief, the experimental data clearly reflect dynamic regular structures in the elastic protein-based polymers with related structures and corresponding behaviours in the natural elastin protein.

4. DISCUSSION

4.1 Relevance of proposed mechanisms for protein entropic (ideal) elasticity

The kernel for the classical theory of rubber elasticity originated with K. H. Meyer in 1932, which according to Flory (1968) can be stated as *"... the orientation of the molecules of a piece of rubber when it is stretched would entail a decrease in entropy, and thus could account for the retractive force."* A common restatement has been that a collection of disordered chains becomes more aligned as the elastomer is stretched, and that this alignment of chains constitutes the decrease in entropy on extension. Flory's restatement in 1968 was given in terms of two more fundamental subsidiary hypotheses: (1) The restoring force originates within the chain molecules by distortion of the distribution of their configurations and not from interactions between chains. (2) The restoring force is due "exclusively to the *entropy* of the chain configuration." For ideal or perfect elastomers, we have no quarrel with these subsidiary hypotheses, but those elastomers exhibiting hysteresis appear not to be consistent with the first hypothesis.

Obviously with respect to protein elasticity, we do disagree with the derivative dogma (Flory, 1968; Hoeve and Flory, 1958, 1974) that only random chain networks comprised of a Gaussian distribution of end-to-end chain lengths can satisfy the two hypotheses, which has been a tenet of the classical theory of rubber elasticity. Clearly, entropic elasticity exhibited by a single chain limits the source of entropy change to the damping of internal chain dynamics within a single chain and can not be due to the relative orientation of many chain molecules within a random chain network.

4.1.1 The Flory random chain network theory of entropic elasticity?

Flory's publications describe a Gaussian distribution of end-to-end chain lengths that results from a random chain network, and they assert that the decrease in entropy due to extension or compression arises from distortion of the network from this most probable Gaussian distribution (Flory 1953, 1968). Hoeve and Flory (1958, 1974) concluded that the entropic elasticity of elastin arises from such a random chain network. There are four principal reasons why this perspective is to be questioned. These are (1) a limited potential for cross-links in the fixed sequence of elastin, (2) the above spectroscopic evidence for regular, non-random, dynamic structural features in components of elastin, (3) the above report that single chains of repeating sequences of elastin exhibit entropic elasticity, and (4) irreversible loss of elastic force due to heating above 60°C due to thermal denaturation.

4.1.1.1 *Relevance of the probability of cross-link formation to structure:* In rubber, each repeating unit is a potential cross-link, and, on vulcanization, any pair of repeating units can be made into a cross-link wherever two chain segments are sufficiently proximal. In elastin, only lysine residues form the cross-links, and yet there are only some forty lysine residues for an elastin protein of about 800 residues, i.e., one lysine in every twenty residues. Furthermore, the lysine residues are arranged in an orderly manner along the sequence. Most commonly, four lysine residues combine to form a single cross-link, called a desmosine, and essentially all of the lysine residues in fibrous elastin have been formed into cross-links. Such cross-linking cannot be achieved within a random chain network. Achievement of such rare cross-linkages require elements of order (Urry, 1976).

4.1.1.2 *Low frequency motions provide much entropy to chain structures:* Motions due to rotations about backbone bonds in a chain molecule that exhibit intense relaxations limited to

localized frequency intervals, that is, intense mechanical resonances, can only result from polymers containing regular, non-random, albeit dynamic structures. For model elastin systems including purified fibrous elastin, such mechanical relaxations are observed near 1 kHz and 5 MHz (see Figures 6, 7 and 8, Buchet, et al, 1988; Urry et al, 1985a, Luan et al, 1988). As will be treated below, these relaxations provide an ample source of entropy to structured elastin systems. These contributions to entropy increase greatly as the frequency of the relaxation is lower, and they are contributions to the free energy of protein structure that have yet to be adequately treated in the current computations of low energy protein structures. Most importantly for entropic elasticity, low frequency motions provide an abundant and ready source of entropy decrease on extension.

4.1.1.3 *Entropic elastomeric force arising from a single chain:* At a fixed extension in the AFM single-chain force-extension curves of Figure 3, there is only one end-to-end chain length. The entropic elastic force measured at a given extension cannot have arisen from displacement of a network of chains from a Gaussian distribution of end-to-end chain lengths. The decrease in entropy that provides the entropic restoring force in the single chain experiment must arise from a damping of internal chain dynamics of the single chain. There are no other degrees of freedom from which the decrease in chain entropy can arise.

4.1.1.4 *Loss of elastomeric force of elastin-based systems due to thermal denaturation:* In Figure 1 above, it was noted that poly(GVGVP) exhibits a slow irreversible denaturation when held at temperatures above 60°C. This same phenomenon is apparent in the thermoelasticity studies on fibrous elastin, as originally noted by Dorrington and McCrum (1977). In the thermoelasticity experiments of Figure 9 (Urry 1988a, 1988b), the elastomer is equilibrated at 40°C and at that temperature is extended to 60%. At this fixed length, the temperature is lowered to about 20°C and slowly raised to 80°C. The force dramatically increases as the temperature is raised through the range of the inverse temperature transition from 20 to 40°C.

Then, the force/T(°K) tends to remain nearly constant from 40 to 60°C, especially for X^{20}–poly(GVGVP). The value of lnf/T begins to decrease above 60°C in a time dependent manner. When using a rate of increase of 4°C per 30 min, 8°C/hr, there is a decrease in lnf/T, and, when the temperature is returned to 40°C, there has occurred an irreversible loss of force. The decrease in force above 60°C is more dramatic on raising the temperature more slowly, e.g., when raising the temperature at a rate of 1°C/hr. Irreversible thermal denaturation is most dramatically seen when kept above 60°C for a longer time. Furthermore, a plot of ln(elastic modulus) versus time at 80°C is linear in evidence of a first order process (Urry 1988a, 1988b). Quite interestingly while heating above 60°C decreases force, it also shortens the length at which zero force is obtained, as to be expected for a filamentous, β-spiral-like structure, that became randomized by thermal denaturation.

As discussed in relation to Eqns. (7) and (8) above, a slope of zero for plots like those in Figure 9 would mean an ideal (entirely entropic) elastomer. As clearly seen for X^{20}–poly(GVGVP) in the 40 to 60°C temperature range when the data is collected at the rate of 30 min per data point, a near zero slope is obtained. Commonly an f_E/f ratio of 0.1 is obtained for X^{20}–poly(GVGVP) (Luan et al 1989). Because of the steep positive slope between 20 and 40°C, due to the hydrophobic folding and assembly of the inverse temperature transition, and because of the slow irreversible thermal denaturation above 60°C, the slope, obtained in the thermoelasticty experiment from which the entropic contribution is estimated, depends on the rate at which the data is collected and the temperature interval over which it is collected.

A steep rise in force in the 20 to 40°C temperature interval for fibrous elastin in Figure 9A, though less steep than seen in Figure 9B for X^{20}–poly(GVGVP), demonstrates the effect of the inverse temperature transition within elastin itself. More dramatic for fibrous elastin is the loss of elastomeric force on raising the temperature above 60°C. This finding of a slow loss of force at elevated temperature would not have been so apparent in the limited time of a single day to perform the experiment (without the advantage of computerized equipment), as was the case when Hoeve et al (1958) carried out their original study on fibrous elastin. For the

thermoelasticity study of fibrous elastin shown in Figure 9, however, the rate of loss of force at elevated temperature is even greater than for X^{20}–poly(GVGVP).

Additionally, the plot of ln(elastic modulus) versus time for fibrous elastin maintained at 80°C, as determined by a stress-strain curve every 24 hrs, is a straight line with a half-life of approximately 10 days (Urry 1988b). Another important feature of the data for determining half-life is that the length at which zero force is obtained decreases with time at 80°C. Remarkably, this means that the loss of force in Figure 9 and the progressive loss of elastic modulus exhibited by a series of stress-strain curves at 80°C is not due to structural rearrangement to an extended state under load or for that matter due to slipping in the grip. Instead, extended periods of time at high temperature results in a denaturation, which entails a randomization of linear filamentous structures to denatured, more nearly, globular structures. This has analogy to the loss of percent water by weight for time above 60°C in Figure 1.

What is clearly being observed in the thermoelasticity data of elastin-based systems in Figure 9, in the half-life studies for the elastic modulus at 80°C, and in the structural change above 60°C in Figure 1 is a slow thermal denaturation of protein-based elastomers. Since random chain networks do not exhibit thermal denaturation, these elastin-based systems are not properly described as random chain networks. *Thus, the evidence is clear and abundant; elastin-based systems contain regular repeating conformations and those ordered structures denature.*

4.1.2 Solvent entropy changes as a source of entropic elastic force?

4.1.2.1 *Effect of removal of solvent entropy change during inverse temperature transition:* The change in solvent entropy is fundamental to the occurrence of an inverse temperature transition. This transition has been extensively utilized to perform the family of energy conversions that sustain living organisms (Urry 1993, 1997), and therefore the inverse temperature transition is extensively characterized. One approach to testing whether the change in solvent entropy contributes to the elastomeric force is to utilize an approach due to Flory, that

is to reduce the heat of the inverse temperature transition to near zero by an appropriate solvent mixture. Hoeve and Flory (1958) had used a mixture of 30% ethylene glycol by weight in water in their thermoelasticity study that deduced a dominant entropic elastic force for fibrous elastin. When Luan et al (1989) compared the thermoelasticity-derived f_E/f ratio of X^{20}–poly(GVGVP) in water and in 30% ethylene glycol, the values were the same, 0.1. Based on the approximations of Eqns (7) and (8), X^{20}–poly(GVGVP) is a dominantly entropic elastomer in both solvent systems. The effect of adding the ethylene glycol is to reduce the heat of the transition to near zero. Now, since the entropy of the desolvation process is the heat of the transition divided by the temperature of the transition, $\Delta H_t/T_t$, the solvent entropy change would be approaching zero, and yet the solvent mixture, instead of reducing the elastomeric force, remarkably resulted in a substantial increase in force. The conclusion is that there is no experimental basis for believing that solvent entropy change contributed to elastomeric force.

4.1.2.2 *The polymer chains bear the force; solvation changes alter the fraction of chain segments that sustain the force*: The force of deformation must be borne by the chains; it cannot be borne by solvent. At fixed length, raising the temperature of a band of elastomer from below to above the temperature of the inverse temperature transition increases the force. Alternatively, increasing chemical potential to lower the transition temperature from above to below the operating temperature at fixed length causes an increase in elastomeric force (Urry et al 1997, 1988a, 1988b). These results are due to an increase in hydrophobic folding and assembly of the chains. Since this is the case at fixed length, the fraction of a chain length that is not folded must be further extended. Accordingly, in order to maintain a fixed length the unfolded segments must be further extended. This provides for the increase in entropic elastic force by means of a decrease in configurational entropy and not directly due to a change in solvent entropy..

4.1.3 Entropic elasticity due to damping of internal chain dynamic on extension

4.1.3.1 *Molecular structure of poly(GVGVP)*: In order to understand the concept of the damping of internal chain dynamics on extension, the structure given in Figure 10 is helpful. The Pro-Gly containing elastomeric sequential polypeptides exhibit a repeating β-turn structure as schematically shown in Figure 10A, and the β-turn is given in crystallographic detail in Figure 10B. On raising the temperature the inverse temperature transition results in the optimization of intramolecular and intermolecular hydrophobic association. Intramolecularly, this results in a helical structure called a β-spiral, which is shown schematically as a helix in Figure 10C, in more detail with β-turns schematically shown as spacers between turns of the helix in Figure 10D, and in atomic stereo detail in Figure 10E. Intramolecularly, the β-spirals associate to form multi-stranded twisted filaments, as depicted in Figure 10F. As there is water within the β-spiral and as a result of the β-turns functioning as spacers, the peptide segments connecting β-turns are free to undergo large amplitude torsional oscillations.

4.1.3.2 *Unrolled perspective of β-spiral showing suspended segment between β-turns*: Shown in Figure 11 is an unrolled perspective of the polypentapeptide β-spiral showing a suspended segment between β-turns where peptide moieties are free to undergo large amplitude torsional oscillations. In particular, the ψ_4-ϕ_5 pair of torsion angles and the ψ_5-ϕ_1 pair of torsion angles couple in each case to result in rocking motions of the respective peptides, i.e., in peptide librations. The point to be made is that the peptide moieties can undergo large torsional oscillations due to the absence of steric interactions in the hydrophobically folded β-spiral structure. This freedom of motion of the peptide moieties of the suspended segment within the β-spiral structure gives much entropy to the structure and is considered to be a primary source of the mechanical resonances of Figures 6, 7 and 8, as will be treated below.

4.1.3.3 *Effect of extension on the amplitude of the torsional oscillations and on chain entropy*: The magnitude of the torsional (dihedral angle) excursions for a single pentamer

sandwiched within a turn of β-spiral (three pentamers) for a 1.5 kcal/mol-residue cut-off energy is shown in Figure 12A when using the ECEPP molecular mechanics calculations of the Scheraga approach. Dihedral angle oscillations of 160° are possible. Lambda oscillational plots of ψ_i-ϕ_{i+1} for the two peptide moieties of Figure 11 are given in Figure 13 for the relaxed and extended (130%) states of poly(GVGVP) where the correlated motions of the pair of angles is apparent by the data points falling on a line with a slope of –1.

The effect of a 130% extension of the β-spiral pitch, shown structurally in Figure 12B and in the plots of Figure 13, is a dramatic decrease in the amplitude of the torsional oscillations allowed within a 1.5 kcal/mol-residue cut-off energy. Using an enumeration of states approach with each change of 5° in any torsion angle counted as a new state, the decrease in numbers of states for a 0.6 kcal/mol-residue cut-off energy (i.e., within an RT) is from a W^r of 342 to a W^e of 24. Using Eqn (10), this gives for ΔS a value of –5.28 cal/mol-deg/pentamer. If the Boltzmann summation over all energies is used, the value is –5.06 cal/mol-deg/pentamer (Urry et al 1985c).

The plots of Figure 13C show similar reductions in freedom of motion to the 130% extension on replacement of the Gly_5–residue by a D-Ala_5-residue. An expected reduction in the intensity of the 5 MHz relaxation has been observed and both are calculable using the peptide dipole reorientations of the pentapeptide moiety in the β-spiral structure (Venkatachalam and Urry, 1986). Furthermore, replacement of the Gly_5–residue by an L-Ala_5-residue resulted in complete loss of elasticity (Urry et al, 1983).

Alternatively, when using the molecular dynamics approach of Karplus, the expression becomes,

$$\Delta S = R \ln[\Pi_i \Delta\phi_i^e \Delta\psi_i^e / \Pi_i \Delta\phi_i^r \Delta\psi_i^r] \qquad (11)$$

where the product Π_i is over the rms (root mean square) torsion angle fluctuations $\Delta\phi_i^e$ and $\Delta\psi_i^e$ for the extended state divided by the product of the rms torsion angle fluctuations $\Delta\phi_i^r$ and $\Delta\psi_i^r$ for the relaxed state as obtained from the molecular dynamics trajectories for the relaxed and

130% extended states. The set of rms torsion angle fluctuations for the relaxed and extended states are given in Table 1, where the decreases in amplitude of the torsional oscillations as the result of extension are apparent. Using Eqn (11), the calculated decrease in entropy is –5.5 cal/mol-deg/pentamer for the 130% extension (Chang and Urry, 1989). Whether the calculation of entropy is by means of an enumeration of states in configuration space or the amplitude of the torsional oscillations in a molecular dynamic simulation, the calculated entropy change for a 130% extension is the same.

The $\Delta\phi$-$\Delta\psi$ representation of entropy change on extension of Eqn (11) provides an opportunity for a particularly insightful sense of entropy. Figure 14 plots in three dimensions the magnitude of the $\Delta\phi$, $\Delta\psi$ values for a chain segment of three torsion angles. As such, the volume is recognized by Eqn (11) as being proportional to the configurational entropy of the chain segment. The decrease in magnitude of the torsion angle oscillations on extension is seen as a decrease in volume, which is proportional to the decrease in the configurational entropy of the chain segment due to extension. Volume in configuration space provides a representation of chain entropy and a visualization of the decrease in entropy on extension. Obviously for a single chain of N-residues fixed at its ends, entropy of the chain can be represented as a volume in 2N-dimensional configurational space, and extension decreases the volume in N-dimensional configuration space, in a manner represented in Figure 14 for three dimensions. In particular, the values in Table 1 are actually the rms $\Delta\phi$ and $\Delta\psi$ for the relaxed state and the extended state. Especially for the suspended segment the decrease in rms $\Delta\phi$ and $\Delta\psi$ values are substantial on extension, leading to the calculated decrease in entropy on extension.

4.1.3.3 *Calculation of contribution of force due to decrease in freedom of motion on extension*: From Eqns (4) and (5) we have that

$$f_S = - T(\partial S/\partial L)_{V,T}. \qquad (12)$$

At physiological temperatures, 310K, and for an extension from .35 to .8 nm for a pentamer within the β-spiral structure of Figure 10E with a calculated decrease in entropy of 5.5 cal/mol-

deg/pentamer, the calculated value for the entropic contribution to the elastomeric force is 24 pN for a single chain of β-spiral.

To put this in terms of an elastic modulus in units of N/m^2, it is necessary to estimate the number of β-spirals per m^2. From Figure 1 the functional state is 37% peptide by weight. Taking the density of the peptide to be 1.3 gm/cm^3, there would be some 10^{17} β-spirals/m^2. The result would be 24 x 10^5 N/m^2. The calculated result is an order of magnitude higher than the experimental value of 1.6 x 10^5 N/m^2 for 20 Mrad cross-linked $(GVGVP)_{251}$. Several factors would be expected to result in a lower experimental elastic modulus for the matrix. Firstly, in the cross-linked matrix the β-spirals would be randomly oriented with respect to direction of extension. Secondly, the β-spirals occur as part of a multi-stranded twisted filament as shown in Figure 10F, which would somewhat restrict the freedom of motion of the torsional oscillations and result in a lower entropy change on extension. *What has been demonstrated, however, is that the damping of internal chain dynamics on extension provides an abundant source of entropic restoring force in elastin-based systems.* Furthermore, given the entropic elasticity of single chains demonstrated by the AFM single-chain force-extension curves for many different polymers, damping of internal chain dynamics on extension would seem to be a fundamental source for the development of entropic elastic force in chain molecules.

4.2 Dependence of entropy and structural free energy on oscillator frequency

One final point should be noted in this report. It is the significance of the occurrence of intense low frequency mechanical motions in elastin-based systems. The insight comes from the expression for the dependence of entropy on frequency of a harmonic oscillator as given in Figure 15. From the expression for the partition function of the harmonic oscillator (Dauber et al 1981), it is seen that the slope for the frequency dependence of entropy is –4.6 EU/logν_i. The extrapolation of the harmonic oscillator treatment to low frequency motions is surely not quantitative, but it is nonetheless informative. While the contribution of a classical vibration is

the order of 5 cal/mol-deg (EU), giving a Gibbs free energy of 1.5 kcal/mol at 298K, the contribution of the 5 MHz relaxation, seen in Figures 7 and 8, would be some 30 cal/mol-deg or 9 kcal/mol, and that for the acoustically activated mechanical resonance near 1 kHz, reported in Figure 6A, would approach 47 cal/mol-deg or 14 kcal/mol. From this it should be apparent that the mechanical relaxations of Figures 6, 7 and 8 arising from torsional oscillations are fundamental in providing for the entropic elasticity of elastin-based systems. On a more general note, computations of protein structure that do not include these important low frequency contributions to the free energy would seem to be limited in their treatment of the structure/function issue.

ACKNOWLEDGMENTS: The work was supported in part by the Office of Naval Research under contract Nos. N00014-00-C-0178 and N00014-00-C-0404.

REFERENCES

Buchet, R., Luan, C.-H., Prasad, K.U., Harris, R.D. & Urry, D.W. (1988). Dielectric Relaxation Studies on Analogs of the Polypentapeptide of Elastin, *J. Phys. Chem.* **92**, 511-517.

Butt, H. J. & Jaschke, M. (1995). Calculation of Thermal Noise in Atomic Force Microscopy. *Nanotechnology*, **6**,1-7.

Chang, D. K. & Urry, D. W. (1989). Polypentapeptide of Elastin: Damping of Internal Chain Dynamics on Extension. *J. Computational Chem.* **10**, 850-855.

Clausen-Schaumann, H.; Rief, M.; Tolksdorf, C. & Gaub, H. E. (2000). Mechanical Stability of Single DNA Molecules. *Biophys. J.*, 78.

Cleveland, J.P., Manne, S., Bocek, D., & Hansma, P.K. (1993). A Nondestructive Method for Determining the Spring Constant of Cantilevers for Scanning Force Microscopy. *Rev. Sci. Instrum.* , **64,** 403-405.

Cook, W.J., Einspahr, H.M., Trapane, T.L., Urry, D.W. & Bugg, C.E. (1980). Crystal Structure and Conformation of the Cyclic Trimer of a Repeat Pentapeptide of Elastin, Cyclo-(L-Valyl-L-prolylglycyl-L-valylglycyl)$_3$. *J. Am. Chem. Soc.* 102, 5502-5505,.

Cox, B.A., Starcher, B.C. & Urry, D.W. (1974). Coacervation of Tropoelastin Results in Fiber Formation. *J. Biol. Chem.* **249**, 997-998.

Cox, B.A., Starcher, B.C. & Urry, D.W. (1973). "Coacervation of α-Elastin Results in Fiber Formation," *Biochim. Biophys. Acta* **317**, 209-213.

Dauber, P., Goodman, M., Hagler, A. T., Osguthorpe, D., Sharon, R. & Stern, P. (1981). In *ACS Symposium Series No. 173, Suypercomputers in Chemistry* Lykos, P. & Shavitt, I., eds, pp.161-191. American Chemical Society, Washington, D. C.

Dorrington, K. L. & McCrum, N. G. (1977). Elastin as a Rubber. *Biopolymers* **16,** 1201-1222.

Eyring, H., Henderson, D., Stover, B. J. & Eyring, E. M. (1964). *Statistical Mechanics and Dynamics*, p.92. John Wiley & Sons Inc, New York.

Flory, P. J. (1953). *Principles of Polymer Chemistry* Cornell University Press, Ithaca, New York, Figure 121.

Flory, P. J. (1968). Molecular Interpretation of Rubber Elasticity, *Rubber Chem. and Tech.*, **41**: G41-G48.

Flory, P. J., Ciferri, A. & Hoeve, C. A. J. (1960). The Thermodynamic Analysis of Thermoelastic Measurements on High Elastic Materials. *J. Polymer Sci.* XLV, 235-236.

Gotte, L., Giro, G., Volpin, D. & Horne, R. W. (1974). The Ultrastructural Organization of Elastin *J. Ultrastruct. Res.* **46**, 23-33.

Grinberg, N. V., Dubovik, A. S., Grinberg, V. Y., Kuznetsov, D. V., Makhaeva, E. E., Grosberg, A. U. & Tanaka, T. (1999). Studies of the Thermal Volume Transition of Poly(N-isopropylacrylamide) Hydrogels by High Sensitivity Differential Scanning Microcalorimetry. 1. Dynamic Effects. *Macromolecules* **32,** 1471-1475.

Hoeve, C. A. J. & Flory, P. J. (1962). Elasticity of Crosslinked Amorphous Polymers in Swelling Equilibrium and Dilutents. *J. Polymer Sci.,* **60**, 155-164.

Hoeve, C. A. J. & Flory, P. J. (1958). The Elastic Properties of Elastin. *J. Amer. Chem. Soc.* **80**, 6523-6526.

Hoeve, C. A. J. & Flory, P. J. (1974). Elastic Properties of Elastin. *Biopolymers* **13**, 677-686.

Li, B., Alonso, D. O. V. & Daggett, V. (2000). The Molecular Basis for the Inverse Temperature Transition of Elastin, *J. Mol. Biol.* **305**, 581-592.

Luan, C.-H., Harris, R. D. & Urry, D. W. (1988). Dielectric Relaxation Studies on Bovine Ligamentum Nuchae," *Biopolymers* **27**, 1787-1793.

Luan, C.-H., Jaggard, J., Harris, R. D. & Urry, D. W. (1989). On the Source of Entropic Elastomeric Force in Polypeptides and Proteins: Backbone Configurational vs. Side Chain Solvational Entropy, *Intl. J. Quant. Chem.: Quant. Biol. Symp.* **16**, 235-244.

Manno, M., Emanuele, A., Martorana, V., San Biagio, P. L., Bulone, D., Palma-Vitorelli, M. B., McPherson, D. T., Xu, J., Parker, T. M., & Urry, D. W. (2001). "Interaction of processes on different time scales in a bioelastomer capable of performing energy conversion. *Biopolymers*, in press

Oesterhelt, F.; Rief, M., & Gaub, H. E. (1999). Single Molecule Force Spectroscopy by AFM Indicates Helical Structure of Poly(ethylene-glycol) in Water. *New J. Phys.* **1**, 6.1-6.11

Partridge, S. M., Davis, H. F. & Adair, G. S. (1955). The Chemistry of Connective Tissues. I. Soluble Proteins Derived from Partial Hydrolysis of Elastin. *Biochem. J.* **61,** 11-21.

Partridge, S. M. & Davis, H. F. (1955). The Chemistry of Connective Tissues. II. Composition of Soluble Proteins Derived from Elastin. *Biochem. J.* **61,** 21-30.

Partridge, S. M. (1966). Biosynthesis and Nature of Elastin Structures. *Federation Proceedings* **25**, 1023-1029.

Partridge, S. M. (1967). Diffusion of Solutes in Elastin Fibers. *Biochim. Biophys. Acta* **140**, 132-141.

Rief, M., Oesterhelt, F., Heymann, B., & Gaub, H.E. (1997). Single Molecule Force Spectroscopy on Polysaccharides by Atomic Force Microscopy Science. *Science* **275**, 1295-1297.

San Biagio, P.L. Madonia, F. Trapane, T.L. & Urry, D.W. (1988). Overlap of Elastomeric Polypeptide Coils in Solution Required for Single-Phase Initiation of Elastogenesis, *Chem. Phys. Letters*. **145**, 571-574.

Sciortino, F. K., Prasad, K. U., Urry, D. W. & Palma, M. U. (1993). Self-Assembly of Bioelastomeric Structures From Solutions: Mean Field Critical Behavior and Flory-Huggins Free-Energy of Interaction," *Biopolymers* **33**, 743–52.

Sheiba, L. (May 14, 1996). Broad Band Method and Apparatus for the Precise Measurement of the Complex Modulus of Viscoelastic Materials. U.S. Patent 08/645,878, Pending.

Urry, D.W. (1976). On the Molecular Mechanisms of Elastin Coacervation and Coacervate Calcification, *Faraday Discussions of The Chem. Soc.* No. **61**, 205-212.

Urry, D.W. (1988a). Entropic Elastic Processes in Protein Mechanisms. I. Elastic Structure Due to an Inverse Temperature Transition and Elasticity Due to Internal Chain Dynamics, *J. Protein Chem.* **7**, 1-34.

Urry, D.W. (1988b). Entropic Elastic Processes in Protein Mechanism. II. Simple (Passive) and Coupled (Active) Development of Elastic Forces, *J. Protein Chem.* **7**, 81-114.

Urry, D.W. (1993). Molecular Machines: How Motion and Other Functions of Living Organisms Can Result from Reversible Chemical Changes, *Angew. Chem. (German)* **105**, 859-883, 1993; *Angew. Chem. Int. Ed. Engl.*, **32**, 819-841.

Urry, D.W. (1997). Physical Chemistry of Biological Free Energy Transduction as Demonstrated by Elastic Protein-based Polymers, invited FEATURE ARTICLE, *J. Phys. Chem.*B, **101**,11007-11028.

Urry, D.W., Long, M.M. & Sugano, H. (1978). Cyclic Analog of Elastin Polyhexapeptide Exhibits an Inverse Temperature Transition Leading to Crystallization. *J. Biol. Chem.* **253**, 6301-6302.

Urry, D.W., Venkatachalam, C.M., Long M.M. & Prasad, K.U. (1982). Dynamic β-Spirals and A Librational Entropy Mechanism of Elasticity. In *Conformation in Biol.* (R. Srinivasan and R.H. Sarma, Eds.), pp.11-27. G.N. Ramachandran Festschrift Volume, Adenine Press, USA.

Urry, D.W. & Venkatachalam, C. M. (1983). "A Librational Entropy Mechanism for Elastomers with Repeating Peptide Sequences in Helical Array," *Int. J. Quant. Chem.: Quant. Biol. Symp.* **10**, 81-93.

Urry, D.W., Wood, S.A., Harris, R.D. & Prasad, K.U. (1984). Polypentapeptide of Elastin as an Elastomeric Biomaterial, In *Polymers as Biomaterials* (S.W. Shalaby, T. Horbett, A.S. Hoffman and B. Ratner, Eds.) . pp.17-32. Plenum Publishing Corporation, New York, New York

Urry, D.W., Henze, R., Redington, P., Long M.M. & Prasad, K.U. (1985a). Temperature Dependence of Dielectric Relaxations in α-Elastin Coacervate: Evidence for a Peptide Librational Mode, Biochem. *Biophys. Res. Commun.* **128**, 1000-1006.

Urry, D.W., Trapane, T. L. & Prasad, K.U. (1985b). Phase-Structure Transitions of the Elastin Polypentapeptide-Water System Within the Framework of Composition-Temperature Studies. *Biopolymers* **24**, 2345-2356.

Urry, D. W., Venkatachalam, C. m., Wood, S.A. & Prasad, K. U. (1985c). "Molecular Structures and Librational Processes in Sequential Polypeptides: From Ion Channel Mechanisms to Bioelastomers," In *Structure and Motion: Membr., Nucleic Acids and Proteins,* (E. Clementi, G. Corongiu, M.H. Sarma and R.H. Sarma, Eds.), pp.185-203. Adenine Press, Guilderland, New York.

Urry, D.W., Harris, R.D., & Prasad, K.U. (1988a). Chemical Potential Driven Contraction and Relaxation by Ionic Strength Modulation of an Inverse Temperature Transition, *J. Am. Chem. Soc.* **110,** 3303-3305.

Urry, D.W., Haynes, B., Zhang, H., Harris, R.D., & Prasad, K.U. (1988b). Mechanochemical Coupling in Synthetic Polypeptides by Modulation of an Inverse Temperature Transition," *Proc. Natl. Acad. Sci.* USA **85**, 3407-3411.

Urry, D. W., Peng, S.Q., Xu, J. & McPherson, D. T. (1997). Characterization of Waters of Hydrophobic Hydration by Microwave Dielectric Relaxation, *J. Amer. Chem. Soc.,* **119**, 1161–1162.

Urry, D. W., Hugel, T., Seitz, M., Gaub, H., Sheiba, L., Dea, J., Xu, J., & Parker, T. (in press) Elastin: A Representative Ideal Protein Elastomer, *Philos. Trans. R. Soc. London [Biol].*

Venkatachalam, C. M. & Urry, D. W. (1986). "Calculation of Dipole Moment Changes Due to Peptide Librations in the Dynamic β-Spiral of the Polypentapeptide of Elastin," Înt. J. Quant. Chem.: Quant. Biol. Symp., ***12,*** *15-24*

Vrhovski, B., Jensen, S., & Weiss, A. S. (1997). Coacervation Characteristics of Recombinant Human Tropoelastin. *Eur. J. Biochem.* **250**, 92-98.

Volpin, D., Urry, D.W., Pasquali-Ronchetti, I. & Gotte, L. (1976). Studies by Electron Microscopy on the Structure of Coacervates of Synthetic Polypeptides of Tropoelastin. *Micron.* **7**, 193-198.

Weis-Fogh, T. & Andersen, S. O. (1970). New Molecular Model for the Long-range Elasticity of Elastin. *Nature* **227**, 718-721.

Wu, W. J., Vrhovski, B., & Weiss, A. S. (1999). Glycosaminoglycans Mediate the Coacervation of Human Tropoelastin Through Dominant Charge Interactions Involving Lysine Side Chains. *J. Biol. Chem.* **274**, 21719-21724

FIGURE LEGENDS

Figure 1: Plot of the percent water by weight as a function of temperature for poly(GVGVP) showing a stable intermediate structured state of 63% water by weight between 30 and 60°C, a state that slowly denatures above 60°C to form a state containing 32% water by weight. Plotted from the data of Urry et al 1985b. Amphiphilic (LCST, lower critical solution temperature) polymers such as PNIPAM, poly(N-isopropyl acrylamide), exhibit only a single, sharper transition, and it is to what is generally considered a disordered state with about 30% water by weight. Plotted from the data of Grinberg et al 1999.

Figure 2: Schematic diagram of an atomic force microscope apparatus adapted for varying the z-direction for obtaining force-extension curves of single-chains.

Figure 3: Single-chain force-extension curves for Cys-$(GVGVP)_{nx251}$-Cys at a temperature below the onset temperature for hydrophobic folding and assembly for this composition. The initial trace is given at the bottom and subsequent traces of the same chain without intervening detachment are displaced vertically by 250 pN. The second and fifth curves exhibit perfect reversibility. The curves marked by an asterisk and the initial curve were the result of a period of at least 30 s in the relaxed state, where one possibility is that some hydrophobic back-folding occurs. Reproduced with permission Urry et al, 2002.

Figure 4: Single-chain force-extension curves for Cys-$(GVGIP)_{nx260}$-Cys at a temperature above the onset temperature for hydrophobic folding and assembly for this composition. In each case the energy expended in deformation is greater than that recovered on relaxation. In addition there appears to be a complex relaxation curve. Reproduced with permission Urry et al, 2002.

Figure 5: A. Block diagram of the instrumentation used to determine the absorption per unit volume of elastic samples in the acoustic range. B. Example of the use of two samples that differ in length by a factor of two as required for the analysis of Sheiba (1996) to be utilized.

Figure 6: A. Plots of the loss factor (absorption per unit volume) for a series of elastomers. The bottom curve is of natural rubber and the slightly higher structure-less curve is for polyurethane, which is recognized as a rubber with a high loss factor in the acoustic absorption range. The upper four curves are of 20 Mrad cross-linked $(GVGVP)_{260}$. As the temperature is raised above the temperature for the inverse temperature transition of hydrophobic folding and assembly for this composition, the intensity for a localized relaxation grows dramatically. To the best of our knowledge, these model elastic protein-based polymers exhibit the greatest sound absorption for the 100 Hz to 10,000 Hz frequency range. This demonstrates the formation of a regular structure for $(GVGIP)_n$ in contrast to the lack of a regular structure for the classical rubbers. Reproduced with permission from Urry et al, 2002.

B. The imaginary (absorptive) part of the dielectric permittivity of poly(GVGIP). The same phenomenon of increased absorption on passing through the temperature range of the inverse temperature transition is observed in the 100 Hz to 10,000 Hz frequency range as exhibited by the same composition in the acoustic absorption range. In this case the temperature is increased to 40°C and the intensity of the relaxation continues to rise.

Figure 7: A. The real part of the dielectric permittivity for poly(GVGIP).

B. The imaginary (absorptive) part of the dielectric permittivity of poly(GVGIP). The same phenomenon of increased absorption on passing through the temperature range of the inverse temperature transition is observed in the 1 MHz to 100 MHz range as exhibited by the same composition in the acoustic absorption range in Figure 6. Reproduced with permission from Buchet et al 1988. Such low frequency motions provide a source of entropic elasticity and low

energy for the structural state of the elastic protein-based polymers. Reproduced with permission from Buchet et al, 1988.

Figure 8: A. The real part of the dielectric permittivity of α-elastin showing an increasing relaxation near 5 MHz with increasing temperature from below to above the temperature range for the inverse temperature transition. The data for α-elastin is nearly identical to that found for poly(GVGVP) shown in the insert for a single temperature below and one above that of the inverse temperature transition. This demonstrates that the same relaxation occurs in a fragment of the natural elastic fiber as has been so thoroughly characterized in the model elastic proteins, poly(GVGVP) and poly(GVGIP). Reproduced with permission from Urry et al, 1985a.
B. The imaginary (absorptive) part of the dielectric permittivity of natural fibrous elastin showing an increasing relaxation near 5 MHz with increasing temperature from below (23°C) to above (58°C) the temperature range for the inverse temperature transition. The same relaxation is seen at 58°C with a somewhat higher intensity and a slightly higher frequency is found for the 20 Mrad cross-linked poly(GVGVP). It seems quite evident that dynamic structured states occur in the natural elastic fiber as demonstrated for the model elastic protein-based polymer. Adapted with permission from Luan et al, 1988.

Figure 9: Thermoelasticity curves for A. fibrous elastin and B. 20 Mrad cross-linked poly(GVGVP). See text for discussion. Whether or not a near zero slope, i.e., an $f_E/f << 1$, is obtained depends on the rate at which the temperature is raised. This is due to a slow denaturation at temperatures above 60°C. Reproduced with permission from Urry 1988a, 1988b.

Figure 10: Description of the proposed molecular structure of poly(GVGVP). See text for discussion.

Figure 11: Unrolled perspective of one-half turn of a β-spiral showing the suspended segment between β-turns. Due to the near collinearity of the bonds on each side of a peptide moiety, the peptide moiety can undergo rocking motions. In particular, the indicated suspended segment there are two peptide moieties with the ψ_4-ϕ_5 pair of torsion angles and the ψ_5-ϕ_1 pair of torsion angles. These pairs of torsion angles couple in each case to result in rocking motions of the respective peptides, referred to as peptide librations. Such motions provide much entropy to the β-spiral structure and to all protein structures that allow for these coupled motions and it is a decrease in this chain dynamics on extension that is a dominant source of entropic elasticity exhibited by single chains.

Figure 12: Stereo view of the torsional oscillations possible within a 2 kcal/mol-residue cut-off energy for the central pentamer of one turn (three pentamers) of the β-spiral structure of poly(GVGVP) in the relaxed state in A. and in the 130% extended state in B. See text for discussion. Reproduced with permission from Urry and Venkatachalam, 1983.

Figure 13: Lambda plots of the torsion angles attending the peptide moieties of the suspended segment of poly(GVGVP) and an analogue. The slopes of negative one demonstrate the correlated motions of the β-spiral structure of poly(GVGVP) in A and B and of the D-Ala (A') analog, poly(GVA'VP). Extension to 130% dramatically decreases the number of states of the polymer that are available within a given energy cut-off as does the substitution of the D-residue. The decrease in number of states, as discussed in the text, represent a decease in entropy of the structure. Reproduced with permission from Urry et al, 1982, Urry and Venkatachalam, 1983, Venkatachalam and Urry 1986.

Figure 14: Representation of entropy as a volume in a $\Delta\phi_i$-$\Delta\psi_i$ configuration space. See text for further discussion.

Figure 15: Plot of the above equation for entropy as a function of log(oscillator frequency) using the partition function of an harmonic oscillator. On the left-hand ordinate is plotted the entropy in cal/mol-deg (EU, entropy units), and on the right-hand ordinate is plotted the Gibbs free energy in kcal/mol at 298°K. This illustrates the increasing contribution of low frequency oscillations to the entropy of a polypeptide chain.

Table 1 Listing of the ϕ and ψ torsion angles for the central six pentamers of $(VPGVG)_{11}$ and the root mean square (RMS) fluctuations of those torsion angles, i.e., the $\Delta\phi_i$ and $\Delta\psi_i$, in columns for the relaxed and 130% extended states arising from 45 picosecond equilibration time and 80 picosecond of molecular dynamics simulation for each state.

	angle	relaxed	extended	angle	relaxed	extended	angle	relaxed	extended
β-turns	ψ_{16}	10·87	14·17	ψ_{26}	27·33	07·64	ψ_{36}	20·19	14·84
	ϕ_{17}	09·86	15·18	ϕ_{27}	11·71	08·33	ϕ_{37}	08·99	10·47
	ψ_{17}	47·59	46·68	ψ_{27}	11·70	13·51	ψ_{37}	21·53	32·96
	ϕ_{18}	61·70	47·41	ϕ_{28}	08·61	10·36	ϕ_{38}	11·15	10·66
	ψ_{18}	09·37	16·05	ψ_{28}	09·33	08·16	ψ_{38}	11·09	27·29
	ϕ_{19}	14·25	08·67	ϕ_{29}	09·70	07·31	ϕ_{39}	12·70	10·24
suspended segments	ψ_{19}	44·09	10·99	ψ_{29}	47·32	10·48	ψ_{39}	52·00	12·50
	ϕ_{20}	41·94	09·29	ϕ_{30}	48·57	11·39	ϕ_{40}	55·88	08·37
	ψ_{20}	14·50	11·15	ψ_{30}	42·56	10·62	ψ_{40}	40·67	11·08
	ϕ_{21}	27·13	24·17	ϕ_{31}	11·43	11·38	ϕ_{41}	36·44	19·06
β-turns	ψ_{21}	09·39	22·73	ψ_{31}	12·17	09·21	ψ_{41}	12·97	14·80
	ϕ_{22}	09·94	08·00	ϕ_{32}	09·90	08·93	ϕ_{42}	11·59	07·33
	ψ_{22}	11·58	16·13	ψ_{32}	15·30	10·80	ϕ_{42}	11·34	13·17
	ϕ_{23}	16·37	09·33	ϕ_{33}	09·60	07·62	ψ_{43}	09·23	09·76
	ψ_{23}	14·33	14·25	ψ_{33}	09·88	09·43	ϕ_{43}	10·60	12·53
	ϕ_{24}	11·39	29·20	ϕ_{34}	11·86	09·71	ϕ_{44}	11·06	12·82
suspended segments	ψ_{24}	19·53	37·87	ψ_{34}	63·80	08·36	ψ_{44}	41·89	35·22
	ϕ_{25}	25·02	23·06	ϕ_{35}	91·70	10·20	ϕ_{45}	48·98	31·31
	ψ_{25}	49·32	32·10	ψ_{35}	15·03	11·51	ψ_{45}	42·05	56·89
	ϕ_{26}	31·43	27·24	ϕ_{36}	21·49	18·66	ϕ_{46}	21·55	30·33

Reproduced with permission Chang and Urry, 1989

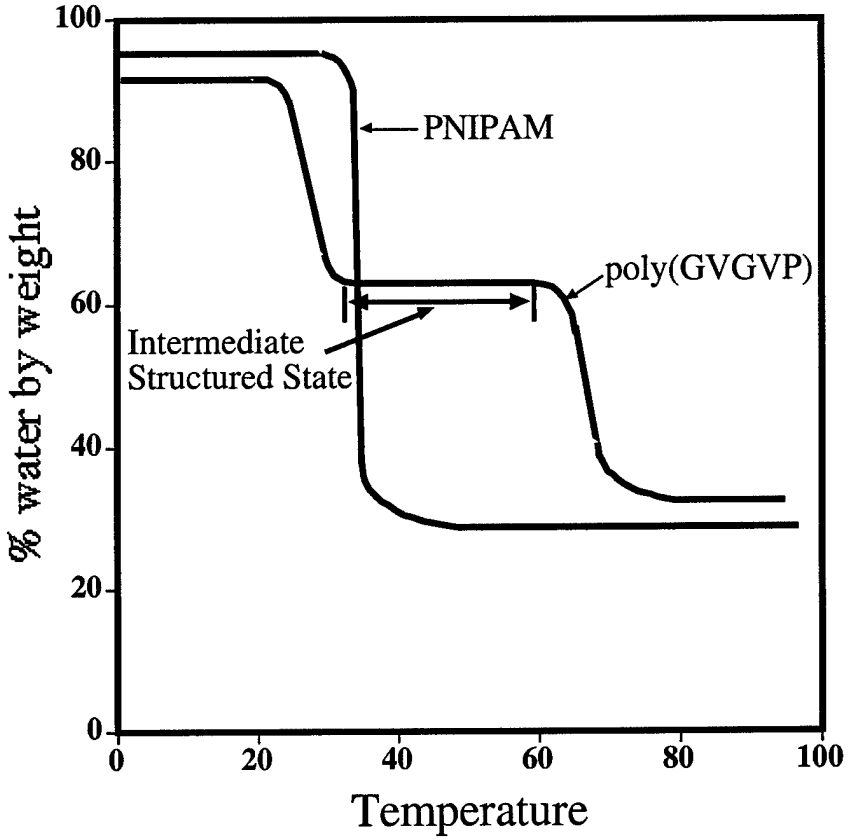

Figure 1: Plot of the percent water by weight as a function of temperature for poly(GVGVP) showing a stable intermediate structured state of 63% water by weight between 30 and 60°C, a state that slowly denatures above 60°C to form a state containing 32% water by weight. Plotted from the data of Urry et al 1985b. Amphiphilic (LCST, lower critical solution temperature) polymers such as PNIPAM, poly(N-isopropyl acrylamide), exhibit only a single, sharper transition, and it is to what is generally considered a disordered state with about 30% water by weight. Plotted from the data of Grinberg et al 1999.

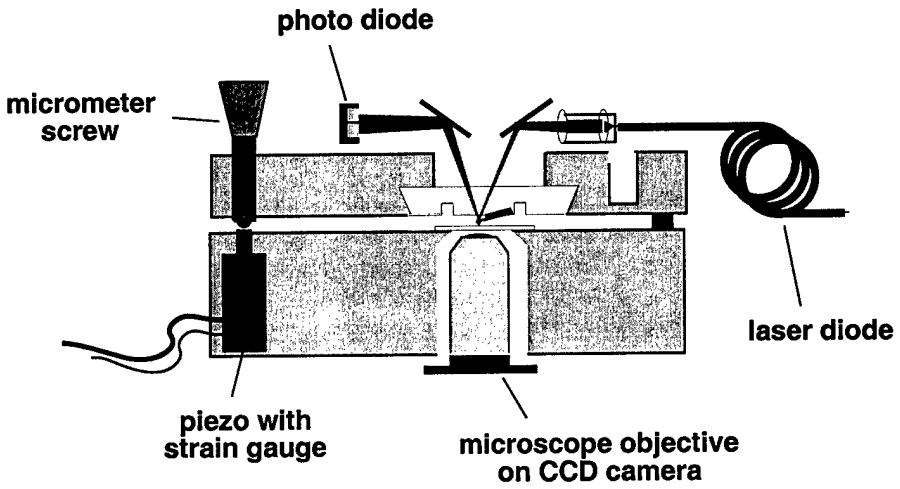

Figure 2: Schematic diagram of an atomic force microscope apparatus adapted for varying the z-direction for obtaining force-extension curves of single-chains.

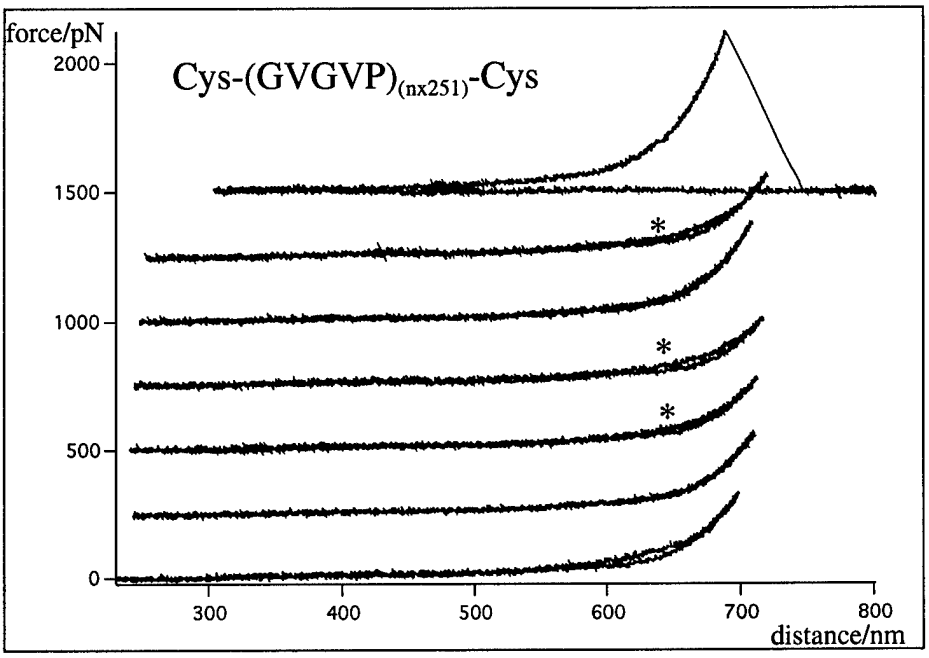

Successive traces from bottom to top, shifted by 250 pN. Before the traces with the *where taken, the chain was at least for 30 s in the relaxed state.

Figure 3: Single-chain force-extension curves for Cys-$(GVGVP)_{nx251}$-Cys at a temperature below the onset temperature for hydrophobic folding and assembly for this composition. The initial trace is given at the bottom and subsequent traces of the same chain without intervening detachment are displaced vertically by 250 pN. The second and fifth curves exhibit perfect reversibility. The curves marked by an asterisk and the initial curve were the result of a period of at least 30 s in the relaxed state, where one possibility is that some hydrophobic back-folding occurs. Reproduced with permission Urry et al, 2002

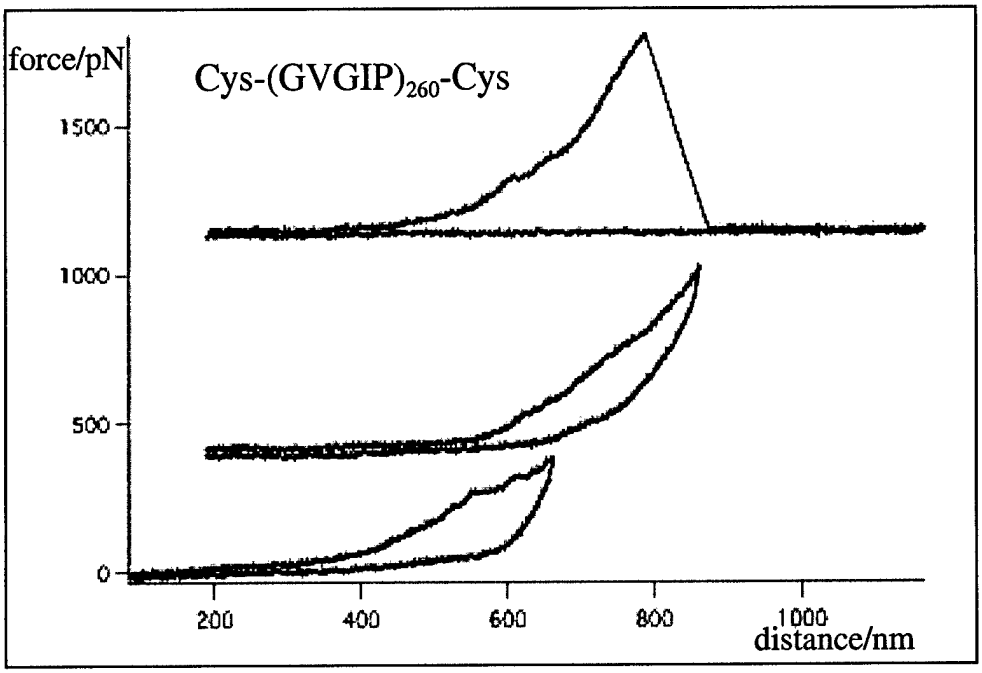

Figure 4: Single-chain force-extension curves for Cys-$(GVGIP)_{nx260}$-Cys at a temperature above the onset temperature for hydrophobic folding and assembly for this composition. In each case the energy expended in deformation is greater than that recovered on relaxation. In addition there appears to be a complex relaxation curve. Reproduced with permission Urry et al, 2002.

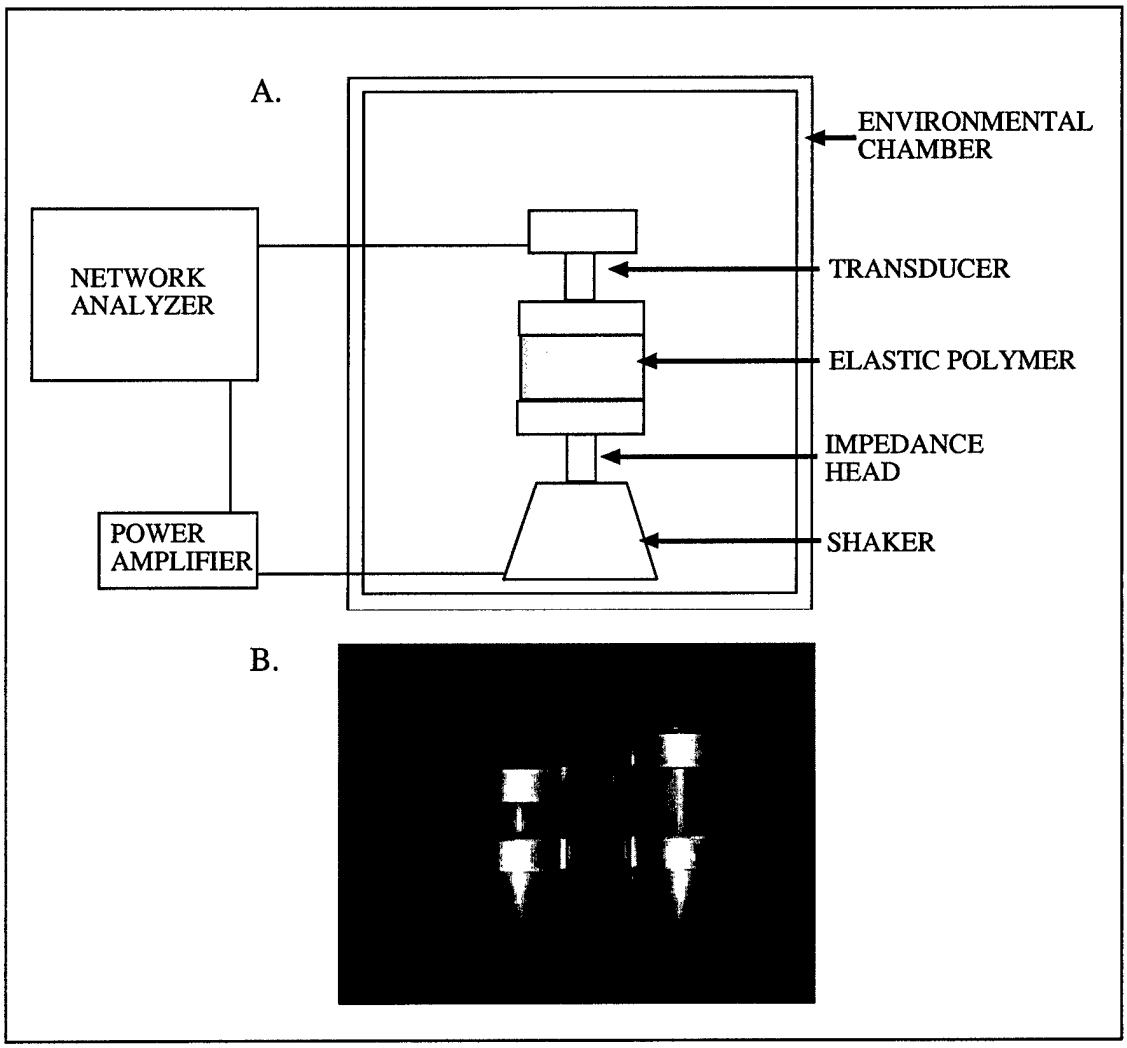

Figure 5: A. Block diagram of the instrumentation used to determine the absorption per unit volume of elastic samples in the acoustic range. B. Example of the use of two samples that differ in length by a factor of two as required for the analysis of Sheiba (1996) to be utilized.

A. $(GVGIP)_{260}$ Acoustic Absorption

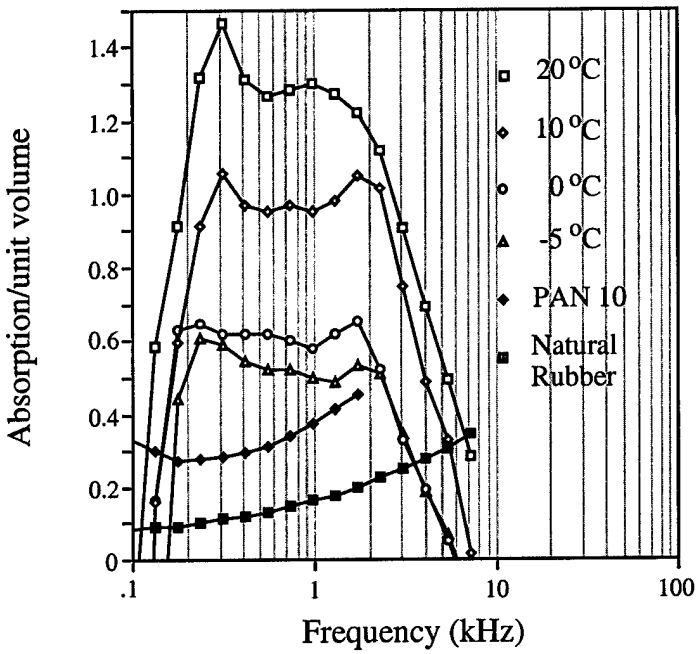

B. $(GVGIP)_{320}$ Dielectric Relaxation

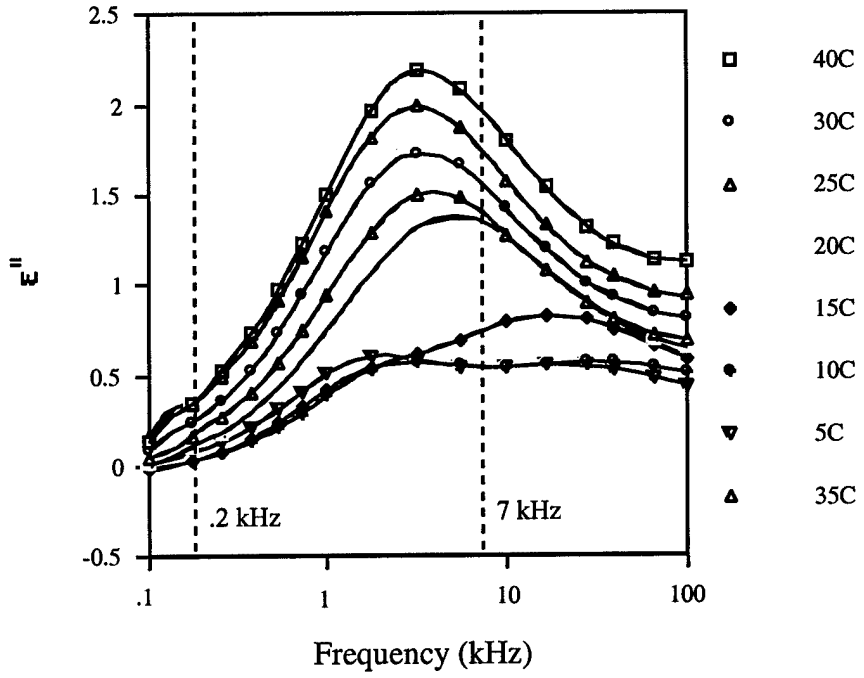

Figure 6: See the figure legend list.

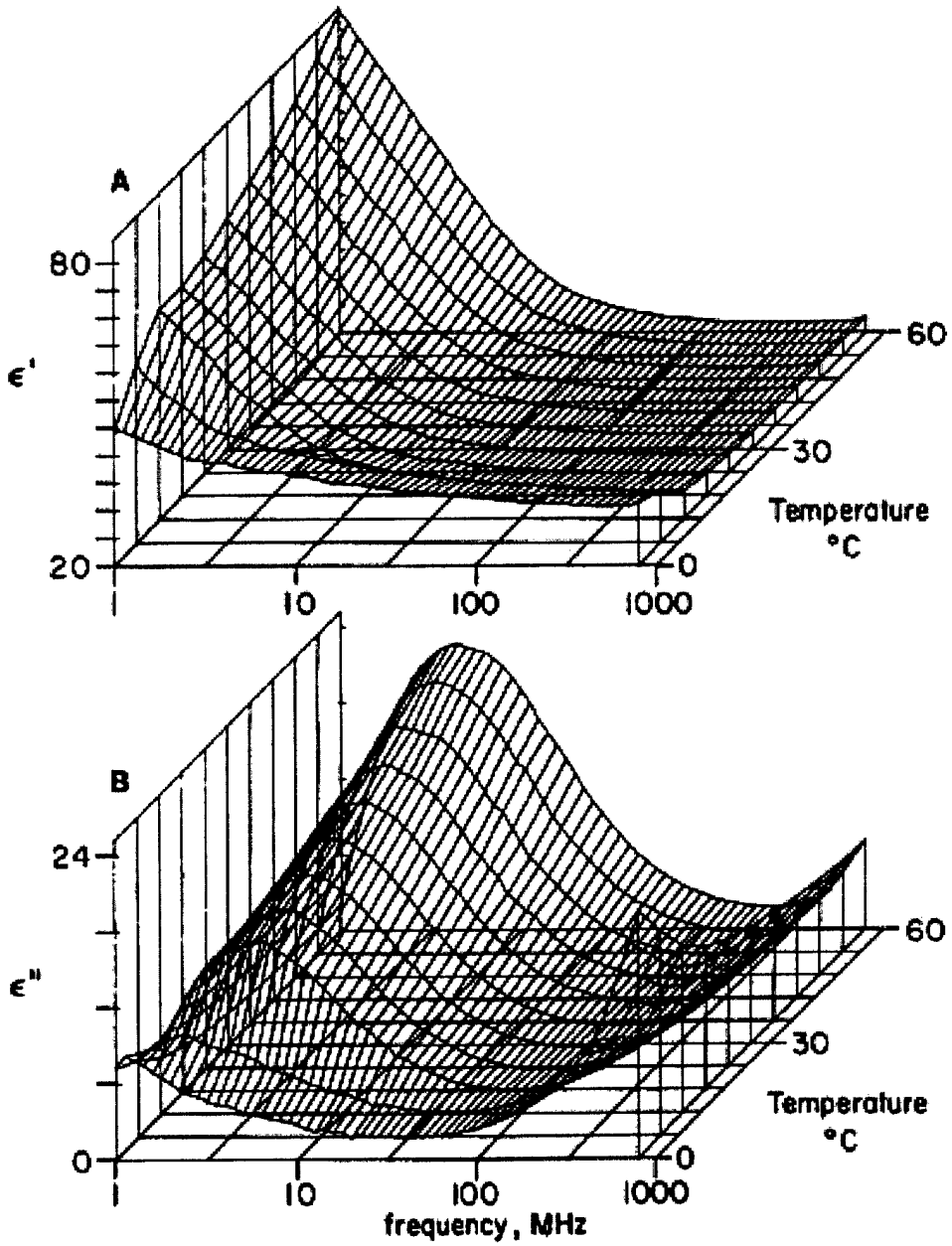

Figure 7: A. The real part of the dielectric permittivity for poly(GVGIP).

B. The imaginary (absorptive) part of the dielectric permittivity of poly(GVGIP). The same phenomenon of increased absorption on passing through the temperature range of the inverse temperature transition is observed in the 1 MHz to 100 MHz range as exhibited by the same composition in the acoustic absorption range in Figure 6. Reproduced with permission from Buchet et al 1988. Such low frequency motions provide a source of entropic elasticity and low energy for the structural state of the elastic protein-based polymers. Reproduced with permission from Buchet et al, 1988.

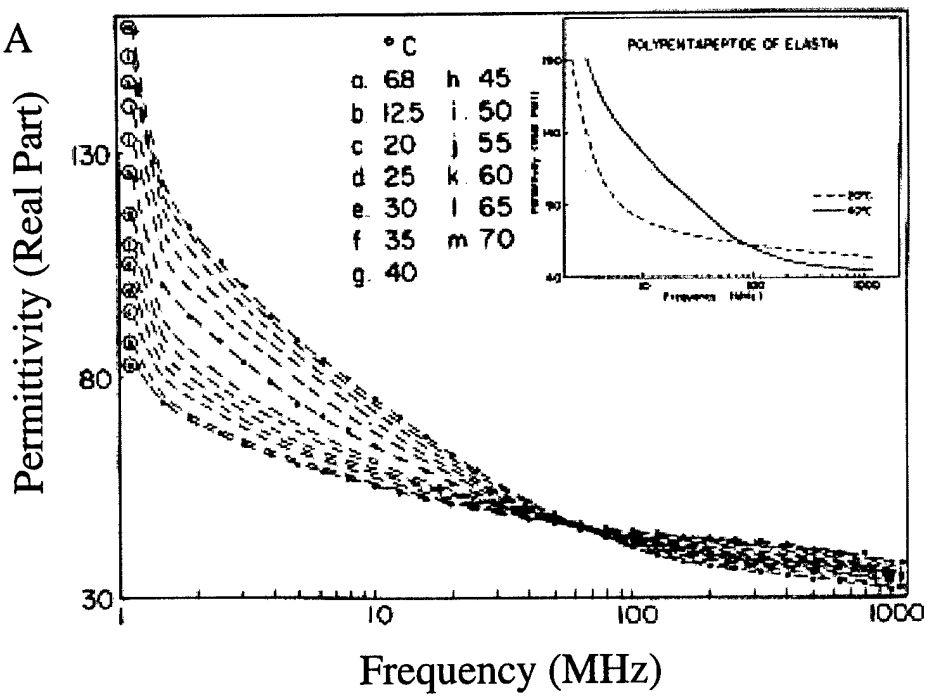

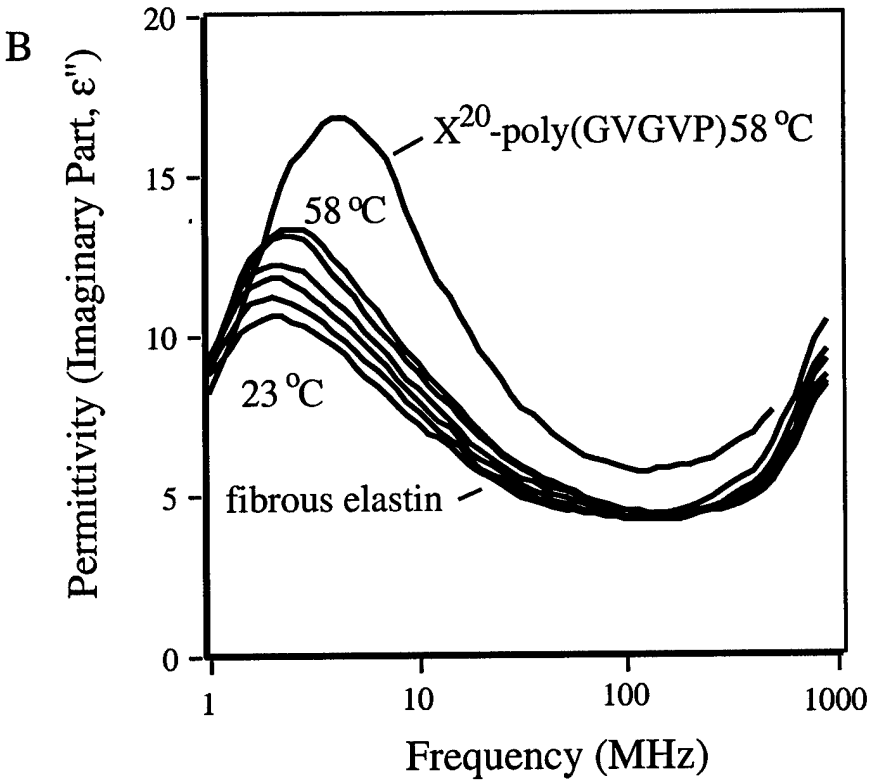

Figure 8: See the figure legend list.

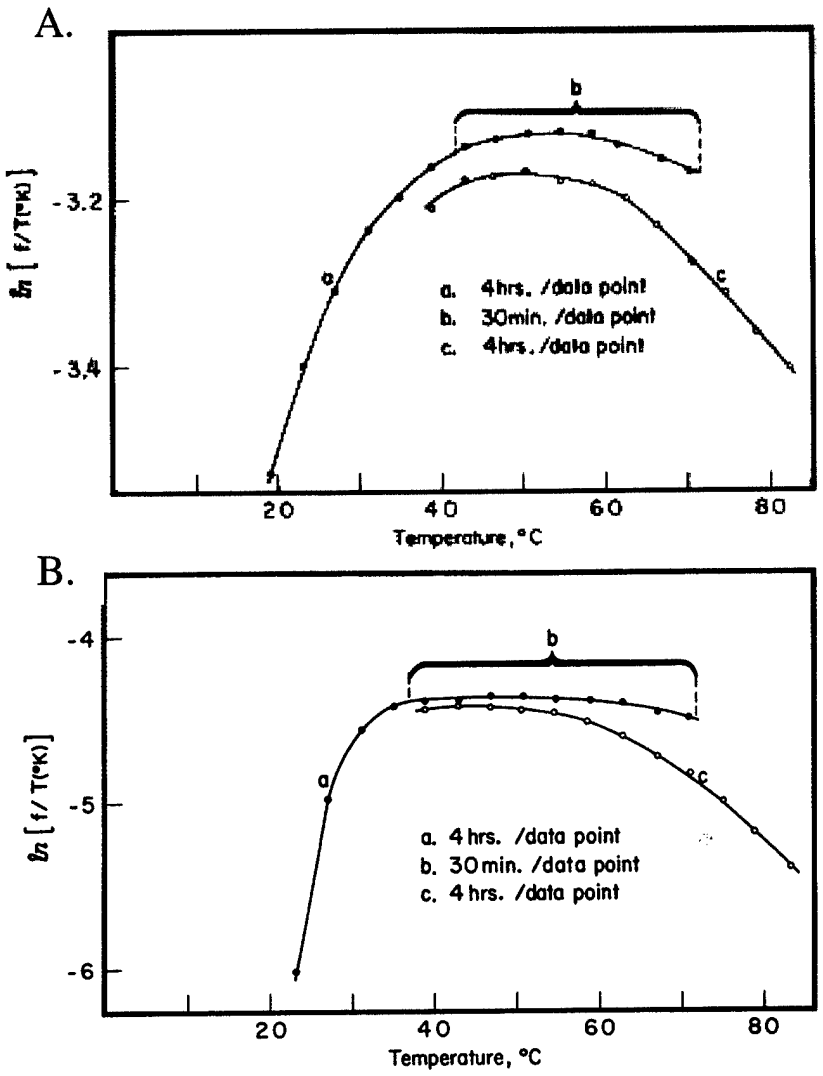

Figure 9: Thermoelasticity curves for A. fibrous elastin and B. 20 Mrad cross-linked poly(GVGVP). See text for discussion. Whether or not a near zero slope, i.e., an $f_E/f << 1$, is obtained depends on the rate at which the temperature is raised. This is due to a slow denaturation at temperatures above 60°C. Reproduced with permission from Urry 1988a, 1988b.

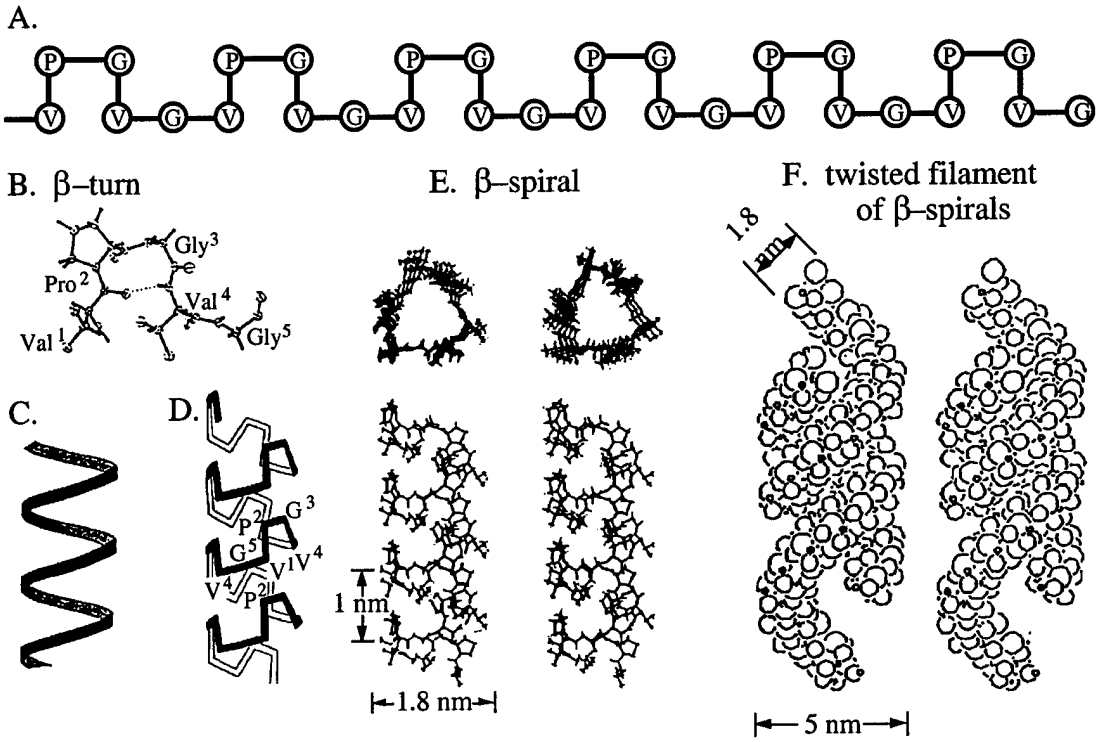

Figure 10: Description of the proposed molecular structure of poly(GVGVP). See text for discussion.

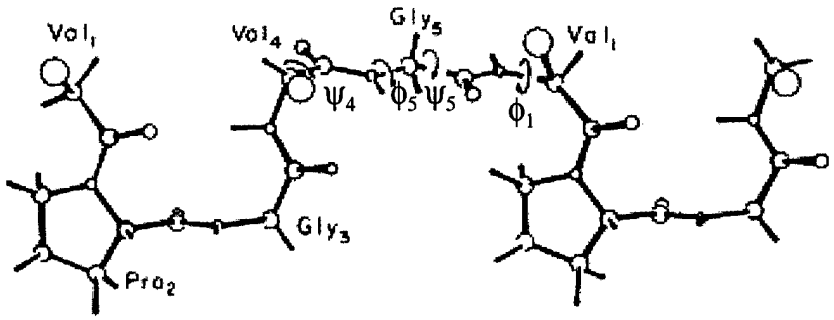

Figure 11: Unrolled perspective of one-half turn of a β-spiral showing the suspended segment between β-turns. Due to the near collinearity of the bonds on each side of a peptide moiety, the peptide moiety can undergo rocking motions. In particular, the indicated suspended segment there are two peptide moieties with the ψ_4-ϕ_5 pair of torsion angles and the ψ_5-ϕ_1 pair of torsion angles. These pairs of torsion angles couple in each case to result in rocking motions of the respective peptides, referred to as peptide librations. Such motions provide much entropy to the β-spiral structure and to all protein structures that allow for these coupled motions and it is a decrease in this chain dynamics on extension that is a dominant source of entropic elasticity exhibited by single chains.

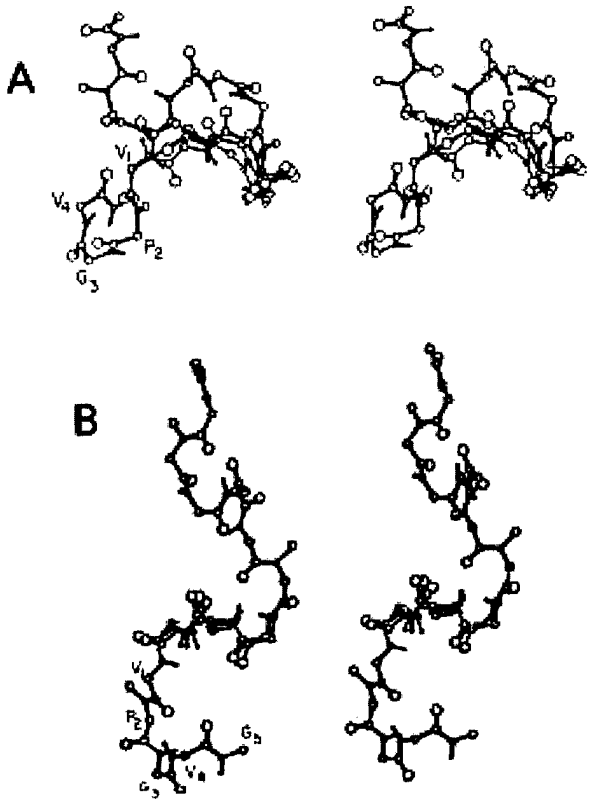

Figure 12: Stereo view of the torsional oscillations possible within a 2 kcal/mol-residue cut-off energy for the central pentamer of one turn (three pentamers) of the β-spiral structure of poly(GVGVP) in the relaxed state in A. and in the 130% extended state in B. See text for discussion. Reproduced with permission from Urry and Venkatachalam, 1983.

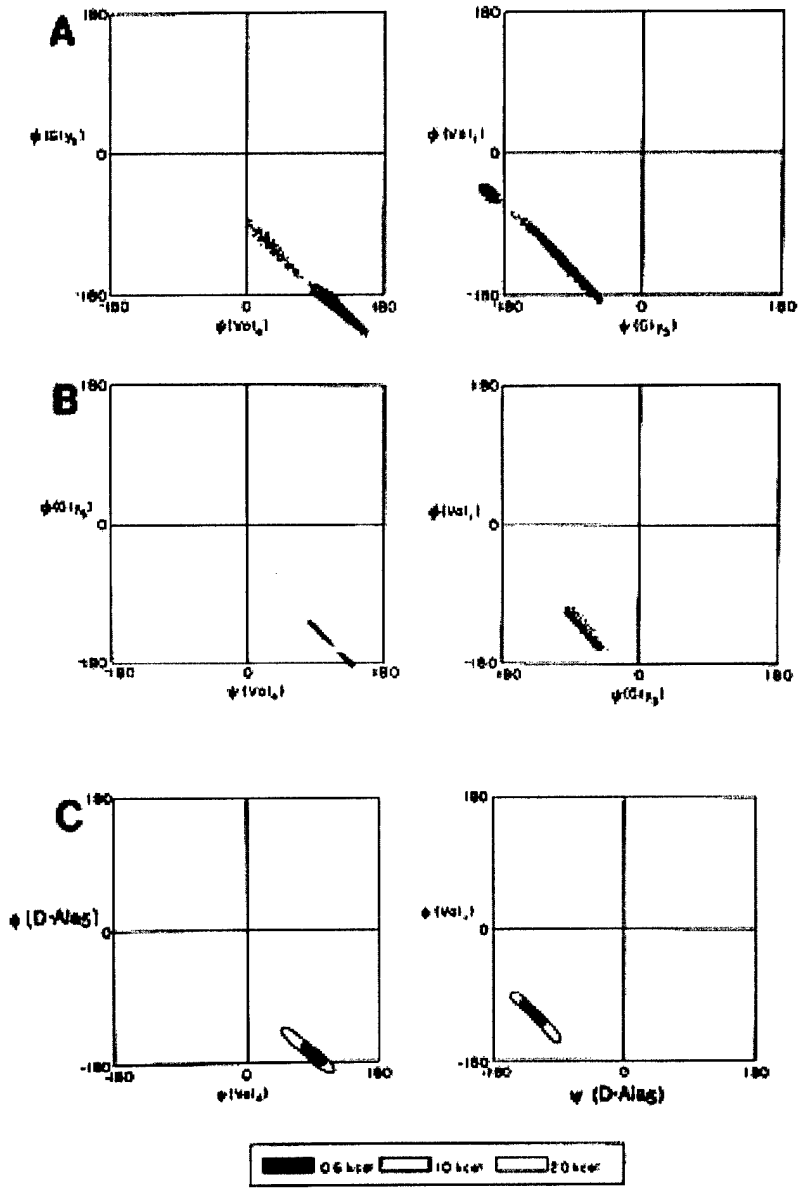

Figure 13: Lambda plots of the torsion angles attending the peptide moieties of the suspended segment of poly(GVGVP) and an analogue. The slopes of negative one demonstrate the correlated motions of the β-spiral structure of poly(GVGVP) in A and B and of the D-Ala (A') analog, poly(GVA'VP). Extension to 130% dramatically decreases the number of states of the polymer that are available within a given energy cut-off as does the substitution of the D-residue. The decrease in number of states, as discussed in the text, represent a decease in entropy of the structure. Reproduced with permission from Urry et al, 1982, Urry and Venkatachalam, 1983, Venkatachalam and Urry 1986.

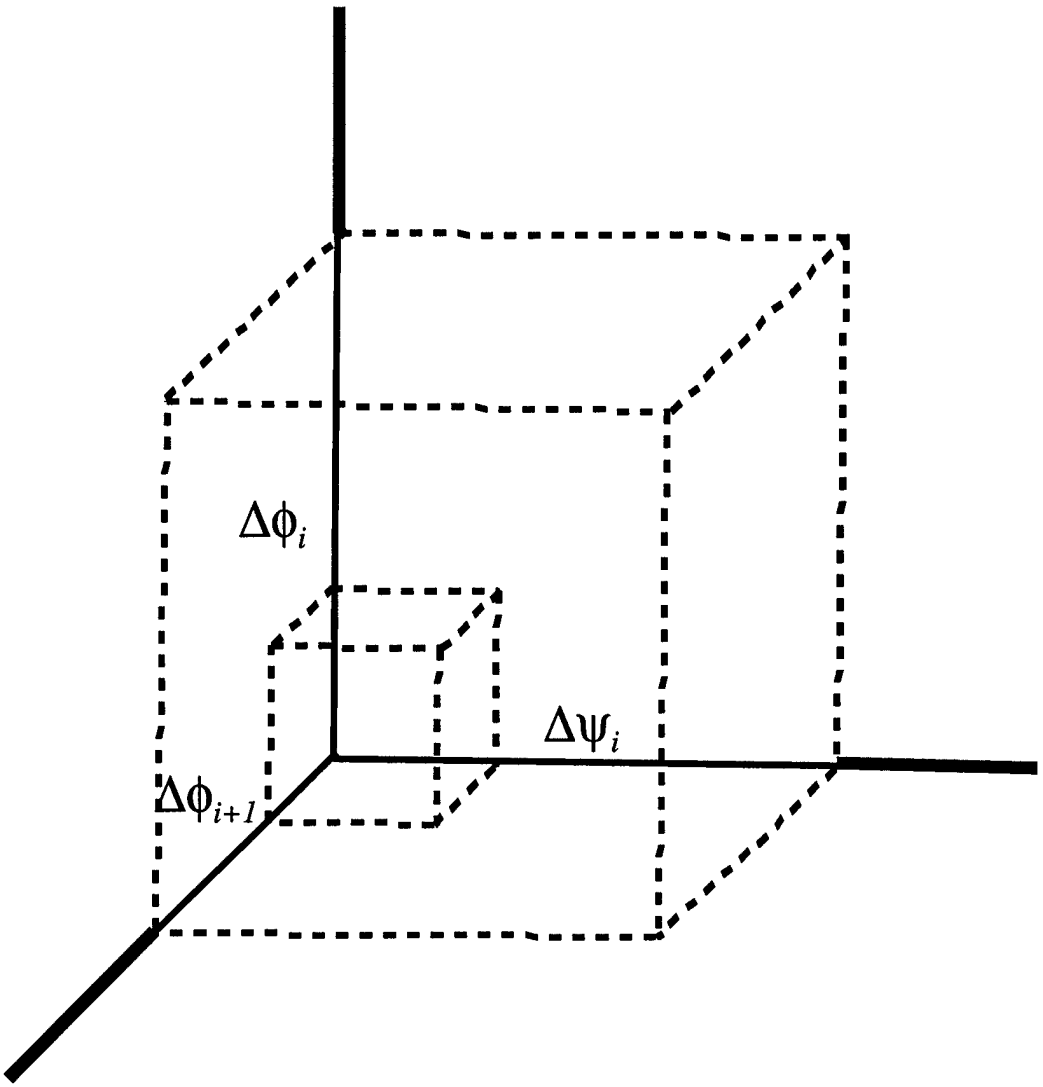

Figure 14: Representation of entropy as a volume in a $\Delta\phi_i$-$\Delta\psi_i$ configuration space. See text for further discussion.

$$S_i = R[\ln(1-e^{-h\nu_i/kT})^{-1} + (h\nu_i/kT)(e^{h\nu_i/kT}-1)^{-1}]$$

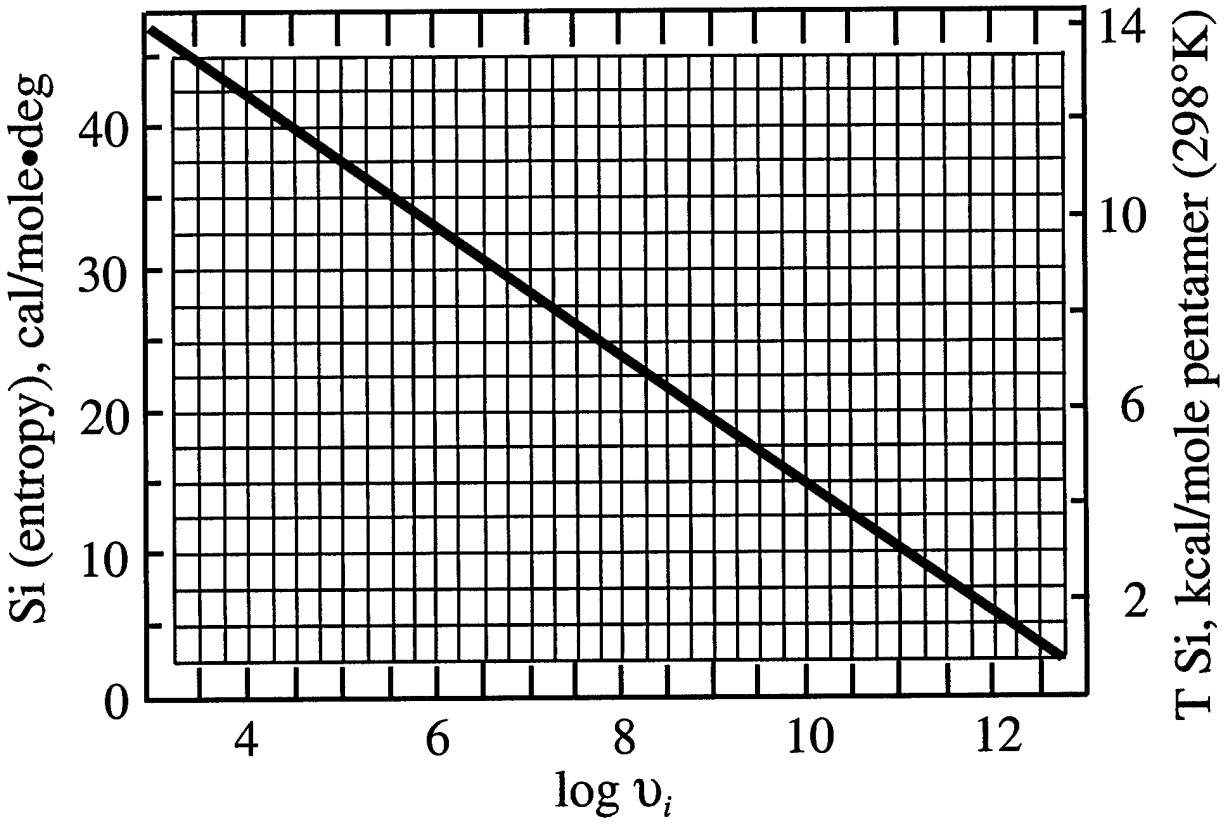

Figure 15: Plot of the above equation for entropy as a function of log(oscillator frequency) using the partition function of an harmonic oscillator. On the left-hand ordinate is plotted the entropy in cal/mol-deg (EU, entropy units), and on the right-hand ordinate is plotted the Gibbs free energy in kcal/mol at 298°K. This illustrates the increasing contribution of low frequency oscillations to the entropy of a polypeptide chain.

Journal of Muscle Research and Cell Motility 23: 543–559, 2002.

Mechanics of elastin: molecular mechanism of biological elasticity and its relationship to contraction

D.W. URRY[1,2,*] and T.M. PARKER[2]
[1]*University of Minnesota, Twin Cities Campus, BioTechnology Institute, 1479 Gortner Avenue, St. Paul, MN 55108-6106;* [2]*Bioelastics Research Ltd., 2800 Milan Court, Suite 386, Birmingham, AL, 35211-6918, USA*

Abstract

Description of the mechanics of elastin requires the understanding of two interlinked but distinct physical processes: the development of entropic elastic force and the occurrence of hydrophobic association. Elementary statistical-mechanical analysis of AFM single-chain force–extension data of elastin model molecules identifies damping of internal chain dynamics on extension as a fundamental source of entropic elastic force and eliminates the requirement of random chain networks. For elastin and its models, this simple analysis is substantiated experimentally by the observation of mechanical resonances in the dielectric relaxation and acoustic absorption spectra, and theoretically by the dependence of entropy on frequency of torsion-angle oscillations, and by classical molecular-mechanics and dynamics calculations of relaxed and extended states of the β-spiral description of the elastin repeat, $(GVGVP)_n$. The role of hydrophobic hydration in the mechanics of elastin becomes apparent under conditions of isometric contraction. During force development at constant length, increase in entropic elastic force resulting from decrease in elastomer entropy occurs under conditions of increase in solvent entropy. This eliminates the solvent entropy change as the entropy change that gives rise to entropic elastic force and couples association of hydrophobic domains to the process. Therefore, association of hydrophobic domains within the elastomer at fixed length stretches interconnecting dynamic chain segments and causes an increase in the entropic elastic force due to the resulting damping of internal chain dynamics. Fundamental to the mechanics of elastin is the inverse temperature transition of hydrophobic association that occurs with development of mechanical resonances within fibrous elastin and polymers of repeat elastin sequences, which, with design of truly minimal changes in sequence, demonstrate energy conversions extant in biology and demonstrate the special capacity of bound phosphates to raise the free energy of hydrophobic association.

Introduction

As a brief introduction to the mechanics of elastin, noted are the composition and sequence of bovine elastin, the inverse phase transition behavior of the elastin and related protein components, and the conformational aspects of the most representative repeating sequence of elastin.

Composition and sequence of elastin

The single-residue T_t-based hydrophobicity plots of Figure 1 (Urry, 1997) provide a simple way to gain perspective of the composition and sequence of bovine elastin and to make comparisons with other extracellular proteins, for example human fibronectin. The longest repeating sequence $(GVGVP)_{11}$ is labeled W4 based on the nomenclature of the Sandberg group (Sandberg *et al.*, 1981, 1985). Additional, less extensive repeats are also apparent. Of the nearly 40 lysine (Lys, K) residues, all but two or three are used in forming cross-links. Generally, four Lys residues come together to form a tetrasubstituted pyridinium. By contrast, in the vulcanization of rubber every monomer is a potential cross-link, which allows for cross-link formation whenever two chains are in contact. In elastin only 5% of the residues participate in cross-link formation and these are often distributed along the chain in pairs. Such a situation requires a regular structure in order to bring this limited number of residues into adequate proximity for covalent cross-link formation.

There are only three negatively charged aspartic acid (Asp, D) and no glutamic acid residues in bovine elastin. The more hydrophobic phenylalanine (Phe, F) and tyrosine (Tyr, Y) residues are also apparent. The almost complete absence of charged groups combined with a substantial quantity of hydrophobic residues are responsible for the hydrophobic association between chains that result in parallel-aligned twisted filaments as seen in electron micrographs of negatively stained tropoelastin and α-elastin (Cox *et al.*, 1973, 1974) and in fibrous elastin (Gotte *et al.*, 1974).

By comparison, a sequence that results in a series of globular repeating units of hydrophobically folded β-barrels is seen in the single-residue T_t-based hydrophobicity plots for fibronectin in the lower part of Figure 1 (Kornblihtt *et al.*, 1985). In this case there are

*To whom correspondence should be addressed: E-mail: durry98@aol.com

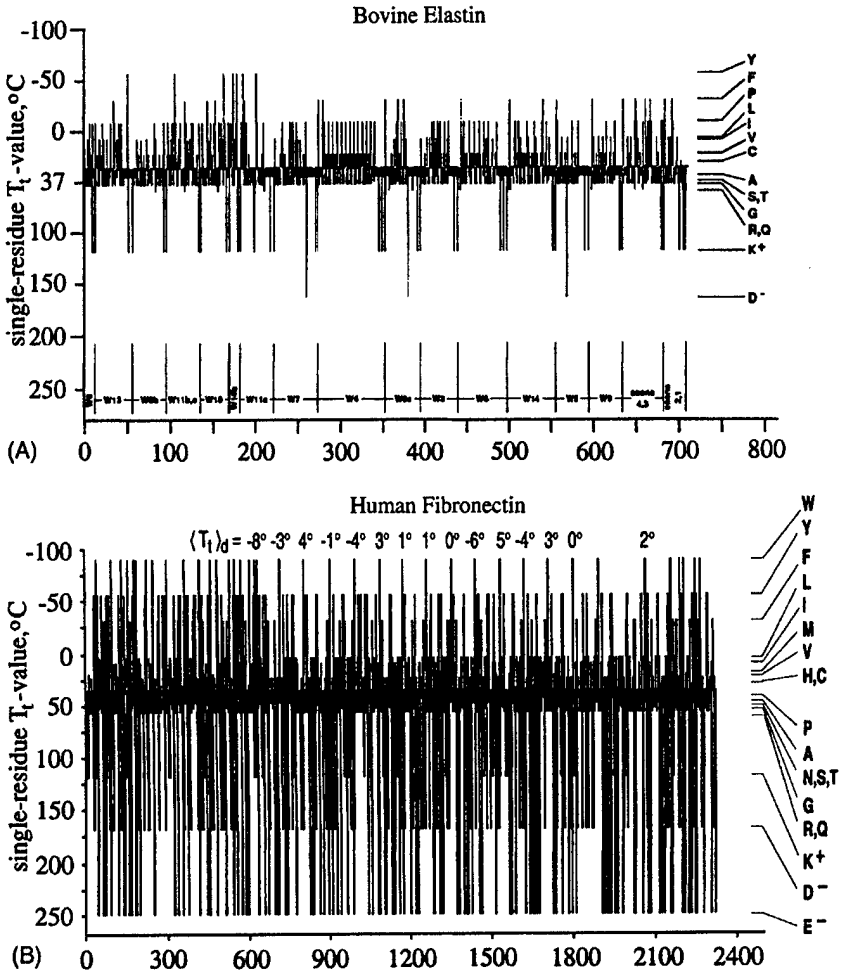

Fig. 1. Single residue T_t-based hydrophobicity plots for bovine elastin (A) and human fibronectin (B) (see text for discussion). Part A reproduced with permission from Urry *et al.* (1995), Part B reproduced with permission from Urry and Luan (1995a).

many more charged Glu, Asp and Lys residues, and the periodicity of the repeating globular units becomes apparent through the repeating tryptophan (Trp, W) residues. This most hydrophobic residue, W, repeating approximately every 90 residues identifies type III domains of fibronectin, which also appear as a repeating unit in titin (connectin). Such repeating globular units give a sawtooth pattern to the single-chain force–extension curves of titin (Rief *et al.*, 1997; Gaub and Fernandez, 1998), which is very different from the smooth single-chain force–extension curves given by elastin models (Urry *et al.*, 2002a, b).

Inverse temperature transition of elastin and component sequences

Increase in order of elastic protein upon raising the temperature

Tropoelastin (precursor protein of fibrous elastin), α-elastin (chemical fragmentation product from fibrous elastin) and high-molecular-weight polymers of repeating sequences of elastin are water soluble at low temperatures, but produce phase separation upon raising the temperature. The initial aggregates of the phase transition, when placed on a carbon-coated EM grid and negatively stained with uranyl acetate/oxalic acid, are observed to form parallel aligned filaments comprised of twisted filaments with interesting periodicities in the optical diffraction patterns of the micrographs (Volpin *et al.*, 1976a, b). Furthermore, cyclic analogues containing pentapeptide and hexapeptide repeats crystallize during temperature increase and redissolve upon lowering the temperature. Clearly, the order in elastin and elastin-based polymers increases with increasing the temperature.

This ordering of protein upon raising the temperature is consistent with the second law of thermodynamics: a structured hydration that surrounds the dissolved hydrophobic groups becomes less ordered bulk water during the phase separation of hydrophobic association (Urry *et al.*, 1997a, b).

This phase transition leading to a fundamental increase in order of the polymer on raising the temperature is called an inverse temperature transition.

Phase diagram

Phase diagrams of the inverse temperature-dependent behavior of elastin-based polymers is seen in Figure 2 (Sciortino *et al.*, 1990, 1993). In the usual polymer phase diagram the polymers are insoluble below and soluble above the binodal (coexistence or coacervate) line. For elastin-based polymers solubility is inverted. With elastin-based polymers solubility occurs below and insolubility occurs above the coexistence line. The shape of the coexistence line is also inverted: while for the usual petroleum-based polymers the line is concave towards the concentration (volume–fraction) axis, for elastin-related polymers it is convex. In case of the elastin-based polymers the coexistence line is also called the T_t-divide. Each point (called T_t) along the T_t-divide corresponds, for a given concentration, to the onset temperature of aggregation.

Elastin-based polymers exhibit a latent heat of transition. Accordingly, within the temperature range of the transition the chemical potential of the polymers in solution and in the phase-separated state are the same. This enables the derivation of the Gibbs free energy of hydrophobic association, ΔG_{HA} (see below). The more hydrophobic elastin-based polymers that associate at lower temperatures have lower values of ΔG_{HA}.

Conformational aspects of the $(GVGVP)_n$ of elastin

The structure of $(GVGVP)_n$, shown in Figure 3, was developed by using methodologies of peptide synthesis, NMR, molecular-mechanics and dynamics calculations

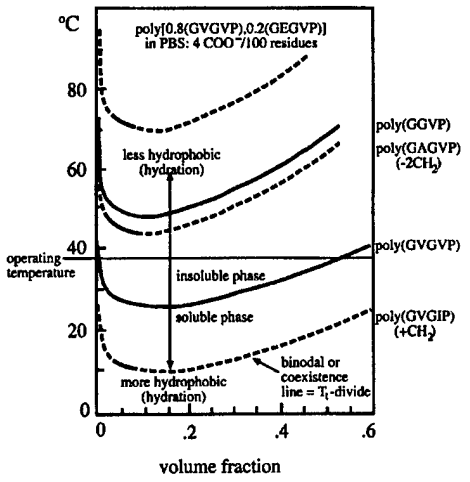

Fig. 2. Schematic representation of phase diagrams for several model elastic proteins based on the elastin repeat, $(GVGVP)_n$ (see text for discussion). Solid curves adapted with permission from Sciortino *et al.* (1990) and (1993).

(Venkatachalam and Urry, 1981; Chang *et al.*, 1989), crystal structure of cyclic analogues (Cook *et al.*, 1980) and the NMR- and computationally characterized relationship between cyclic and linear structures (Urry *et al.*, 1981, 1989), and Raman, absorption and circular dichroism spectroscopies.

The structure involves a series of β-turns, ten-atom hydrogen-bonded rings from the Val^1 C—O to the Val^4 N—H (Figure 3A and B) which, upon raising the temperature, wrap up into a helical structure called the β-spiral (shown schematically in Figure 3C and D and in detail in Figure 3E). It is shown that the β-turns

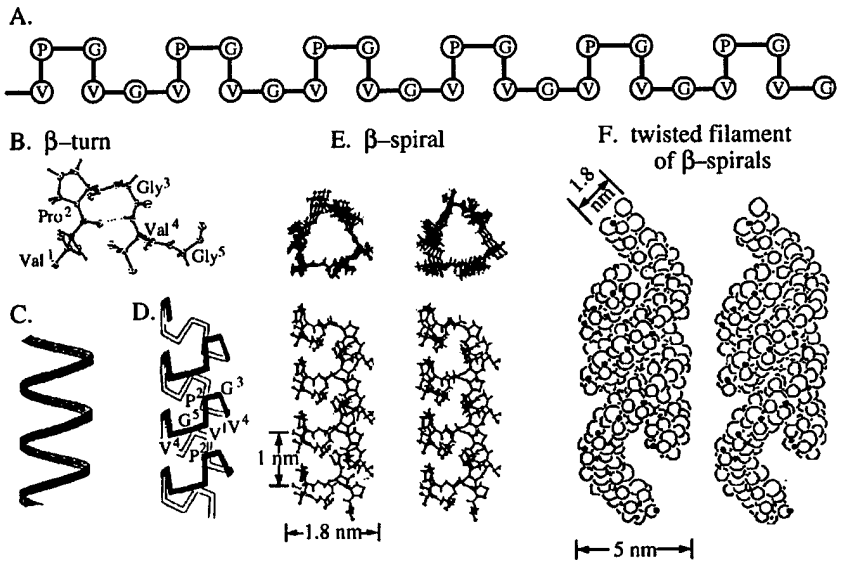

Fig. 3. Representations of the proposed molecular structure of $(GVGVP)_n$ (see text for discussion).

function as hydrophobic spacers between the turns of the β-spiral and that the β-spirals associate hydrophobically to form twisted filaments of the dimensions found in the transmission electron micrographs of negatively stained incipient aggregates as noted above (Volpin *et al.*, 1976a, b). Hydrophobic folding of β-spirals and the hydrophobic association of β-spirals to form twisted filaments occur in a cooperative manner.

General considerations of entropic elastic force

Components of elastic force and their delineation

Internal energy (f_E) and entropy (f_S) components of elastic force

The total elastic force (f) can be thermodynamically described as

$$f = (\partial E/\partial L)_{V,T,n} - T(\partial S/\partial L)_{V,T,n}, \tag{1}$$

where E is the internal energy; S the entropy; T the absolute temperature in °K, and V, T, and n indicate that the change in length (∂L) occurs at constant volume, temperature and composition. Accordingly, the total elastic force comprises two components, the internal energy component (f_E) and the entropic component (f_S):

$$f = f_E + f_S. \tag{2}$$

Experimental delineation of the relative magnitudes of f_E and f_S

Following Flory *et al.* (1960) the total force can also be written as

$$f = (\partial E/\partial L)_{V,T,n} + T(\partial f/\partial T)_{V,L,n} \tag{3}$$

which is equivalent to

$$f_E/f = -T(\partial \ln[f/T]/\partial T)_{V,L,n}. \tag{4}$$

Equation (4) shows that the ratio of the internal energy component of force to the total force can be determined experimentally by plotting $\ln[f/T]$ as a function of temperature while maintaining the elastic element at constant volume, at fixed length and without a change in composition. Under these experimental conditions, the slope of the plot multiplied by ($-T$°K) provides the f_E/f ratio.

Statistical mechanical expression for entropy

The Boltzmann relation

The Boltzmann relation provides the bridge from a statistical mechanical description of molecular structure to experimentally determined thermodynamic quantities. It is an elegant yet simple statement of entropy (S) in terms of thermodynamic probability (W, the number of *a priori* equally probable states accessible to the system) (Eyring *et al.*, 1964), i.e.,

$$S = R \ln W. \tag{5}$$

R (1.987 cal/deg mol) is the gas constant. $R=Nk$, where N is Avogadro's number (6.02×10^{23}/mol) and k Boltzmann's constant (1.38×10^{-16} erg/deg K). W is a volume in phase space, a $2N$-dimensional space, which fundamentally provides a description of a molecule in terms of the momentum (p_i) and coordinate (q_i) of each its i atoms.

Description of entropy using partition functions for different degrees of freedom

In practice, the description of the molecule is achieved by the product of partition functions, which group according to the degrees of freedom of the molecular system. In general, the $2N$ degrees of freedom group as three translational degrees of freedom, three rotational degrees of freedom and the remainder are internal degrees of freedom that comprise vibrations and torsional oscillations (rotations about bonds). In the measurement of elasticity, the single chain molecule or the cross-linked matrix is fixed at both ends. In this case, there are holonomic constraints on the molecular system in that there are neither whole-molecule translational nor rotational degrees of freedom. Thus, we are left only with internal chain dynamics.

Frequency dependence of entropy for the harmonic oscillator representation of internal chain dynamics

The harmonic oscillator partition function (f_v) provides a relatively simple and yet informative representation of internal chain dynamics.

$$f_v = [1 - \exp(-h\nu_i/kT)]^{-1}. \tag{6}$$

When placed in Equation (5) and expressed in terms of the frequency-dependence of entropy (S) we obtain (Dauber *et al.*, 1981),

$$S_i = R\{\ln[1 - \exp(-h\nu_i/kT)]^{-1} + (h\nu_i/kT)[\exp(h\nu_i/kT) - 1]^{-1}\}. \tag{7}$$

Equation (7) is plotted in Figure 4 with S_i on the left-hand ordinate and with the free-energy contribution (TS_i) on the right-hand ordinate.

The interesting features of Figure 4 are that the vibrational modes occur at high frequencies where the contribution to entropy is small, and the torsional oscillations occur at much lower frequencies where the contribution to entropy is much larger. As discussed below, the mechanical resonances exhibited by elastin models and fibrous elastin occur at frequencies near 1 kHz and 5 MHz, i.e., near 3 and 6 on the abscissa of Figure 4. Accordingly, it becomes reasonable to neglect

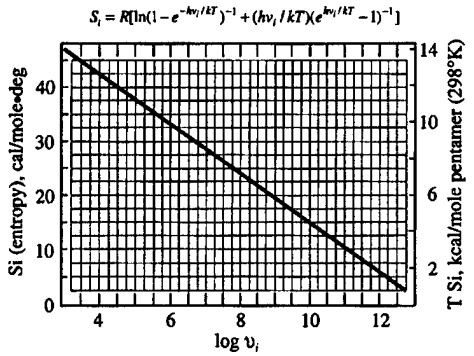

Fig. 4. Plot, based on the harmonic oscillator partition function, of the entropy of the oscillator as a function of log(oscillator frequency). On the left-hand ordinate is plotted the entropy in cal/mol deg (EU, entropy units), and on the right-hand ordinate is plotted the entropic contribution to the Gibbs free energy in kcal/mol pentamer at 298°K. This illustrates the increasing contribution of low frequency oscillations to the entropy and free energy of a protein chain segment. Adapted with permission from Urry *et al.* (1988).

changes in vibrational frequencies on extension and to consider those configurational and dynamic changes due to changes in torsion angles.

Expression for the change in entropy on extension
The change in entropy upon extension is written,

$$\Delta S = (S^{e} - S^{r}) = R\ln(W^{e}/W^{r}), \qquad (8)$$

where e and r stand for the extended and relaxed states. With Equation (8) it becomes possible to use both molecular mechanics and dynamics calculations of the molecular structure described in Figure 3 to calculate the contribution of torsional freedom of the structure to entropy in both the relaxed and extended states.

The physical basis for entropic elasticity in elastin

In an ideal or perfect elastomer the energy repeatedly invested in extension is repeatedly and completely recovered during relaxation. Ideality increases as the elastic force results from a decrease in entropy upon extension, because this occurs without stressing bonds to the breaking point. Elastin models and elastin itself in water provide examples of such entropic elastomers with about 90% of the elastic force being entropic, that is, the f_E/f ratio of Equation (4) is about 0.1. This is essential to human life expectancy, because the half-life of elastin in the mammalian elastic fiber is on the order of 70 years. This means that the elastic fibers of the aortic arch and thoracic aorta, where there is twice as much elastin as collagen, will have survived some billion demanding stretch-relaxation cycles by the start of the seventh decade of life. This represents an ultimate in ideal elasticity.

Three main mechanisms proposed for the entropic elasticity of elastin

The classical (random chain network) theory of rubber elasticity
In 1958 Hoeve and Flory reported studies on the nature of elasticity of the bovine fibrous protein, elastin, as representative of the mammalian elastic fiber. Because they were able to determine a very low f_E/f ratio, they concluded that the elastic fiber was without order, that is, it was a random chain network. They re-affirmed it in the spring of 1974 in a Biopolymers paper (Hoeve and Flory, 1974) stating that 'A network of random chains within the elastic fibers, like that in a typical rubber, is clearly indicated.' In order to emphasize this perspective further, the following statement appeared in the legend to Figure 1 of that paper: 'Configurations of chains between cross-linkages are much more tortuous and irregular than shown.' In part because Paul Flory received the Nobel Prize in 1974 for his work on macromolecules, this perspective became firmly set in the minds of the interested scientific community.

The solvent (bulk water ↔ hydrophobic hydration) entropy mechanism
It appeared that the sole purpose of the Hoeve and Flory 1974 paper, which presented neither new experimental data nor theoretical analysis, was to refute the publication of a new mechanism. The new mechanism for the entropic elasticity of elastin was published by Weis-Fogh and Anderson (1970) with the title 'New Molecular Model for the Long-range Elasticity of Elastin.' The proposed new mechanism, stated in the terms of present adherents, was that upon extension hydrophobic side-chains become exposed to the water solvent. The result is formation of low-entropy water of hydrophobic hydration. Here we refer to this as the solvent (bulk water ↔ hydrophobic hydration) mechanism for entropic elasticity. This mechanism has been given credibility by groups using computational methods on $(GVGVP)_n$ in water (Wasserman and Salemme, 1990; Alonso *et al.*, 2001). One of the many arguments marshaled by Hoeve and Flory (1974) against this mechanism was that polymer backbone, not solvent, must bear the force.

The damping of internal chain dynamics on extension
In the hydrophobically folded β-spiral structure (Figure 3), the presence of suspended segments between the β-turns is immediately apparent. With water surrounding the suspended segments and no steric hindrance to limit rotation about backbone bonds of the suspended segments, the peptide moieties would be expected to rock or 'librate'. These suspended segments are probably free to undergo large torsion-angle oscillations, and the amplitude of these torsional oscillations might be damped during extension (Urry, 1982). We devised experimental (physical and chemical) and computational tests of the structure with a focus on the freedom of

motion of the suspended segments. The chemical tests (replacement of the Gly residues with D- and L-alanines) resulted in the predicted limited torsional oscillations and elasticity (Urry *et al.*, 1983a, b, 1984, 1991). The principal physical tests involved dielectric and NMR relaxation methodologies (Henze and Urry, 1985; Urry *et al.*, 1985a, b, c, 1986; Buchet *et al.*, 1988). Remarkably, in the dielectric relaxation characterization, where the only dipole moments were those of the backbone peptide moieties, intense localized relaxations developed as the model elastic protein underwent the inverse temperature (phase) transition. Furthermore, molecular mechanics and dynamics calculations demonstrated the decrease in amplitude of torsion-angle oscillations within the suspended segment during extension (Urry, 1982; Chang and Urry, 1989). Indeed, by treating the dynamics of the pentameric unit the oscillating dipole moment reproduced the dielectric relaxation results (Venkatachalam and Urry, 1986). Thus, the concept of the damping of internal chain dynamics by extension as a source of entropic elastic force became established (Chang and Urry, 1989). Key experimental and computational results are treated in more detail below.

Key experimental data relevant to the proposed mechanisms

Atomic force microscopy (AFM) single-chain force–extension results

The remarkable capacity to obtain single-chain force–extension curves provides new insights into the mechanism of entropic elasticity. Figure 5A shows a series of single-chain force–extension curves for a single molecule of Cys-$(GVGVP)_{n\times251}$-Cys (Urry *et al.*, 2002a). Starting from the bottom, a series of extension–relaxation cycles are displayed. The second trace, during which the molecule was extended from an end-to-end distance of 200–700 nm and then returned to the starting length, demonstrates perfect reversibility at the rate of stretch and within the resolution of the technique. Since all of the energy of deformation was recovered during relaxation, we observe an ideal elastomer! For the third, fourth and sixth traces, a resting time of 30 s near 200 nm was allowed, and these traces demonstrated barely detectable imperfect overlap of extension and relaxation curves. The fifth trace without the 30 s resting time near 200 nm again exhibited perfect reversibility. Finally on the seventh extension of the chain the continuity from substrate to cantilever tip became severed and the force dropped to zero just above 700 nm.

The slight hysteresis of traces one, three, four and six, may be due to backfolding of the chain on itself, interaction of a second chain picked up at low extension or possibly even non-specific adsorption of the single chain to surface at low extension and at a position along the chain of within 100 nm of extended length from the attachment point. Regardless of the source of the barely detectable non-overlap of several of the traces, ideal

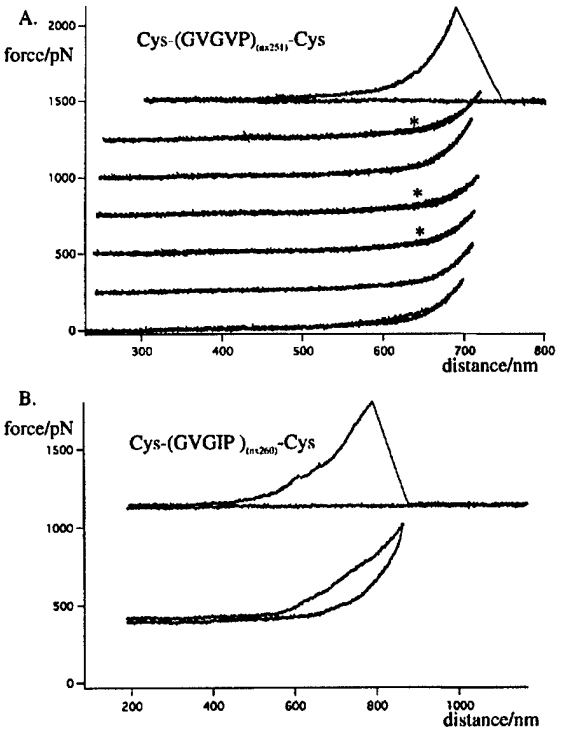

Fig. 5. AFM single-chain force–extension curves of the model elastic proteins based on elastin, Cys-$(GVGVP)_{n\times251}$-Cys (A) and Cys-$(GVGIP)_{n\times260}$-Cys (B), showing the ideal elasticity due to perfect reversibility of traces 2 and 5 from bottom of A and marked hysteresis in the lower trace of B. See text for discussion. Reproduced with permission from Urry *et al.* (2002a).

(entropic) elasticity has been observed in a single chain. No longer can the change from a Gaussian distribution of end-to-end chain lengths within a random chain network be insisted upon as the structural representation of entropic elasticity. The ideal single-chain force–extension curves require high dilution, and a higher dilution yet is required for more hydrophobic protein-based polymers where the tendency for aggregation is greater. This and additional data tell us that these perfectly reversible force–extension curves are due to single-chains. A single chain does not constitute a random chain network; and a single chain with ends fixed in space does not comprise a Gaussian distribution of end-to-end chain lengths. It seems that this eliminates the basic tenets of the random chain network theory of entropic elasticity as regards these elastic protein-based polymers. Furthermore, random chains do not exhibit mechanical resonances, e.g., intense localized Debye-type relaxations as observed in the dielectric relaxation spectra near 5 MHz and 3 kHz, and intense localized absorption maxima as observed in the acoustic absorption and loss permittivity spectra. These points constitute only the more apparent elements of the argument.

In addition, on the basis of the elementary statistical mechanical analysis given above, it would seem that the

source of entropic elasticity must come from a decrease in internal chain dynamics upon extension.

Reduction of mean solvent-entropy change increases rather than decreases entropic elastic force

Formation of hydrophobic hydration is exothermic (Butler, 1937). Accordingly, when the temperature of the dissolved protein with its hydrophobic hydration is raised from below to above the inverse temperature transition, an endothermic transition due to the conversion of hydrophobic hydration to bulk water occurs. The transition from *hydrophobic hydration to bulk water* represents a positive change in entropy. By finding a suitable solvent that allows the transition but reduces the heat of the transition to near zero, it becomes possible to determine whether a decrease in elastic force occurs due to the loss of the contribution of the negative solvent-entropy change to the entropic elastic force. In other words, if a decrease in solvent entropy occurs as bulk water becomes ordered (in the form of hydrophobic hydration) by exposure of hydrophobic groups during extension, then the extent to which this contributes to entropic elastic force could be measured as a decrease in entropic elastic force.

In our experimental approach (based on Hoeve and Flory (1958)) ethylene glycol was added to suppress the solvent interaction with the protein. In particular, as shown in the differential calorimetry data of Figure 6A increasing the amount of ethylene glycol decreases the heat and lowers the temperature of the transition. By 30% ethylene glycol in water the heat of the transition is minimal. The entropy change attending the transition is calculated by dividing an increment of heat released over the temperature of the increment and summing over all increments of the transition. Accordingly, the decrease in heat of the transition seen in Figure 6A would be expected to result in a decrease in the entropic elastic force due to a decrease in the magnitude of the negative entropy of hydration on extension. In fact, as seen in Figure 6B, the entropic elastic force reached is greater in 30% ethylene–70% water.

The thermoelasticity studies on γ-irradiation-cross-linked poly(GVGVP) of Figure 6B are carried out by stretching the elastomer to a fixed extension of 50% at 37°C. Then held at that fixed length, the temperature is re-equilibrated below that of the onset for the inverse temperature transition, and the temperature is very slowly raised to 55°C. As regards the contribution of solvent entropy change to entropic elastic force, it is expected that the force reached would be less for the ethylene glycol containing solution by a fraction indicative of the contribution of solvent entropy change to the elastic force. The observation that the force actually increased, rather than decreased does not favor the solvent entropy mechanism.

As shown in Equation (4), the value of f_E/f is given by $-T(\partial \ln[f/T]/\partial T)_{V,L,n}$. Using the temperature range from 45 to 55°C, the f_E/f ratio is found to be no more than 0.1. Based on this analysis using Equation (4), the f_S/f value would be 0.9 or greater, and yet this entropic elastic force would appear not to come from a change in solvent entropy. Even more telling is the increase in force at fixed length, $(\partial f/\partial T)_L$, as the temperature is raised through the range of the inverse temperature transition. As will be discussed below, this thermally driven isometric contraction shows an increase in force under conditions of an increase rather than the required decrease in solvent entropy.

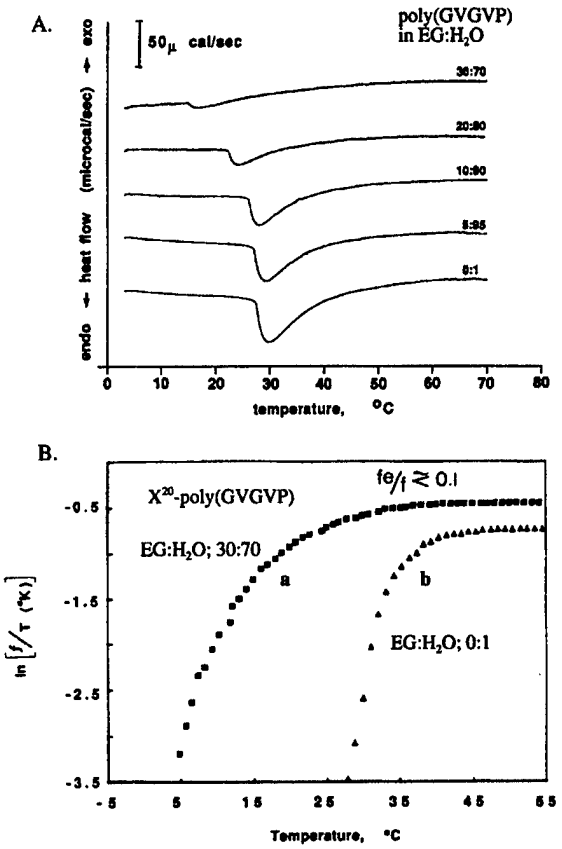

Fig. 6. (A) Differential calorimetry curves as a function of ethylene glycol (EG) in water. Note the decrease in the heat and lowering of the temperature range of the transition as the amount of ethylene glycol is raised to 30%. B. Thermoelasticity curves, plots of $\log(f/T)$ vs. T at fixed length, for 20 Mrad γ-irradiation cross-linked poly(GVGVP). The f_E/f ratio, determined from the slope above 45°C for both solvent conditions, is less than or equal to 0.1, that is the entropic component of elastic force is 90% or greater. Significantly, addition of ethylene glycol (EG) results in an increase in entropic elastic force suggesting that solvent entropy change is not a contribution to the entropic elastic force. Reproduced with permission from Luan *et al.* (1989).

Presence of mechanical resonances in elastin models and elastin itself

(i) *Mechanical resonances in the acoustic frequency range*: The elastic models of elastin based on the pentameric repeat (GVGVP) and analogues thereof, such as (GVGIP), exhibit mechanical resonances in the

acoustic frequency range of 100 Hz to 7 kHz. This is seen in Figure 7A for γ-irradiation-cross-linked $(GVGIP)_{260}$, which exhibits a mechanical resonance of increasing absorption intensity as the temperature is raised from below to above the range of the inverse temperature transition (Urry *et al.*, 2002a). By contrast, natural rubber and polyurethane (a particularly good elastomer for sound absorption), exhibit only broad low-intensity absorption as might be expected for a random chain network. For a random chain the frequency for rotation about each polymer backbone bond will be different, whereas for an elastomer with a regular repeating structure such as that in Figure 3 mechanical resonances such as those in Figure 7A can result. For our purposes the observation of a mechanical resonance is evidence for a non-random structure, and therefore challenges the classical theory of rubber elasticity.

Low-frequency dielectric relaxation studies also demonstrate mechanical resonances with absorption in the acoustic frequency range. As seen in Figure 7B, the imaginary part (ε″) of the dielectric permittivity of cross-linked $(GVGIP)_{320}$ exhibits a relaxation that also increases in intensity as the temperature is raised from

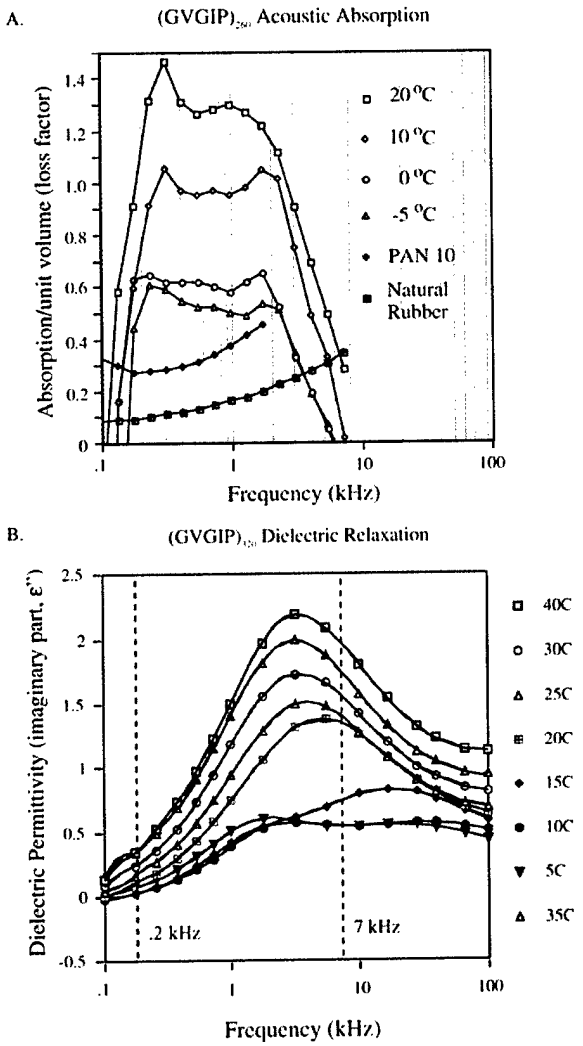

Fig. 7. Mechanical resonances seen in the acoustic absorption frequency range. The repeating pentamers, as they fold into the regularly repeating structure of Figure 3 on raising the temperature, develop a mechanical resonance wherein all pentamers absorb energy over the same frequency range. Although the physical means of exciting the mechanical resonance is different in A and B, an acoustic wave in A and an oscillating electric field in B, the maxima of these low frequency mechanical resonances are only shifted by a few kHz. A second higher frequency mechanical resonance is observed for this same elastic model protein in the dielectric relaxation near 5 MHz, 1000 kHz to higher frequency, as seen in Figure 8 for both the real and imaginary parts of the dielectric permittivity. Part A, acoustic absorption/unit volume (loss factor), reproduced with permission from Urry *et al.* (2002a) and part B, imaginary part of the low frequency dielectric relaxation spectra, reproduced with permission from Urry *et al.* (2002b).

below to above the temperature of the inverse temperature transition (Urry *et al.*, 2002b). As the excitation energy is not that of a compressional acoustic wave, but rather an oscillating electric field, it is interesting to see that the repeating unit of five residues acts as a single unit with an oscillating net dipole that displays mechanical resonance in a similar frequency range. It may be further noted in Figure 7B that the absorption intensity increases by more than 50% upon going from 20 to 40°C. Because of this, the acoustic absorption exhibited by $(GVGIP)_n$ at 20°C in Figure 7A would be expected to increase by an additional 50% upon increasing the temperature further, to 40°C. This would make the absorption per unit volume of $(GVGIP)_n$ much larger than that exhibited by natural rubber or urethane.

(ii) *Mechanical resonances in the MHz range*: Dielectric relaxation studies demonstrate mechanical resonances near 5 MHz for $(GVGVP)_n$, $(GVGIP)_n$, $(GVGLP)_n$ (Buchet *et al.*, 1988), α-elastin and fibrous elastin purified from bovine *ligamentum nuchae*. The data of Figure 8A give the real part of the dielectric permittivity (ε′) for α-elastin, a 70 kDa chemical fragmentation product of natural fibrous elastin (Urry *et al.*, 1988a) and for the elastin model poly(GVGVP) (inset) (Henze and Urry, 1985). ε″ for poly(GVGVP) and fibrous elastin is shown in Figure 8B (Luan *et al.*, 1988).

As seen in Figure 1, there is much more to elastin than poly(GVGVP), of the W4 sequence, although it is the most prominent repeating sequence in bovine elastin. The relaxations for 100% poly(GVGVP) are expected to

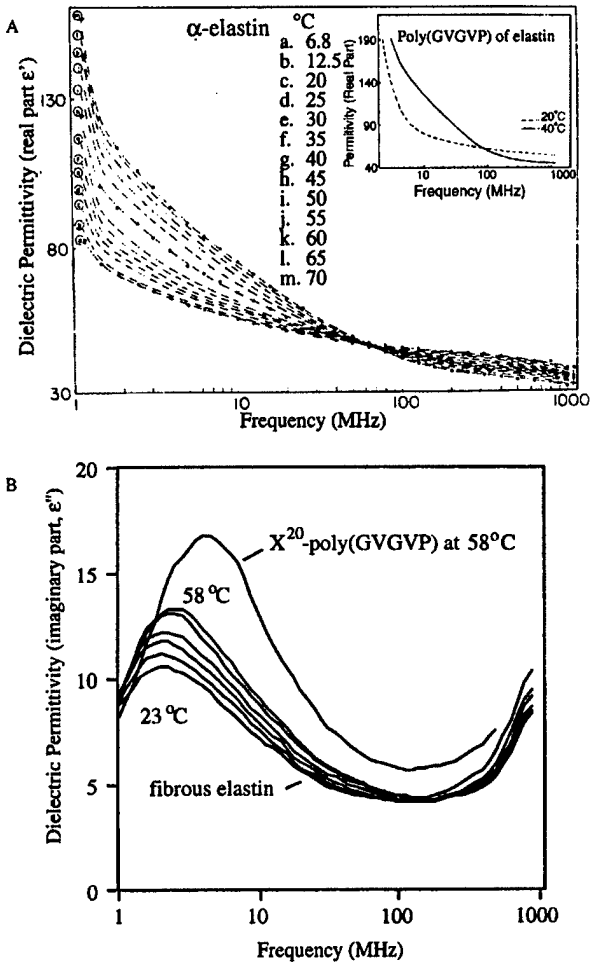

Fig. 8. Dielectric relaxation spectra in the 1–1000 MHz frequency range of α-elastin (part A), the poly(GVGVP) of elastin (inset of part A and part B), and fibrous elastin (part B). In all cases as the temperature is raised there develops an intense mechanical relaxation centered near 5 MHz as repeating elements of these protein systems hydrophobically fold into regular, albeit obviously dynamic, structures. In the case of poly(GVGVP) each pentamer folds into the same conformation, in which the peptide moieties (the only entities with dipole moments) undergo coordinated rocking motions with a resulting oscillating mean dipole moment. The rocking of the mean dipole moments of the pentamers resonate, in this case move, at the same frequency in response to an alternating electric field, that is, they exhibit a mechanical resonance centered near 5 MHz. A similar mechanical resonance is observed near 1 kHz in Figure 7. Part A reproduced with permission from Urry *et al.* (1988a), and part B reproduced with permission from Luan *et al.* (1988).

be more intense than that of α-elastin and fibrous elastin. It is indeed surprising that the frequency overlap and intensity is as close as found. It is apparent that other repeating sequences, or quasi repeats, exhibit dielectric relaxations at slightly lower frequencies.

Importantly, mechanical resonances near 5 MHz and 1 kHz indicate the presence of regularly repeating dynamic structures. Extension of such structures reasonably gives rise to an entropic elastic force upon extension by the damping of internal chain dynamics represented by mechanical resonance. Molecular mechanics and dynamics calculations based on the molecular structure shown in Figure 3 will demonstrate just how effectively the structure can explain the experimental elasticity and relaxation data.

Entropy calculations based on the elastin model, $(GVGVP)_n$

Calculations of structures and the entropies of the structures have used conventional molecular mechanics and dynamics programs such as CHARMM (Karplus and McCammon, 1983; Karplus and Kushick, 1981), AMBER (Weiner and Kollman, 1981), and Scheraga's ECEPP (Momany *et al.*, 1974, 1975). The satisfying feature of these quite distinct computational approaches is that they give essentially identical results whether carried out within our group by different researchers or by different groups. It is important, however, that the constraints and boundary conditions should properly reflect the conditions considered. Paramount among the constraints is adherence to the elasticity experiment in which the ends of the molecular structure are fixed at whatever selected degree of extension.

Molecular mechanics calculations using Scheraga's ECEPP approach for energy surfaces in ϕ–ψ configuration space

(i) *Calculation of entropy change during extension by an enumeration of states approach for relaxed and extended states*: In Scheraga's approach the internal energy of a chosen chain segment (in our case the pentamer permutation, $V_1P_2G_3V_4G_5$) is calculated as a function of a pair of adjacent torsion angles. Normally, the ϕ and ψ torsion angles are identical to those in the Ramachandran plot. In our case since the primary sites of motion are the peptide moieties of the suspended segment ($V_4G_5V_1$), such that the two ϕ–ψ plots, now called lambda plots, become ϕ_5–ψ_4 and ϕ_1–ψ_5.

In the enumeration of states approach, a 5° change in a single torsion angle is counted as a new state, and the number of states is counted for the chosen cut-off energy for both the relaxed and 130% extended structures (Urry *et al.*, 1982; Urry and Venkatachalam, 1983; Urry *et al.*, 1985c; Urry, 1991). A single pentamer is calculated within the relaxed and extended β-spiral structures, and 0.6, 1.0 and 2.0 kcal/mol-pentamer cut-off energies are used as well as an energy weighting using the Boltzmann summation over states. Table 1 gives the number of states where the entropy is simply calculated by Equation (9) using the example of 1 kcal/mol-pentamer,

$$\Delta S = (S^e - S^r) = R\ln(W^e/W^r) = R\ln(58/762) = -5.1 \text{ cal/mol-pentamer.} \quad (9)$$

This, of course, is −1.02 cal/mol-residue as given in Table 1.

(ii) *Calculation of dielectric relaxation data from pentamer molecular mechanics*: With the aid of the Onsager equation for polar liquids (Onsager, 1931; Bottcher, 1973) it becomes possible to use the structures obtained above and to sum the dipole moments of the states of Table 1. In addition, the same can be done for $V_1P_2G_3V_4A'_5$) where the A' stands for the D-Ala amino acid residue (Venkatachalam and Urry 1986 and printers erratum as corrected below; Urry, 1991). Comparison of experimental and calculated values is particularly satisfying. 'In view of this result, it seems reasonable to consider a cutoff energy of 1.5 kcal mol^{-1}. This value of energy cutoff leads to a mean dipole moment change of 3.8 Debye per pentamer in good agreement with the value obtained from dielectric relaxation studies. Similar dielectric studies on D.Ala^5-polypentapeptide indicate a dipole moment of about one-third of that found for the polypentapeptide at 37°C... This is in very good agreement with the dipole changes obtained from

Table 1. Perspective of entropy of the poly(GVGVP) β-spiral by enuneration of states

Cutoff energy (kcal/mol)	Number of states		Entropy change per residue
	Relaxed (r)	Extend (e)	
2	1853	162	−0.97
1	762	58	−1.02
0.6	342	24	−1.06
	Using Boltzmann sum over states $f = \sum_i e^{-\epsilon_i/kT}$		
2	$\Delta S = R\ln(f^e/f^r) + \frac{E^e - E^r}{T}$		−1.01

molecular mechanics calculations presented here' (Venkatachalam and Urry 1986).

The above calculated results utilize the 5 MHz mechanical resonance. They further demonstrate how readily calculations based on the dynamic structure given in Figure 3 calculate experimental dielectric relaxation data with inherent relevance to entropic elastic force. The values for entropy change calculated using the molecular mechanics approach, when used in the second term of Equation (1), provide excess entropic elastic force as expected (see Urry *et al.*, 2002a, b).

Molecular dynamics calculations using Karplus' CHARMm and Kollman's AMBER programs

As the motions of the torsional oscillations are dynamic, it is appropriate to consider molecular dynamics calculations using the Karplus software program adapted by Polygen, Inc. (now Molecular Simulations), called CHARMm, version 20.3. For these Newtonian classical mechanics simulations the potential energy functions and parameters suggested by the Karplus group (Brooks *et al.*, 1983) were used in a software program. The root-mean-square (RMS) fluctuations of the torsion angles, $\Delta\phi_i$ and $\Delta\psi_i$ for the relaxed and extended (130%) of $(GVGVP)_{11}$ as given in Table 2 are used in Equation (10).

$$\Delta S = R \ln[\Pi_i \Delta\phi_i^e \Delta\psi_i^e / \Pi_i \Delta\phi_i^r \Delta\psi_i^r] \qquad (10)$$

The calculated change in entropy upon extension of −1.1 cal/mol deg-residue is in remarkable agreement with the previously described molecular-mechanics calculations.

Furthermore, Wasserman and Salemme (1990) using the AMBER software program of the Kollman group (Weiner and Kollman, 1981), but also including a medium of water molecules, obtained essentially identical results. It must be concluded, damping of internal chain dynamics is an abundant source of decrease in chain entropy that is sufficient to account for the entropic elastic force.

As Wasserman and Salemme (1990) included water molecules in their calculations, and an ordering of water molecules was found as the hydrophobic side chains became exposed on chain extension, they considered this decrease in solvent entropy as a possible source of the entropic elastic force. As will be shown below, solvent entropy change does not make a significant contribution to the entropic elastic force development during isometric contractions.

Relationship between hydrophobic association–dissociation, elastic force and energy conversion in elastin mechanics

By introducing glutamate (Glu, E) the ideal elastomer in Figure 5A becomes a chemo-mechanical transducer capable of converting the chemical energy of proton concentration changes into the mechanical energy of isotonic and isometric contractions (See Figure 9A and B). An analysis of this data in combination with that of Figure 6B resolves the issue of the role of changes in solvent entropy in elastic force development and energy conversion.

Table 2. RMS fluctuations of torsion angles (ϕ and ψ) of $(VPGVG)_{11}$ (45 ps of equilibration time and 80 ps of molecular dynamics simulation). Reproduced with permission from Chang and Urry (1989)

	Angle	Relaxed	Extended	Angle	Relaxed	Extended	Angle	Relaxed	Extended
β-turns	ψ_{16}	10.87	14.17	ψ_{26}	27.33	07.64	ψ_{36}	20.19	14.84
	ϕ_{17}	09.86	15.18	ϕ_{27}	11.71	08.33	ϕ_{37}	08.99	10.47
	ψ_{17}	47.59	46.68	ψ_{27}	11.70	13.51	ψ_{37}	21.53	32.96
	ϕ_{18}	61.70	47.41	ϕ_{28}	08.61	10.36	ϕ_{38}	11.15	10.66
	ψ_{18}	09.37	16.05	ψ_{28}	09.33	08.16	ψ_{38}	11.09	27.29
	ϕ_{19}	14.25	08.67	ϕ_{29}	09.70	07.31	ϕ_{39}	12.70	10.24
Suspended	ψ_{19}	44.09	10.99	ψ_{29}	47.32	10.48	ψ_{39}	52.00	12.50
	ϕ_{20}	41.94	09.29	ϕ_{30}	48.57	11.39	ϕ_{40}	55.88	08.37
Segments	ψ_{20}	14.50	11.15	ψ_{30}	42.56	10.62	ψ_{40}	40.67	11.08
	ϕ_{21}	27.13	24.17	ϕ_{31}	11.43	11.38	ϕ_{41}	36.44	19.06
β-turns	ψ_{21}	09.39	22.73	ψ_{31}	12.17	09.21	ψ_{41}	12.97	14.80
	ϕ_{22}	09.94	08.00	ϕ_{32}	09.90	08.93	ϕ_{42}	11.59	07.33
	ψ_{22}	11.58	16.13	ψ_{32}	15.30	10.80	ψ_{42}	11.34	13.17
	ϕ_{23}	16.37	09.33	ϕ_{33}	09.60	07.62	ϕ_{43}	09.23	09.76
	ψ_{23}	14.33	14.25	ψ_{33}	09.88	09.43	ψ_{43}	10.60	12.53
	ϕ_{24}	11.39	29.20	ϕ_{34}	11.86	09.71	ϕ_{44}	11.06	12.82
Suspended	ψ_{24}	19.53	37.87	ψ_{34}	63.80	08.36	ψ_{44}	41.89	35.22
	ϕ_{25}	25.02	23.06	ϕ_{35}	91.70	10.20	ϕ_{45}	48.98	31.31
Segments	ψ_{25}	49.32	32.10	ψ_{35}	15.03	11.51	ψ_{45}	42.05	56.89
	ϕ_{26}	31.43	27.24	ϕ_{36}	21.49	18.66	ϕ_{46}	21.55	30.33

$\Delta S = R \ln \frac{\Pi_i \Delta\phi_i^e - \Delta\psi_i^e}{\Pi_i \Delta\phi_i^r - \Delta\psi_i^r}$.

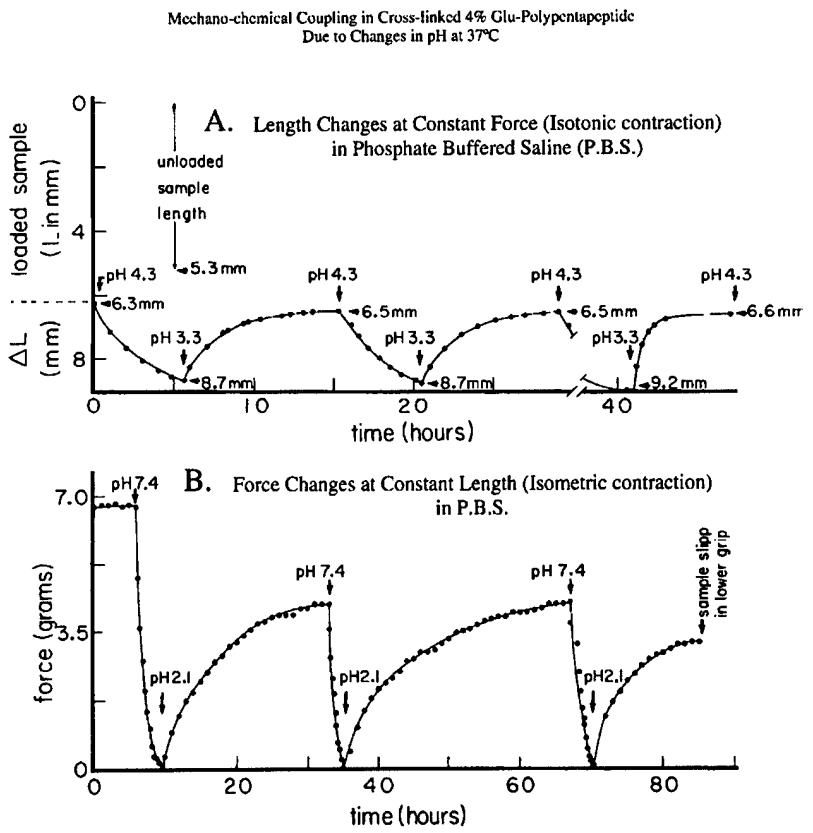

Fig. 9. Mechano-chemical coupling by 20 Mrad γ-irradiation cross-linked of poly[0.8(GVGVP),00.2(GEGVP)] under isotonic (A) and isometric (B) conditions. In part B under isometric contraction conditions there occurs an increase in entropic elastic force resulting from a decrease in entropy of the elastomer while there occurs an increase in the entropy of the solvent as hydrophobic hydration becomes bulk water. Therefore the increase in entropic elastic force cannot be the result of the solvent entropy change. Reproduced with permission from Urry *et al.* (1988b).

Chemically driven isotonic $(\partial L/\partial\mu_H)_f$ and isometric $(\partial f/\partial\mu_H)_L$ contractions

The elastin model protein of interest is poly $[x_V$-(GVGVP),x_E(GEGVP)], where x_V and x_E are the mole fractions with $x_V + x_E=1$ and for the case where $x_E=0.2$. Upon γ-irradiation cross-linking an elastic matrix is formed which can be studied under isotonic and isometric conditions. Results are shown in Figure 9A and B (Urry *et al.*, 1988b). The isotonic contraction $(\partial L/\partial\mu_H)_f$ in Figure 9A is the change in length at constant load (force) resulting from an increase in the concentration of proton, that is, the increase in chemical potential of proton $(\partial\mu_H)$. The isometric contraction $(\partial f/\partial\mu_H)_L$ in Figure 9B is the change in force at constant length due to an increase in proton.

Both of these contractions result from hydrophobic association due to protonation of the carboxylate group. The underlying physical process is the competition for hydration between the charged carboxylate and the hydrophobic side chains of the valine (Val, V) residues (Urry, 1997). This competition, described as an apolar–polar repulsive free energy of hydration, results in increasing positive cooperativity of the acid–base titration curves that correlate with increasingly larger pK_a shifts. As Val residues are replaced by more hydrophobic phenylalanine (Phe, F) residues, the pK_a shifts increase (up to 6 pH units or more) and positive cooperativity increases with Hill coefficients of up to 8 or more (Urry, 1997). The apolar–polar repulsive free energy of hydration is related to the change in Gibbs free energy for hydrophobic hydration, $\Delta G_{HA}(\chi)$, of a phosphate as discussed in relation to Equations (17) and (19) below, but first the source of entropic elastic force is addressed.

Isometric contractions, $(\partial f/\partial T)_L$ and $(\partial f/\partial\mu_H)_L$, confirm basis for entropic elastic force

From Equation (1) the entropic component of the elastic force, f_S, is proportional to $-\Delta S$, that is, an increase in entropic elastic force results from a decrease in entropy. Also the formation of hydrophobic hydration from bulk water constitutes an inherently negative ΔS, and, of course, the loss of hydrophobic hydration constitutes a positive change in entropy. This change in solvent

entropy due to formation of hydrophobic hydration has been credited as an important contribution to entropic elastic force (Weis-Fogh and Anderson, 1970; Wasserman and Salemme, 1990, Alonso *et al.*, 2001). Therefore, the immediate question becomes whether experimental results support or eliminate a decrease in solvent entropy as a source of entropic elastic force.

Thermally driven isometric contraction (Figure 6B)
Figure 6B shows the classic thermoelasticity study for determining the f_E/f ratio for γ-irradiation-cross-linked poly(GVGVP). Because extension is fixed, a thermally driven isometric contraction also occurs over the temperature range of the inverse temperature transition of hydrophobic association. During hydrophobic association, hydrophobic hydration becomes bulk water. Therefore, the solvent entropy change is positive. Any contribution to the entropic elastic force due to changes in hydrophobic hydration during this thermally driven isometric contraction would necessarily result in a decrease in force. Yet the experimental result of Figure 6B shows the development of an elastic force that is 90% entropic, while the change in solvent entropy is of the opposite sign. Clearly, the change in solvent entropy is not contributing to the estimated 90% entropic elastic force. Having eliminated solvent entropy change as the source of entropic elastic force during a thermally driven isometric contraction, we now analyze the solvent entropy change attending a chemically driven isometric contraction.

Chemically driven isometric contraction (Figure 9B)
As seen in Figure 9B, at fixed extension of the γ-irradiation-cross-linked elastic matrix comprised of poly[0.8(GVGVP),0.2(GEGVP)], protonation of four carboxylates per 100 residues results in development of elastic force. A thermoelasticity characterization of this matrix at low pH gives the same result of dominantly entropic elasticity as found in curve b of Figure 6B for poly(GVGVP) in the absence of carboxyl moieties.

The process of protonation allows reconstitution of hydrophobic hydration to such an extent that the temperature range for hydrophobic association drops below that of the operating temperature (Urry, 1993, 1997). The result is a contraction due to hydrophobic association. Again, during an isometric contraction (this time chemically driven), hydrophobic hydration becomes less ordered bulk water. The solvent entropy increases during the development of entropic elastic force due to a decrease in entropy.

In addition to eliminating solvent entropy change as a source of entropic elastic force, the isometric contraction results provide the conceptual bridge between the fundamental source of entropic elastic force and contraction by hydrophobic association.

Hydrophobic association effects elastic force development by extending (and thereby damping internal dynamics of) interconnecting chain segments

Clam-shaped globular proteins that open and close due to hydrophobic association
The top part of Figure 10 shows a series of clam-shaped globular proteins strung together near the open end by elastic bands and maintained at fixed extension. In this isometric state, there is depicted an equilibrium between open and closed states. Obviously, shifting the equilibrium toward the closed state would increase the force measured at the force transducer, whereas shifting toward the open state would lower the force on the interconnecting elastic bands. Thus, any process that increased hydrophobic association would increase the elastic force. Now in the lower part of Figure 10, we relate this perspective to the β-spiral representation of Figure 3C.

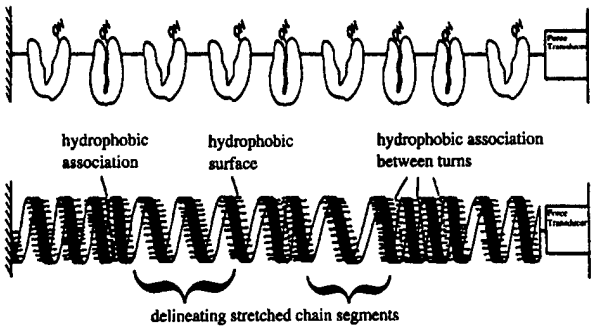

Fig. 10. Cartoon of the relationship between hydrophobic association and entropic elastic force development. Above: A series of clam-shaped globular protein strung together by elastic bands with an equilibrium between open and hydrophobically associated closed states. Clearly, as the equilibrium shifts toward more closed states, the force, sustained by the interconnecting elastic segments, increases. Below: Representation of the β-spiral structure of poly(GVGVP) at an intermediate state of hydrophobic association between turns of the β-spiral. Clearly, as more hydrophobic association occurs between turns, the interconnecting elastic chain segments become further extended with an increase in damping of internal chain dynamics giving rise to greater entropic elastic force. Reproduced with permission from Urry (1990).

Schematic representation of an equilibrium between hydrophobically associated and dissociated turns of a β-spiral held at fixed extension

The bottom half of Figure 10 uses the representation of the β-spiral given in Figure 3C to depict an equilibrium between associated and dissociated turns of the β-spiral. As more of the turns are involved in hydrophobic association, those not involved become extended to a greater extent. Thus, as more hydrophobic association occurs, the interconnecting segments become increasingly extended. By the entropic mechanism of the damping of internal chain dynamics on extension, the entropic elastic force increases.

Opening and closing of the clam-shaped globular proteins of the upper part of Figure 10 (Urry, 1990) would be detectable under conditions of force-clamp atomic force spectroscopy. Such traces have been observed using titin-based elastic constructs comprised of a series of hydrophobically folded β-barrels (Oberhauser *et al.*, 2001). Because of the continuous nature of increases in hydrophobic association between turns of the β-spiral represented in the lower part of Figure 10, such force-clamp traces for poly(GVGVP) would not have such steps, unless sensitivity were sufficient to detect the addition of a repeating unit to hydrophobic association.

Thus, the changes in entropic elastic force and in hydrophobic association are two distinct physical processes that become interlinked when occurring within the same chain system. Hydrophobic association causes the extension of interconnecting dynamic chain segments with the result of the damping of internal chain dynamics within those non-hydrophobically associated interconnecting chain segments.

Derivation of Gibbs free energy for hydrophobic association ΔG_{HA}

The role of hydrophobic association in the development of entropic elastic force has been delineated above. The next step is to derive an expression for the Gibbs free energy of hydrophobic association and to relate it to processes that direct elastic–contractile processes.

(i) *At the temperature of the inverse temperature transition*, $\mu_{HA} = \mu_{HD}$ and $\Delta G = 0$: The chemical potential (μ) is the Gibbs free energy per mole ($\Delta G/\Delta n$). By the Gibbs phase rule, at the temperature of the inverse temperature transition for hydrophobic association the chemical potential of the hydrophobically disassociated (dissolved) state (μ_{HD}) and the chemical potential of the hydrophobically associated state (μ_{HA}) are equal. Therefore, at the temperature of the inverse temperature transition (T_t), $\Delta G_t = \Delta H_t - T_t\Delta S_t = 0$, where ΔH_t is the heat of the transition and ΔS_t is the entropy change for the transition. Accordingly at the value of T_t for a given elastic model protein composition, $\Delta H_t = T_t\Delta S_t$.

By way of example, consider the two different compositions of model elastic proteins, $(GVGVP)_n$ and $(GVGIP)_n$. These two polypentapeptides differ only by a single CH_2 moiety per pentamer. In particular, the R-group for the V residue, $-CH(CH_3)_2$, differs from the R-group of the I residue, $-CH(CH_3)-CH_2-CH_3$, by the addition of a single CH_2 moiety. At the temperature for each of their respective phase transitions where $\mu_{HA}=\mu_{HD}$, we can write,

$$\Delta H_t(\text{GVGVP}) = T_t(\text{GVGVP})\Delta S_t(\text{GVGVP}) \qquad (11)$$

and

$$\Delta H_t(\text{GVGIP}) = T_t(\text{GVGIP})\Delta S_t(\text{GVGIP}). \qquad (12)$$

Butler (1937) showed that each addition of a CH_2 moiety in the series of normal alcohols from methanol to *n*-pentanol on dissolution in water resulted in an average exothermic heat $(\Delta H)/CH_2$ of −1.4 kcal/mol-CH_2 and a change of the term, $(-T\Delta S)/CH_2$, of a +1.7 kcal/mol-CH_2. While there are many important points to make about this fundamental finding, we use it here simply as a justification to rewrite Equation (12) as

$$\Delta H_t(\text{GVGIP}) = \Delta H_t(\text{GVGVP}) + \Delta H_t(CH_2), \qquad (13)$$

and

$$T_t(\text{GVGIP})\Delta S_t(\text{GVGIP}) = T_t(\text{GVGIP})[\Delta S_t(\text{GVGVP}) + \Delta S_t(CH_2)]. \qquad (14)$$

Substituting Equations (13) and (14) into Equation (12) and subtracting Equation (11) gives

$$[\Delta H_t(CH_2) - T_t(\text{GVGIP})\Delta S_t(CH_2)] = [T_t(\text{GVGIP}) - T_t(\text{GVGVP})]\Delta S_t(\text{GVGVP}). \qquad (15)$$

The left hand side of Equation (15) is recognized as an expression for the change in Gibbs free energy due to addition of the CH_2 moiety. On consideration of the phase transition being analyzed, the left hand side of Equation (5) becomes the change in Gibbs free energy of hydrophobic association due to the addition of a single CH_2 moiety, $\Delta G_{HA}(CH_2)$, that causes the inverse temperature transition of hydrophobic association to occur at a lower temperature for $(GVGIP)_n$.

$$\Delta G_{HA}(CH_2) = [T_t(\text{GVGIP}) - T_t(\text{GVGVP})] \times \Delta S_t(\text{GVGVP}). \qquad (16)$$

The right hand side of Equation (16) is negative because $T_t(\text{GVGIP}) < T_t(\text{GVGVP})$ and $\Delta S_t(\text{GVGVP})$ is positive for a transition whereby hydrophobic hydration becomes less ordered bulk water during hydrophobic association, that is, as insolubility ensues.

The addition of a CH_2 moiety per pentamer is one of very many ways whereby the value of T_t can be changed. A T_t-based hydrophobicity scale has been developed for substitution of each of the naturally occurring amino

acid residues and chemical modifications thereof by systematically increasing the mole fraction of pentamers containing the change X and extrapolating to the value of T_t that would occur for poly(GXGVP) (Urry, 1997). Therefore, the value of T_t may be greater than 100°C as for poly(GEGVP) when the glutamic acid residue, E, is ionized as the carboxylate, where T_t=250°C. On the other hand, the value of T_t may be less than 0°C as for poly(GWGVP) when the tryptophan is the residue, where T_t=−90°C. For the amino acids with functional side chains the T_t-value changes upon changing the state of the side chain from carboxyl to carboxylate, or the redox state of an attached redox couple. The most dramatic change in the T_t-value occurs upon phosphorylation of a Ser, Thr, or Tyr residue (Pattanaik *et al.*, 1991). Furthermore, adding salt to the solution of a neutral polymer such as poly(GVGVP) itself lowers the value of T_t (Urry, 1993), but the ΔT_t is 10 times greater when the salt ion-pairs with a charged side chain (Urry and Luan, 1995a; Urry *et al.*, 1997a).

So we generalize to any experimental variable, χ, that alters the value of T_t of a reference model elastic protein and write,

$$\Delta G_{HA}(\chi) = [T_t(\chi) - T_t(\text{reference})]\Delta S_t(\text{reference}), \tag{17}$$

or

$$\Delta G_{HA}(\chi) = \Delta T_t(\chi)\Delta S_t(\text{reference}), \tag{18}$$

where T_t is the value of a reference polymer and state has been changed to $T_t(\chi)$ by the experimental variable χ. All of these energy inputs can now be described in terms of their effect on the free energy of hydrophobic association, $\Delta G_{HA}(\chi)$.

Relevance of Gibbs free energy for hydrophobic association to energizing by phosphorylation

Phosphorylation of poly[30(GVGIP),(RGYSLG)] by the cardiac cyclic AMP-dependent protein kinase at the serine (Ser, S) residue of the polymer goes to an average of 47% completion by the following reaction (Pattanaik *et al.*, 1991; A. Pattanaik, personal communication).

$$\begin{aligned}&\text{ATP} + \text{poly[30(GVGIP),(RGYSLG)]}\\ &\quad = \text{ADP} + \text{poly[30(GVGIP),}\\ &\qquad \text{(RGYS(—OPO}_3^{2-}\text{)LG)]}.\end{aligned} \tag{19}$$

The value of T_t for this polymer before phosphorylation was approximately 20°C and the change in the value of T_t extrapolated as defined to a reference state of one phosphate per GVGIP becomes 860°C, which is represented as $T_t(—OPO_3^{2-})$. If we now use the experimentally derived value of ΔS_t(GVGIP) = 9.32 cal/mol (pentamer) deg as the ΔS_t(reference) (Luan and Urry, 1999) of Equation (17), the change in Gibbs free energy for hydrophobic association due to phosphorylation, $\Delta G_{HA}(—OPO_3^{2-})$, is +7.8 kcal/mol. For the reaction of Equation (19) with an equilibrium constant of $K = 47/53 = 0.9 = \exp(-\Delta G/RT)$, the change in Gibbs free energy for the reaction is 0.06 kcal/mol. Thus, the calculated value for the free energy contributed by the terminal phosphate of ATP would be 0.06–7.8 = −7.7 kcal/mol, which is remarkably close to the free energy of hydrolysis of the terminal phosphate of ATP of 7.3 kcal/mol (Voet and Voet, 1995).

Accordingly, phosphorylation raises the free energy of the hydrophobically associated state, that is, it results in hydrophobic disassociation, and phosphate removal drives hydrophobic association, e.g., contraction, more effectively than any other chemical change measured so far. Expectations are that the binding of ATP, and most effectively ADP plus phosphate, would dramatically raise the free energy of the hydrophobically associated state as evidenced by an increase the value of T_t. This $\Delta T_t(—OPO_3^{2-})$ and $\Delta G_{HA}(—OPO_3^{2-})$ can be only partially modulated by ion-pairing, for example, with magnesium, of the phosphates at the binding site.

Relationship between entropic elasticity and efficiency of energy conversion

The process of stretching an elastomer constitutes an energy input with the expended mechanical energy $f\Delta L$, where f is force and ΔL is the change in length. Accordingly, the mechanical energy is obtained from the area under the force vs. extension curve. For an ideal elastomer, the plot of force vs. extension is perfectly reversible, as shown by the second and fifth traces of Figure 5A for the single-chain force–extension curve of the entropic elastomer, $(GVGVP)_{n\times 251}$. Thus, the input energy is completely recovered on relaxation for an ideal (entropic) elastomer. Since the energy recovered on relaxation can be viewed in the sense of an energy output, an ideal elastomer could be considered a perfect machine for storing energy of deformation.

Often the force vs. length curve obtained on relaxation falls below the force vs. length curve obtained on extension (as seen in the lower curve of Figure 5B); then the material is said to exhibit a hysteresis. In this case the energy recovered on relaxation is less than that expended on extension. The input deformation energy has been dissipated in some way and to an extent indicated by the difference in the areas below the extension and relaxation curves.

When energy conversion occurs by means of an ideal elastic material, it is possible for the energy conversion to occur at high efficiency, whereas when energy conversion occurs using an elastic material that exhibits hysteresis, the efficiency of energy conversion becomes limited at least to an extent determined by the magnitude of the hysteresis. The elasticity of polymeric materials becomes inextricably intertwined with the efficiency of energy conversion. Thus, the increase in

elastic force during the isometric contraction and relaxation of Figure 9B would be exactly reversible for an ideal elastomer as would the isotonic contraction of Figure 9A. This would not be the case for a molecular machine comprised of the elastic polymer functioning in Figure 5B.

An important element, therefore, of an ideal elastomer is to have the energy uptake into the elastomer during extension reside entirely in the backbone modes where it can be recovered on relaxation. Should energy of deformation find its way into side-chain motional modes and into chains not bearing the deformation and irreversibly into solvent, this deformation energy becomes dissipated and unavailable during relaxation, resulting in hysteresis. Comparison of the single-chain force–extension curves of Figure 5 for poly(GVGVP) with poly(GVGIP) provides an example with proposed loss of energy into the side chain motions and interactions of the bulkier isoleucine (I) residue with its added CH_2 moiety into adjacent non-load-bearing chains.

Acknowledgements

The authors wish to acknowledge the support of the Office of Naval Research under contracts, N00014-00-C-0404 and N00014-00-C-0178, and to thank A. Pattanaik for updated details on the phosphorylation study and L. Hayes for assistance in obtaining the hydrophobicity plots and references.

References

Alonso LB, Bennion BJ and Daggett V (2001) Hydrophobic hydration is an important source of elasticity in elastin-based polymers. *J Am Chem Soc* **123:** 11,991–11,998.

Bottcher CJF (1973) *Theory of Electric Polarization.* (vol. 1, p. 178) Elsevier, Amsterdam.

Brooks BR, Bruccoleri RE, Olafson BO, States DT, Swaminathan S and Karplus M (1983) CHARMM: a program for macromolecular energy, minimization, and dynamics calculations. *J Comput Chem* **4:** 187.

Buchet R, Luan C-H, Prasad KU, Harris RD and Urry DW (1988) Dielectric relaxation studies on analogs of the polypentapeptide of elastin. *J Phys Chem* **92:** 511–517.

Butler JAV (1937) The energy and entropy of hydration of organic compounds. *Trans Faraday Society* **33:** 229–238.

Chang DK and Urry DW (1989) Polypentapeptide of elastin: damping of internal chain dynamics on extension. *J Comput Chem* **10:** 850–855.

Chang DK, Venkatachalam CM, Prasad KU and Urry DW (1989) Nuclear overhauser effect and computational characterization of the β-spiral of the polypentapeptide of Elastin. *J Biomol Struct Dynam* **6:** 851–858.

Cook WJ, Einspahr HM, Trapane TL, Urry DW and Bugg CE (1980) Crystal structure and conformation of the cyclic trimer of a repeat pentapeptide of elastin, cyclo-(L-Valyl-L-prolylglycyl-L-valylglycyl)$_3$. *J Am Chem Soc* **102:** 5502–5505.

Cox BA, Starcher BC and Urry DW (1973) Coacervation of α-elastin results in fiber formation. *Biochim Biophys Acta* **317:** 209–213.

Cox BA, Starcher BC and Urry DW (1974) Coacervation of tropoelastin results in fiber formation. *J Biol Chem* **249:** 997–998.

Dauber P, Goodman M, Hagler AT, Osguthorpe D, Sharon R and Stern P (1981) In: Lykos P and Shavitt I (eds) *ACS Symposium Series No. 173. Suypercomputers in Chemistry.* (pp. 161–191) American Chemical Society, Washington, DC.

Eyring H, Henderson D, Stover BJ and Eyring EM (1964) *Statistical Mechanics and Dynamics.* (p. 92) John Wiley & Sons Inc, New York.

Gaub HE and Fernandez JM (1998) The molecular elasticity of individual proteins studied by AFM-related techniques. *AvH-Magazin* **71:** 11–18.

Gotte L, Giro G, Volpin D and Horne RW (1974) The ultrastructural organization of elastin. *J Ultrastruct Res* **46:** 23–33.

Henze R and Urry DW (1985) Dielectric relaxation studies demonstrate a peptide librational mode in the polypentapeptide of elastin. *J Am Chem Soc* **107:** 2991–2993.

Hoeve CAJ and Flory PJ (1958) The elastic properties of elastin. *J Am Chem Soc* **80:** 6523–6526.

Hoeve CAJ and Flory PJ (1974) Elastic properties of elastin. *Biopolymers* **13:** 677–686.

Karplus M and Kushick JN (1981) Method for estimating the configurational entropy of macromolecules. *Macromolecules* **14:** 325–332.

Karplus M and McCammon JA (1983) Dynamics of proteins: elements of function. *Ann Rev Biochem* **53:** 263–300.

Kornblihtt AR, Umezawa K, Vibe-pederson K and Baralle FE (1985) Primary structure of human fibronectin: differential splicing may generate at least 10 polypeptides from a single gene. *EMBO J* **4:** 1755–1759.

Luan C-H, Harris RD and Urry DW (1988) Dielectric relaxation studies on bovine ligamentum nuchae. *Biopolymers* **27:** 1787–1793.

Luan C-H, Jaggard J, Harris RD and Urry DW (1989) On the Source of Entropic Elastomeric Force in Polypeptides and Proteins: Backbone Configurational vs. Side Chain Solvational Entropy. *Int. J. of Quant. Chem.: Quant. Biol. Symp.* **16:** 235–244.

Luan C-H and Urry DW (1999) Elastic, plastic, and hydrogel protein-based polymers. In: Mark JE (ed.) *Polymer Data Handbook,* (pp. 78–89, Table 3A) Oxford University Press, New York, Oxford.

Momany FA, Carruthers LM, McGuire RF and Scheraga HA (1974) Intermolecular potentials from crystal data. III. Determination of empirical potentials and application to the packing configurations and lattice energies in crystals of hydrocarbons, carboxylic acids, amines, and amides. *J Phys Chem* **78:** 1595.

Momany FA, McGuire FF, Burgess AW and Scheraga HA (1975) Energy parameters in polypeptides. VII. Geometric parameters, partial charges, nonbonded interactions, hydrogen bond interactions, and intrinsic torsional potentials for the naturally occurring amino acids. *J Phys Chem* **79:** 2361.

Oberhauser AF, Hansma PK, Carrion-Vasquez M and Fernandez JM (2001) Stepwise unfolding of titin under force-clamp atomic force microscopy. *Proc Natl Acad Sci USA* **98:** 468–472.

Onsager L (1936) Electric moments of molecules in liquids. *J Am Chem Soc* **58:** 1486–1493.

Pattanaik A, Gowda DC and Urry DW (1991) Phosphorylation and dephosphorylation modulation of an inverse temperature transition. *Biochem Biophys Res Comm* **178:** 539–545.

Rief M, Gautel M, Oesterhelt F, Fernandez JM and Gaub HE (1997) Reversible unfolding of individual titin immunoglobulin domains by AFM. *Science* **276:** 1109–1112.

Sandberg LB, Leslie JG, Leach CT, Alvarez VL, Torres AR and Smith DW (1985) Elastin covalent structure as determined by solid phase amino acid sequencing. *Pathol Biol (Paris)* **33:** 266–274.

Sandberg LB, Soskel NT and Leslie JG (1981) Elastin structure, biosynthesis, and relation to disease states. *N Engl J Med* **304:** 566–579.

Sciortino F, Prasad KU, Urry DW and Palma MU (1993) Self-assembly of bioelastomeric structures from solutions: mean field critical behavior and Flory–Huggins free-energy of interaction. *Biopolymers* **33:** 743–752.

Sciortino F, Urry DW, Palma MU and Prasad KU (1990) Self-assembly of a bioelastomeric structure: solution dynamics and the spinodal and coacervation lines. *Biopolymers* **29:** 1401–1407.

Urry DW (1990) Protein folding and assembly: an hydration-mediated free energy driving force. In: Gierasch L and King J (eds) *Protein Folding: Deciphering the Second Half of the Genetic Code.* (pp. 63–71) Am. Assoc. for the Advancement of Sci., Washington, DC.

Urry DW (1991) Thermally driven self-assembly, molecular structuring and entropic mechanisms in elastomeric polypeptides. In: Balaram P and Ramaseshan S (eds) *Mol Conformation and Biol Interactions.* (pp. 555–583) Indian Acad of Sci., Bangalore, India.

Urry DW (1993) Molecular machines: how motion and other functions of living organisms can result from reversible chemical changes, *Angew Chem (German)* **105:** 859–883, 1993; *Angew Chem Int Ed Engl* **32:** 819–841.

Urry DW (1997) Physical chemistry of biological free energy transduction as demonstrated by elastic protein-based polymers (invited FEATURE ARTICLE). *J Phys Chem* B **101:** 11,007–11,028.

Urry DW, Luan C-H and Peng SQ (1995) Molecular Biophysics of Elastin Structure, Function and Pathology, in Proceedings of The Ciba Foundation Symposium No. 192, The Molecular Biology and Pathology of Elastic Tissues, John Wiley & Sons, Ltd., Sussex, UK, pp. 4–30.

Urry DW and Luan C-H (1995a) A New Hydrophobicity Scale and its Relevance to Protein Folding and Interactions at Interfaces, in Proteins at Interfaces 1994, American Chemical Society Symposium Series, (Thomas A. Horbett and John L. Brash, eds.), pp. 92–110, Washington, D.C.

Urry DW and Luan C-H (1995b) Proteins: structure, folding and function. In: Lenaz G (ed.) *Bioelectrochemistry: Principles and Practice.* (pp. 105–182) Birkhäuser Verlag AG, Basel, Switzerland.

Urry DW and Venkatachalam CM (1983) A librational entropy mechanism for elastomers with repeating peptide sequences in helical array. *Int J Quant Chem: Quant Biol Symp* **10:** 81–93.

Urry DW, Chang DK, Krishna R, Huang DH, Trapane TL and Prasad KU (1989) Two dimensional proton nuclear magnetic resonance studies on poly(VPGVG) and its cyclic conformational correlate, cyclo(VPGVG)$_3$. *Biopolymers* **28:** 819–833.

Urry DW, Harris CM, Luan CX, Luan C-H, Gowda DC, Parker TM, Peng SQ and Xu J (1997a) Transductional protein-based polymers as new controlled release vehicles. In: Park K (ed.) *Controlled Drug Delivery: The Next Generation, Part VI: New Biomaterials for Drug Delivery,* (pp. 405–437) Am Chem Soc Professional Reference Book.

Urry DW, Haynes B, Zhang H, Harris RD and Prasad KU (1988b) Mechanochemical coupling in synthetic polypeptides by modulation of an inverse temperature transition. *Proc Natl Acad Sci USA* **85:** 3407–3411.

Urry DW, Henze R, Redington P, Long MM and Prasad KU (1985a) Temperature dependence of dielectric relaxations in α-elastin coacervate: evidence for a peptide librational mode. *Biochem Biophys Res Commun* **128:** 1000–1006.

Urry DW, Hugel T, Seitz M, Gaub H, Sheiba L, Dea J, Xu J and Parker T (2002a) Elastin: a representative ideal protein elastomer. *Philos Trans Roy Soc London [Biol]* **357:** 169–184.

Urry DW, Hugel T, Seitz M, Gaub H, Sheiba L, Dea J, Xu J, Prochazka F and Parker T (2002b) In: Shewry P & Bailey A (eds) *Ideal Protein Elasticity: The Elastin Model.* Cambridge University Press (in press).

Urry DW, Jaggard J, Prasad KU, Parker T and Harris RD (1991) Poly(Val^1-Pro^2-Ala^3-Val^4-Gly^5): a reversible, inverse thermoplastic. In: Gebelein CG (ed.) *Biotechnology and Polymers* (pp. 265–274) Plenum Press, New York.

Urry DW, Jing N, Trapane TL, Luan C-L and Waller M (1988a) Ion interactions with the gramicidin A transmembrane channel: cesium-133 and calcium-43 NMR studies. In: Agnew W, Claudio T and Sigworth F (eds) *Mol Biol of Ionic Channels* **33:** (vol. pp. 51–90) Academic Press, Inc., New York.

Urry DW, Peng SQ, Xu J and McPherson DT (1997b) Characterization of waters of hydrophobic hydration by microwave dielectric relaxation. *J Am Chem Soc* **119:** 1161–1162.

Urry DW, Peng SQ, Hayes LC, McPherson DT, Xu J, Woods TC, Gowda DC and Pattanaik A (1998) Engineering protein-based machines to emulate key steps of metabolism (biological energy conversion). *Biotechnology and Bioengineering* **58:** 175–190.

Urry DW, Trapane TL, Sugano H and Prasad KU (1981) Sequential polypeptides of elastin: cyclic conformational correlates of the linear polypentapeptide. *J Am Chem Soc* **103:** 2080–2089.

Urry DW, Trapane TL, Long MM and Prasad KU (1983a) Test of the librational entropy mechanism of elasticity of the polypentapeptide of elastin: effect of introducing a methyl group at residue-5. *J Chem Soc, Faraday Trans I* **79:** 853–868.

Urry DW, Trapane TL, Wood SA, Walker JT, Harris RD and Prasad KU (1983b) D-Ala$_5$ Analog of the elastin polypentapeptide. Physical characterization. *Int J Pept Protein Res* **22:** 164–175.

Urry DW, Trapane TL, Wood SA, Harris RD, Walker JT and Prasad KU (1984) D-Ala$_3$ Analog of elastin polypentapeptide: an elastomer with an increased Young's modulus. *Int J Pept Protein Res* **23:** 425–434.

Urry DW, Trapane TL, Iqbal M, Venkatachalam CM and Prasad KU (1985b) Carbon-13 NMR Relaxation studies demonstrate an inverse temperature transition in the elastin polypentapeptide. *Biochemistry* **24:** 5182–5189.

Urry DW, Trapane TL, McMichens RB, Iqbal M, Harris RD and Prasad KU (1986) Nitrogen-15 NMR relaxation study of inverse temperature transitions in elastin polypentapeptide and its Cross-Linked Elastomer. *Biopolymers* **25:** S209–S228.

Urry DW, Venkatachalam CM, Wood SA and Prasad KU (1985c) Molecular structures and librational processes in sequential polypeptides: from ion channel mechanisms to bioelastomers. In: Clementi E, Corongiu G, Sarma MH and Sarma RH (eds), *Structure and Motion: Membr, Nucleic Acids and Proteins* (pp. 185–203). Adenine Press, Guilderland, New York.

Urry DW, Venkatachalam CM, Long MM and Prasad KU (1982) Dynamic β-spirals and A librational entropy mechanism of elasticity. In: Srinivasan R and Sarma RH (eds) *Conformation in Biol.* (G.N. Ramachandran Festschrift Volume pp. 11–27). Adenine Press, Guilderland, New York.

Venkatachalam CM and Urry DW (1981) Development of a linear helical conformation from its cyclic correlate. β-spiral model of the elastin poly(pentapeptide), (VPGVG)$_n$. *Macromolecules* **14:** 1225–1229.

Venkatachalam CM and Urry DW (1986) Calculation of dipole moment changes due to peptide librations in the dynamic β-spiral of the polypentapeptide of elastin. *Int J Quant Chem: Quant Biol Symp* **12:** 15–24.

Voet D and Voet JG (1995) *Biochemistry.* 2nd edn. (p. 430, Table I5-3) John Wiley & Sons, Inc., New York.

Volpin D, Urry DW, Cox BA and Gotte L (1976a) Optical diffraction of tropoelastin and α-elastin coacervates. *Biochim Biophys Acta* **439:** 253–258.

Volpin D, Urry DW, Cox BA, Pasquali-Ronchetti I and Gotte L (1976b) Studies by electron microscopy on the structure of coacervates of synthetic polypeptides of tropoelastin. *Micron* **7:** 193–198.

Wasserman ZR and Salemme FR (1990) A molecular dynamics investigation of the elastomeric restoring force in elastin. *Biopolymers* **29:** 1613–1631.

Weiner PK and Kollman PA (1981) AMBER: assisted model building with energy refinement. A general program for modeling molecules and their interactions. *J Comput Chem* **2:** 287–303.

Weis-Fogh T and Andersen SO (1970) New molecular model for the long-range elasticity of elastin. *Nature* **227:** 718–721.